Heat transfer, evaporation and carbon dioxide transfer in soil

by

Xinhua Xiao

A dissertation submitted to the graduate faculty

in partial fulfillment of the requirements for the degree of

DOCTOR OF PHILOSOPHY

Major: Soil Science (Soil Physics)

Program of Study Committee:

Robert Horton, Major Professor

Tom Sauer

Brian Hornbuckle

Mahdi Al-Kaisi

Amy Kaleita-Forbes

Iowa State University

Ames, Iowa

2012

Table of Contents

Abstract

Latent heat flux associated with soil water evaporation connects the surface water balance with the surface energy balance. Soil water evaporation and soil carbon dioxide (CO2) fluxes both involve soil gas transport processes and properties, and both impact the soil environment and physical, chemical, and biological processes occurring in the soil. Accurate and dynamic measurements of soil water evaporation and soil CO2 fluxes enhance the understanding of water, energy, and carbon partitioning at the soil-atmosphere interface and the mechanisms of mass and energy movement in the soil. Most previous work focused on measurements made above the soil surface, and quantitative determinations of in situ water evaporation and carbon dioxide fluxes within soil profile were absent. The objectives of this dissertation were to accurately determine transient soil water evaporation and soil CO2 fluxes with depth in bare soil and in different management zones of a corn field and to evaluate in situ measurement techniques.

Three-needle heat pulse sensors were used to measure subsurface soil water evaporation at depths of 3 mm and below in a bare field. The daily evaporation estimated from the heat pulse method agreed well with the daily evaporation estimated from Bowen ratio and micro-lysimeter methods. The results showed that heat pulse sensors alone could accurately determine subsurface soil water evaporation with time and depth, and surface and subsurface evaporation could be accurately determined with heat pulse measurements combined with Bowen ratio measurements in a bare field. Newly designed 11-needle heat pulse sensors were used at the following locations within a corn field: within-row (ROW), between-rows with roots (BR), and between-rows without roots (BRNR). The

findings showed that heat pulse sensors measured the dynamic soil water evaporation at the three locations. The daily heat pulse evaporation estimates agreed well with micro-lysimeter measurements of daily soil water evaporation at ROW and BR in the corn field. In addition to heat pulse measurements for soil water evaporation, plant transpiration and evapotranspiration (ET) were measured using stem flow gauges and an eddy covariance system in the corn field. The evapotranspiration estimated from the sum of heat pulse evaporation and stem flow transpiration (E+T), eddy covariance ET, and potential evapotranspiration, ET_0, estimated from the Penman-Monteith equation had similar trends. ET_0 was larger than the individually measured E+T and eddy covariance ET. The individually measured E+T and ET_0 had similar values but eddy covariance measurements underestimated ET.

Bare soil CO2 fluxes were determined using a concentration gradient method with in situ measured soil CO2 concentrations and model estimated gas coefficients during natural wetting and drying periods. Results showed that CO2 fluxes decreased with depth and most of the CO2 was produced at shallow soil depths. CO2 fluxes decreased with depth from 0 to 90 mm, and kept stable at depths of 90 to 200 mm. The gradient method determined CO2 fluxes agreed well with surface closed-chamber measured CO2 fluxes. For 10 out of 12 days the daily mean gradient CO2 flux values were within the ranges of the closed-chamber CO2 fluxes values during a soil drying period.

The conclusions of the dissertation were that the heat pulse sensors were able to accurately determine soil water evaporation with time and depth in a bare field and in different soil management zones in a corn field. Soil CO2 fluxes and soil CO2 production

rates with depth in a bare field were accurately determined using a concentration gradient method with in situ CO2 concentration profiles. These simultaneous soil water evaporation and soil CO2 flux measurements could serve as a foundation for testing the numerical models of coupled heat, water, and gas transfer in soil, and could enhance further understanding of the complex soil system, and could guide the management of soil properties and processes.

Chapter 1 General introduction

Soil heat, water evaporation and carbon dioxide (CO_2) are interactive and impact the soil environment and physical, chemical and biological processes occurring in the soil. Latent heat flux associated with soil water evaporation connects the surface water balance with the surface energy balance. Accurate and dynamic measurements of soil water evaporation and soil CO_2 fluxes enhance the understanding of water, energy, and carbon partitioning at the soil-atmosphere interface and the mechanisms of mass and energy movement in the soil.

Eddy covariance and Bowen ratio are widely used micrometeorological approaches for estimating soil water evaporation and /or soil CO_2 flux at field scales (Wolf et al., 2008). Lysimetry (van Bavel, 1961) is a long-established method to determine soil water evaporation directly. Chamber-based methods, including open-chamber and closed-chamber approaches, are established ways to directly measure surface CO_2 efflux at local scale (Norman et al., 1992; Pumpanen et al., 2004). However, each of the methods has advantages and disadvantages. Eddy covariance and Bowen ratio can measure soil water evaporation and / or soil carbon dioxide fluxes at high temporal resolution without soil disturbance (Law et al., 1999). A disadvantage of the methods is that the instruments are stationary, relatively expensive and the underlying vegetation is assumed to be homogeneous. Lysimeter methods provide a direct way to measure soil water evaporation, but they can require significant labor and soil disturbance. Surface chamber methods also may disturb the soil environment, impacting temperature, water content, and rooting, during the measurements. One limitation of the earlier work is that measurements were focused above the soil surface. None of the earlier methods quantitatively determined subsurface soil water evaporation or soil carbon dioxide fluxes in soil profiles. The quantification of in situ surface and subsurface soil water evaporation and soil carbon dioxide not only enhances understanding of the mechanisms of energy and mass movement in the soil, but also provides useful information to aid in managing soil properties and processes. The objectives of this dissertation were to accurately measure transient soil water evaporation and soil CO2 fluxes with depth in a bare soil and soil water evaporation in different management zones of a corn field.

Based on conduction heat transfer theory and mathematical analysis introduced by Carslaw and Jaeger (1946), heat pulse sensors were developed and used to measure soil thermal properties. De Vries (1952) was the first soil scientist to measure soil thermal conductivity with single-needle heat pulse sensors. Later multi-needle heat pulse sensors were introduced to measure soil thermal properties and soil properties by monitoring the temperature response after applying a controlled heat pulse to the soil. Campbell et al. (1991) presented a two-needle heat pulse sensor for measuring soil heat capacity. Bristow et al. (1994) reported that the two-needle heat pulse sensor also could be used to measure thermal conductivity, thermal diffusivity, and volumetric heat capacity. Noborio et al. (1996) showed that heat pulse sensors could be combined with time domain reflectometry (TDR) technology, and Ren et al. (1999) developed a combined thermo-TDR sensor to measure in situ soil thermal properties, water content, and electrical conductivity. Thermo-TDR sensors were extended to simultaneously measure water content, bulk density, air-filled porosity (Ochsner et al., 2001) and soil water liquid fluxes (Ren et al., 2000; Ochsner et al., 2005).

Based on heat pulse theory, Heitman et al. (2008) reported that 3-needle heat pulse sensors could be used to accurately measure transient subsurface soil water evaporation at depths of 3 mm and deeper in a bare soil. The heat pulse method has several advantages, including accurate in situ measurements, simple calculations, and minimal soil disturbance. The method for determining the amount of latent heat involved in soil water evaporation requires measurement of the net sensible heat flux and the change in sensible heat storage of selected soil layers. Measured sensible heat terms enable the determination of a sensible heat balance for each soil layer. Latent heat for evaporation is the residual of the measured sensible heat balance. Numerical simulations provide support for the accuracy of heat pulse measurements for sensible heat balance determination of bare soil water evaporation with time and depth (Sakai et al., 2011).

One objective of this dissertation is to use heat pulse sensors accurately to determine transient soil water evaporation at various soil depths in bare and cropped fields.

Another objective of this dissertation is to accurately determine transient soil CO2 fluxes at various soil depths. Tang et al. (2003), DeSutter et al. (2008) and Turcu et al. (2005) used a concentration gradient method to estimate soil profile CO2 fluxes from measured soil CO2 concentrations and model-estimated gas diffusion coefficients in a corn-soybean rotation field, in an oak-grass savanna and in a laboratory soil column, respectively. However, they only measured CO2 concentrations at a few soil depths. The concentration gradients and gas diffusion coefficients near the soil surface varied largely depending on the methods used to estimate them. DeSutter et al. (2008) used six methods to estimate CO2 concentration gradients and three models to predict diffusion coefficients and found that some gradient method calculations of CO_2 fluxes were more than a hundred times larger than the CO_2 fluxes measured by an automated sampling chamber. To improve estimation of soil CO_2 fluxes, use of high-resolution soil CO_2 measurements with the concentration gradient method was investigated. Soil CO_2 concentrations were measured at 13 soil depths in the 0-200 mm soil layer during natural soil wetting and drying periods. The concentration gradient calculations of CO_2 fluxes were compared with surface CO_2 effluxes determined by closed-chamber measurements.

Soil heat transfer, water evaporation and CO_2 transfer are linked together and interactive. As solar radiation shines on a soil surface and the soil surface warms, heat redistributes and temperature gradients occur in the soil profile affecting soil moisture, surface vegetation and roots in the soil. Likewise, as soil water evaporates from or near the surface, soil temperature gradients increase and liquid water moves upward in the soil. Soil temperature and soil moisture influence soil micro-organisms and root respiration which are both sources of soil CO_2. Accurate measurements of in situ soil water evaporation and CO_2 fluxes enhance the understanding of water, energy, and carbon partitioning at the soil-atmosphere interface and the mechanisms of mass and energy movement in the soil. Simultaneous measurements are helpful for evaluating coupled soil heat, evaporation and CO_2 transfer model and for guiding the management of soil properties and processes.

Dissertation organization

The dissertation contains seven chapters: a general introduction (chapter 1), five research papers (chapters 2, 3, 4, 5 and 6) and a general conclusion (chapter 7). The general introduction reviews previous work on the measurements of soil water evaporation and soil CO_2, and introduces the significance of this dissertation study. The 5 research papers in this dissertation address two topics: soil water evaporation (chapters 2, 3, 4 and 5) and soil CO_2 (chapter 6). I was the first author of chapters 3, 4, 5 and 6. Although I was not the first author of chapter 2, I made significant contributions to the chapter. I designed the experiment, collected the data, analyzed the data and contributed to the writing.

In chapter 2, 3-needle heat pulse sensors are used to measure the dynamics of subsurface soil water evaporation with time and depth from a bare field, and the heat pulse method is evaluated by comparing heat pulse evaporation estimates with Bowen ratio and micro-lysimeter evaporation estimates. In chapter 3, cumulative soil water evaporation from a Bowen ratio measurement is combined with heat pulse cumulative soil water evaporation with time and depth to indicate the dynamics of surface and subsurface soil water evaporation in a bare field. In chapter 4, new 11-needle heat pulse sensors are used to measure soil water evaporation at three locations in a corn field. In chapter 5, evapotranspiration and its components are determined, and the measurement methods are evaluated for use in a corn field. Soil water evaporation is measured with 11-needle heat pulse sensors, plant transpiration is measured with stem flow gauges, and evapotranspiration is measured with an eddy covariance system.

In chapter 6, transient soil CO_2 fluxes and soil CO_2 production are estimated with time and depth in a bare field using a concentration gradient method. The concentration gradient method is evaluated by comparing gradient method CO_2 flux values with surface closed-chamber measurements of soil CO_2 fluxes.

A general conclusion in chapter 7 synthesizes all of the research results and mentions future research directions.

References

Bristow, K.L., G. J. Kluitenberg, and R. Horton. 1994. Measurement of soil thermal properties with a dual-probe heat-pulse technique. Soil Sci. Soc. Am. J. 58:1288-1294.

Campbell, G.S., C. Calissendorf, and J.H. Williams. 1991. Probe for measuring soil specific heat using a heat-pulse method. Soil Sci. Soc. Am. J. 55:291-293.

Carslaw, H.S., and J.C. Jaeger. 1946. Conduction of heat in solids. First ed. Oxford Unversity Press, Oxford.

De Vries, D.A. 1952. A nonstationary method for determining thermal conductivity of soil in situ. Soil Sci. 73:83-89.

DeSutter, T.M., T.J. Sauer, T.B. Parkin, and J.L. Heitman. 2008. A subsurface, closed-loop system for soil carbon dioxide and its application to the gradient efflux approach. Soil Sci. Soc. Am. J. 72:126-134.

Heitman, J.L., R. Horton, T.J. Sauer, and T.M. DeSutter. 2008. Sensible heat observations reveal soil water evaporation dynamics. J. Hydrometeor. 9:165-171.

Law, B.E., D.D. Baldocchi, and P.M. Anthoni. 1999. Below-canopy and soil CO2 fluxes in a ponderosa pine forest. Agric. For. Meteor. 94:171–188.

Noborio, K., K.J. McInnes, and J.L. Heilman. 1996. Measurement of soil water content, heat capacity, and thermal conductivity with a singer TDR probe. Soil Sci. 161:22-28.

Norman, J.M., R. Garcia, and S.B.Verma. 1992. Soil surface CO2 fluxes and the carbon budget of a grassland. J. Geophys. Res. Atmos. 97:18845–18853.

Ochsner, T.E., R. Horton, and T. Ren. 2001. Simultaneous water content, bulk density, and air-filled porosity measurements with thermo-time domain reflectometry. Soil Sci. Soc. Am. J. 65:1618-1622.

Ochsner, T.E., R. Horton, G.J. Kluitenberg, and Q. Wang. 2005. Evaluation of the heat pulse ratio method for measuring soil water flux. Soil Sci. Soc Am. J. 69:757-765.

Pumpanen, J., P. Kolari, H. Ilvesniemi, K. Minkkinen, T. Vesala, S. Niinistö, A. Lohila, T. Larmola, M. Morero, M. Pihlatie, I. Janssens, J. C. Yuste, J. M. Grünzweig, S. Reth. J.A. Subke, K. Savage, W. Kutsch, G. Østreng, W. Ziegler, P. Anthoni, A. Lindroth, P. Hari. 2004. Comparison of different chamber techniques for measuring soil CO2 efflux. Agric. For. Meteor. 123:159–176.

Ren, T., G.J. Kluitenberg, and R. Horton. 2000. Determing soil water flux and pore water velocity by a heat pulse technique. Soil Sci.Soc. Am. J. 64:552-560.

Ren, T., K. Noborio, and R. Horton. 1999. Measuring soil water content, electrical conductivity, and thermal properties with a thermo-time domain reflectometry probe. Soil Sci. Soc. Am. J. 63:450-457.

Sakai, M., S.B. Jones, and M. Tuller. 2011. Numerical evaluation of subsurface soil water evaporation derived from sensible heat balance. Water Resour. Res. 47, W02547, doi:10.1029/2010WR009866.

Tang J., D. D. Baldocchi, Y. Qi, and L. Xu. 2003. Assessing soil CO2 efflux using continuous measurements of CO2 profiles in soils with small solid-state sensors. Agric. For. Meteor. 118: 207–220.

Turcu, V.E., S.B. Jones, and D. Or, 2005. Continuous soil carbon dioxide and oxygen meaurements and estimation of gradient-based gaseous flux. Vadose Zone J. 4:1161-1169.

van Bavel, C.H.M, 1961. Lysimetric measurements of evapotranspiration rates in the eastern United States. Soil Sci. Soc. Am. J. 25:138-141.

Wolf, A., S. Nick, A. Kanat, A.J. Douglas, and L. Emilio. 2008. Effects of different eddy covariance correction schemes on energy balance closure and comparisons with the modified Bowen ratio system. Agric. For. Meteorol. 148:942–952.

Zhang, X., S. Lu, J.L. Heitman, R. Horton and T. Ren. 2012. Subsurface soil-water evaporation with an improved heat-pulse probe. Soil Sci. Soc. Am. J. 76: 3: 876-879.

Chapter 2 Sensible heat measurements indicate depth and magnitude of sub-surface soil water evaporation

A paper published in the Water Resources Research

J.L. Heitman, X. Xiao, R. Horton, and T.J. Sauer

Abstract

Most measurement approaches for determining evaporation assume that the latent heat flux originates from the soil surface. Here, a new method is described for determining *in situ* soil water evaporation dynamics from fine-scale measurements of soil temperature and thermal properties with heat-pulse sensors. A sensible heat balance is computed using soil heat flux density at two depths and change in sensible heat storage between; the sensible heat balance residual is attributed to latent heat from evaporation of soil water. Comparisons between near-surface soil heat flux density and Bowen ratio energy balance measurements suggest evaporation originates below the soil surface several days after rainfall. The sensible heat balance accounts for this evaporation dynamic in mm-scale depth increments within the soil. Comparisons of sensible heat balance daily evaporation estimates to Bowen ratio and mass balance estimates indicate strong agreement (r^2 = 0.84, RMSE = 0.24 mm). Potential applications of this technique include location of the depth and magnitude of sub-surface evaporation fluxes, and estimation of Stage 2-3 daily evaporation without requirements for large fetch. These applications represent new contributions to vadose zone hydrology.

Introduction

Soil-water evaporation is a critical component of both the surface energy balance and the hydrologic cycle, coupling heat and water transfer between land and atmosphere [Berge, 1990]. In drying technology [e.g., Segura and Toledo, 2005; Prat 2007], it is widely recognized that control and location of drying (i.e., evaporation) depends on the balance between heat, liquid, and vapor transport mechanisms. Shifts between atmospheric and soil control on evaporation have been commonly referred to in the soil science and hydrology literature as stages of evaporation [Lemon, 1956]. The inability to quantify near-surface soil processes has prevented a detailed, accurate assessment of near-surface soil water evaporation [Kondo et al., 1990; Yamanaka and Yonetani, 1999]. Because the balance of heat, liquid, and vapor mechanisms in soil is difficult to predict, measurement-based approaches are needed to determine dynamic behavior, particularly in the field [e.g., Cahill and Parlange, 1998]. Heitman et al. [2008] introduced a measurement-based soil sensible heat balance to determine the partitioning of latent heat within the soil, and thereby account for soil-water evaporation in situ. Such an approach offers broad potential utility because it does not require determination of coupled heat and water transfer coefficients [e.g., Nassar and Horton, 1997], characterization of soil-specific hydraulic properties [e.g., Mahrt and Pan, 1984; Wetzel and Chang, 1987], or large fetch. Here we present a conceptual background for the soil sensible heat balance method and provide preliminary tests using comparison to both above-ground (Bowen Ratio) and mass-balance (microlysimeter) estimates of evaporation.

Method

Conceptual Background

The surface energy balance is commonly treated as

$$R_n - G = LE + H \tag{1}$$

where R_n (W m^{-2}) is net radiation, G (W m^{-2}) is surface soil heat flux density, and LE (W m^{-2}) and H (W m^{-2}) are latent and sensible heat flux densities, respectively [c.f. *Cellier et al*., 1996]. Widely used calorimetric and combination approaches for determining G rely on measurement of heat flux density below the surface. A correction is then made for change in sensible heat storage, ΔS (W m^{-2}), between the depth of measurement and the surface [Fuchs, 1986].

$$G = G_o + \Delta S \tag{2}$$

where G_o refers to heat flux density measured at some arbitrary sub-surface depth.

Equation (2) assumes that LE originates at the soil surface rather than within the soil [Mayocchi and Bristow, 1995]. This is a restrictive assumption, because as soil dries from the surface downward, an increasing fraction of soil water evaporation occurs below the surface [Yamanaka et al., 1998]. Micrometeorological methods (e.g., Bowen ratio and eddy covariance) account for LE exclusively at the soil surface, but Gardner and Hanks [1966] suggested that (2) could be adjusted to include LE (i.e., evaporation of soil water) in order to determine evaporation occurring within the soil.

$$\left(G_1 - G_2\right) - \Delta S = LE \qquad (3)$$

where G_1 and G_2 are heat flux densities measured at two different depths and ΔS represents the change in sensible heat storage between these depths (Fig. 1). The hypothesis in this approach is that the residual to the balance of measurable sensible heat terms (G_1, G_2, and ΔS) represents heat partitioned to latent heat with water vaporization in the depth interval between G_1 and G_2.

Instrumentation provided a major limitation for Gardner and Hanks [1966] and allowed mostly qualitative assessment. However, development of the heat-pulse (HP) sensor [Campbell et al., 1991; Bristow et al., 1994; Ham and Benson, 2004] provides new opportunity to implement the heat balance approach. HP sensors generally consist of two or three small (1.3-mm diam.) needles. One needle contains a resistance heater for applying a small heat input, while the remaining needles contain thermocouples for measuring temperature response at a fixed distance (typically 6 mm) from the heater. The temperature response can be evaluated to determine soil thermal properties. The temperature sensing needles of the sensor can also be used to passively determine ambient temperature conditions within the soil. Cobos and Baker [2003] and Ochsner et al. [2006] discussed the use of HP sensors to measure G_o, and Ochsner et al. [2007] discussed HP sensor measurement of ΔS. An advantage to this type of sensor is that it is relatively unobtrusive when compared to more commonly used heat flux plates. It doesn’t appreciably limit water vapor or liquid movement and, thus, can be installed nearer the soil surface.

Heitman et al. [2008] expanded on the approaches of Ochsner et al. [2006, 2007] and Cobos and Baker [2003] to implement (3) by measuring heat flux density at two depths (i.e., G_1 and G_2) and ΔS with a single three-needle HP sensor. In their approach, sensors, oriented perpendicular to the soil surface, are used for three functions (Fig. 2): measurement of ambient temperature (T, °C), volumetric heat capacity (C, J m^{-3} $°C^{-1}$), and thermal conductivity (λ, W m^{-1} $°C^{-1}$). Examples of these data (collected as described in the following section) are presented in Fig. 3A and 3B. The vertical T gradient, dT/dz (°C m^{-1}), is obtained by dividing the T difference by the distance, z (m), between adjacent needles (Fig. 3C). The gradient can then be multiplied by λ to approximate the heat flux densities (G_1 and G_2) at the mid-point depths between adjacent needles (i.e., Fourier's Law) (Fig. 3D). The change in T with time, t (s), at the central needle is combined with C to determine ΔS according to [Ochsner et al., 2007]

$$\Delta S = \sum_{i=1}^{N} C_{i,j-1} \frac{T_{i,j} - T_{i,j-1}}{t_j - t_{j-1}} \left(z_i - z_{i-1}\right) \tag{4}$$

where the subscripts *i* and *j* are index variables for depth layers and time steps, respectively (Fig. 3D). For these calculations, we assume a mean thermal property (i.e., *C* and λ) for each sensor depth increment. Having measurements of G_1, G_2, and ΔS allows implementation of (3) to determine *LE*.

Measurements and Field Locations

Measurements were collected at two research sites located near Ames, IA (41° N, 93° W), the Been field and the Brooks field. HP instrumentation at the Been field was installed in May 2007 and operated for 40 d. A bare surface area (approx. 125 m^2) was maintained throughout the study. The soil at the site is Canisteo clay loam (Fine-loamy, mixed, superactive, calcareous, mesic Typic Endoaquolls). In addition to HP sensors (described below), a Bowen ratio energy balance (BREB) measurement station was located 30 m from the north edge of the bare area. The design of this measurement system was similar to those of Bland et al. [1996] and Sauer et al. [2002]. An air temperature/relative humidity probe (Model HMP45C, Vaisala Inc., Woburn, MA) was used to measure vapor pressure while a thermistor circuit was used to measure air temperature. Both sensors were mounted in aspirated radiation shields with a vertical separation of 1 m and were exchanged every 5 min. A second tripod was used to support a net radiometer (Model Q*7, Radiation and Energy Balance Systems, Seattle, WA) at a height of 2 m. Soil heat flux was measured with two flux plates (Model HFT3.1, Radiation and Energy Balance Systems) at a depth of 0.06 m. Soil temperature measured with type T thermocouples at 0.015 and 0.045 m depths adjacent to each plate were used with measured volumetric water content to determine energy storage change above the flux plates [Sauer and Horton, 2006]. All sensor signals were monitored at a 5 s interval and 5 min averages were stored for analysis. The combined suite of instruments on the BREB station provided estimates of R_n, LE, H, and G. A tipping bucket rain gage was used to record rainfall.

Experiments at the Brooks field were conducted for a 40 d measurement period beginning in late July 2005. Soil at the site is Canisteo silty clay loam. A 100 m^2 area selected for study was cleared of all vegetation and surface residue, and leveled. Estimates of soil water evaporation were obtained periodically with microlysimeters

(MLs) [Evett et al., 1995]. The MLs were constructed from 7.5 cm ID, white polyvinyl chloride pipe, cut to 10-cm length and milled to a wall thickness of 3 mm. The MLs were installed with a drop hammer in the area surrounding the instrument nest and not used until several natural wetting/drying cycles had occurred post-installation. For measurements, the MLs were carefully excavated, sealed at the lower end with thin plastic, weighed in the field with a portable balance, and replaced in the soil. Evaporation estimates were determined from the change in mass upon reweighing at 24 h. At least eight replicate MLs were collected and averaged for each measurement.

HP sensors built following the design of Ren et al. [2001] were used at both field sites. The sensors consisted of three stainless steel needles (1.3 mm diam., 4 cm length) fixed approximately 6 mm apart with an epoxy body at one end. Each needle contained a Type E thermocouple for measuring temperature; the central needle also contained a resistance heater for implementing the HP method. The sensors were calibrated in agar stabilized water to determine the apparent distance between the needles [Campbell et al., 1991]. The sensors were installed via a 10 cm deep trench by pushing the needles from the trench into undisturbed soil. The plane formed by the three needles of each sensor was oriented perpendicular to the soil surface (Fig. 2). Sensors were installed at 6 depths beginning immediately below the soil surface with the central needles of the sensors positioned at 6, 12, 18, 24, 45, and 60 mm. After installation, the sensor lead wires were routed through the trench and the trench was carefully backfilled. The sensors were connected to a data acquisition system on the soil surface, which consisted of a datalogger and multiplexers for the thermocouples and heaters, all housed in a weatherproof enclosure. Power was supplied by a 12 V battery maintained with a solar panel. All heaters were controlled and measured with a single control circuit consisting of a relay and 1-Ω precision resistor. Thermal property measurements were collected each 4 h. Thermal diffusivity and C were determined following the procedures described by Bristow et al. [1994] and Knight and Kluitenberg [2004], respectively. Measurements were corrected for ambient T drift using the T measurements collected prior to HP initiation. A time-scaled change in ambient T was subtracted from the T change observed following application of the heat pulse [Jury and Bellantuoni, 1976; Ochsner et al., 2006]. Soil thermal conductivity λ was computed as the product of the thermal diffusivity and C. Thermocouples in each sensor needle were used to record ambient soil T each 30 min (5-min average). Measurements of T, C, and λ were used together as described above to determine LE for a discrete depth increment with each sensor. Heitman et al. [2008] provides additional details on data handling.

Results and Discussion

Evidence of Evaporation Below the Soil Surface

The general hypothesis in the sensible heat balance approach is that evaporation occurs below the soil surface, and therefore, can be determined by measurements within the soil. A limitation in testing this hypothesis is the proximity to the surface in which the upper-most heat flux G_1 can be measured. The practical limit for G_1 with the design of the heat-pulse sensors used in these experiments is approximately 3 mm, which is the mid-point between needles installed immediately at the surface and the adjacent needle positioned at 6 mm below the surface (Fig. 2). This prevents measurement of evaporation occurring above the 3 mm soil depth where it likely occurs in the day(s) immediately following rainfall or irrigation. However, if the evaporation front does penetrate deeper into the soil, it should be discernable. To test this idea we compare heat flux density measured at the 3 mm soil depth in the Been field with measurements obtained from the BREB measurement station (Fig. 4).

Data in Fig. 4 were collected following a rainfall event on day of year (DOY) 172. If evaporation occurs below 3 mm in the soil, then G_1 at the 3 mm depth should be approximately equal to the sum of LE and G as treated in (1) and measured by the BREB station. It is clear that $LE + G$ exceeds G_1 until DOY 176, suggesting that evaporation is occurring above the 3 mm soil depth. However, on DOY 176 G_1 increases and begins to exceed G. The growing peak magnitude of G_1, while still remaining less than $LE + G$, suggests that some but not all evaporation is occurring below the 3 mm depth. DOY 177 provides an anomaly where G_1 actually exceeds $LE + G$. This result is surprising and suggests error in either the BREB station or G_1. While the magnitude of the 3-mm heat flux density is exceptionally large and cannot be confirmed independently, we note that the magnitude of DOY 177 $LE + G$ also differs from the general trend on DOY 176-181. Despite similar conditions on the days before and after, H measured with the BREB on DOY 177 was uncharacteristically large and suggests some measurement error (data not shown). DOY 177 represents a transition to evaporation below the 3 mm depth in the soil. On subsequent days, G_1 decreases and begins to track closely with the magnitude of $LE + G$. The pattern revealed by this comparison indicates that the measurements of near-surface heat flux density accurately depict $LE + G$ following Stage 1 evaporation.

Subsurface Evaporation Patterns

The comparison between $LE + G$ and G_1 suggests that some evaporation is occurring below the 3 mm depth beginning on DOY 176. To quantify this evaporation we utilize measurements for multiple depth increments below the soil surface, where each depth increment includes G_1, G_2, and ΔS measured by a single sensor. These data are shown for the uppermost sensor in Fig. 3. During this time period, daily maximum ambient T generally increases after rainfall through DOY 178 at the 0, 6, and 12 mm depths (Fig. 3A). Drying in the upper portion of the soil profile also produces declines in both C and λ (Fig. 3B). Accompanying these changes are shifts in the magnitude of dT/dz at the 3 and 9 mm depths. The magnitude of dT/dz is similar with depth through DOY 175 (Fig. 3C). On DOY 176, the peak magnitude of dT/dz at 3 mm begins to increase and thereafter remains relatively large. A shift also occurs at 9 mm on DOY 176, but peak magnitudes remain well below those at 3 mm until DOY 178 when the gradients begin to converge. This indicates that drying occurs deeper in the soil. Driven by dT/dz, heat flux density demonstrates a similar pattern (Fig. 3D). The 3 and 9 mm depth heat flux densities are nearly identical through DOY 175. However, beginning on DOY 176, divergence in the heat flux density with depth indicates significant heat loss (> 150 W m^{-2}) as heat is transferred through the soil. The amount of heat partitioned to ΔS can be quantified and remains consistently small throughout this period (< 25 W m^{-2}). The difference between heat flux density at 3 and 9 mm (i.e. G_1 and G_2) appreciably exceeds ΔS through DOY 178 and thereby provides means for determining LE with (3).

Results for sensors measuring the 3-9, 9-15, 15- 21, and 21-27 mm depth increments are shown in Fig. 5. Note that data are presented as evaporation rate, E (mm h^{-1}), rather than LE. To make this conversion we estimate L as a function of T following *Forsythe* [1964].

The evaporation rate remains near 0 for all measured depth increments through DOY 175, which again indicates that the evaporation zone has not passed below the 3 mm soil depth. All sensible heat transferred through the 3 mm depth is accounted for through ΔS or heat flux density at lower depths. On DOY 176, the peak magnitude of E increases to 0.3 and 0.15 mm h^{-1} during the afternoon at the 3-9 and 9-15 mm depth increments, respectively. The peak magnitude of E continues to increase for both depth increments on DOY 177 before declining on subsequent days. Despite some concerns raised above about observations on DOY 177, the pattern here again suggests a transition. Net evaporation rates are generally highest immediately following rainfall, assuming that atmospheric demand is not limiting [Lemon, 1956]. Thus, the relatively lower E on DOY 176 than 177 does not necessarily suggest less total evaporation. Rather it indicates that evaporation is still occurring in the soil layer above the 3 mm depth on DOY 176. Transition to evaporation at deeper soil depths is beginning to occur on DOY 176 as soil water stored above the 3 mm depth is depleted and cannot meet atmospheric demand. After DOY 177, measurements of the 3-mm heat flux density (Fig. 4) suggest that nearly all evaporation occurs below the 3 mm soil depth. The shifting pattern of evaporation continues on subsequent days as soil water storage is further depleted near the surface and peak E at 9-15 mm begins to exceed E at 3-9 mm (Fig. 5). The declining peak magnitudes of E for all depth increments after DOY 177 are indicative of decreased total evaporation as soil water becomes limiting.

Comparison of Heat Balance Daily Evaporation to Independent Estimates

An advantage of the heat balance approach is that it allows observation of *in situ* evaporation for multiple depth increments below the soil surface, whereas other methods such as Bowen ratio and lysimeters only provide indication of total net evaporation. Yet, this also provides some difficulty for verifying the data presented in Fig. 5. Few means are available for temporal comparison to fine-scale soil water evaporation measurements. In order to provide a means for comparison, we take a daily sum of the values from (3) for all measured depth increments to obtain an estimate of total daily evaporation. These estimates are compared to total daily evaporation determined by microlysimmeters at the Brooks field and the Bowen ratio approach at the Been field in Fig. 6. We assume *a priori* that measurements from the heat-pulse sensors do not capture evaporation occurring above the 3 mm soil depth immediately after rainfall as discussed above. Thus, comparisons in Fig. 6 preclude measurements taken in the first 3 d after rainfall.

Daily evaporation estimates from the independent estimates (microlysimeter and Bowen ratio) ranged from 3.29 to 0.57 mm (Fig. 6). Regression analysis indicates strong correlation between the heat-balance and independent estimates with r^2 = 0.96 and RMSE = 0.20 mm for 20 d of measurements. The regression relationship is also near 1:1 with slope of 0.91 and intercept of ~0.16. Treated independently, the relationship between heat-balance and microlysimeter estimates (available on 9 d) gave slightly lower RMSE (0.11 mm). The range of the compared observations from the microlysimeters was limited to < 1.5 mm daily evaporation by environmental conditions during the Brooks field experiment. However, the increased strength of this relationship may indicate the improved accuracy of the method under predominantly water-limited (i.e., soil-controlled) evaporative conditions. Overall, comparisons between heat balance and independent estimates of total daily evaporation indicate the potential of the heat balance method. Though indirect, these comparisons also provide support for the fine time and depth scale measurements of evaporation from which the heat-balance daily estimates were derived.

Summary and Conclusions

Few if any measurement approaches are currently available for determining *in situ* soil water evaporation. However, developments in the HP measurement technique provide a new opportunity to implement such an approach. Here, measurements of soil temperature and thermal properties obtained with HP sensors were used to determine the sensible heat balance below the soil surface. Heat that cannot be accounted for directly by measurement, the residual to the soil sensible heat balance, is attributed to latent heat with evaporation of soil water. Comparisons of measured near-surface heat flux density with $LE + G$ in the traditional surface energy balance indicate that the soil heat flux is partitioned to LE below the surface, particularly several days after rainfall events. Combination of heat flux density measurements at multiple depths below the soil allows the location and magnitude of evaporation to be quantified, thereby revealing the dynamic evolution of soil water evaporation following rainfall events. Initial comparisons between daily estimates of heat balance evaporation compare favorably with standard independent methods for determining daily evaporation. However, unlike standard micro-meteorological methods, large fetch is not a requirement. Because of its capability to measure evaporation with depth and time in field conditions, which is not available through other current approaches, the sensible heat balance method promises to be a practical and valuable addition for a wide range of vadose zone hydrology investigations.

References

Bristow, K.L., G.J. Kluitenberg, and R. Horton. 1994. Measurement of soil thermal properties with a dual-probe heat-pulse technique, Soil Sci. Soc. Am. J. 58:1288-1294.

Berge, H.F.M. 1990. Heat and Water Transfer in Bare Topsoil and the Lower Atmosphere, Centre for Agricultural Publishing and Documentation, Wageningen, the Netherlands.

Bland, W.L., J.T. Loew, and J.M. Norman. 1996. Evaporation from cranberry, Agric. Forest Meteorol. 81:1-12.

Cahill, A.T., and M.B. Parlange.1998. On water vapor transport in field soils, Water Resour. Res. 34:731-739.

Campbell, G.S., C. Calissendorff, and J. H. Williams. 1991. Probe for measuring soil specific heat using a heat-pulse method, Soil Sci. Soc. Am. J. 55:291-293.

Cellier, P., G. Richard, and P. Robin. 1996. Partition of sensible heat fluxes into soil and the atmosphere, Ag. For. Meteor. 82:245-265.

Cobos, D.R., and J.M. Baker. 2003. In situ measurement of soil heat flux with the gradient method, Vados Zone J. 2:589-594.

Evett, S.R., A.W. Warrick, and A.D. Matthias. 1995. Wall material and capping effects on microlysimeter temperatures and evaporation, Soil Sci. Soc. Am. J. 59:329-336.

Forsythe, W.E. 1964. Smithsonian physical tables, Smithsonian Inst. Publ. 4169, Washington, DC.

Fuchs, M. 1986. Heat flux, in Methods of soil analysis, Part 1, Physical and mineralogical methods, 2nd ed, SSSA Book Series no. 5, edited by A. Klute, pp. 957-968, SSSA, Madison, WI.

Gardner, H.R., and R.J. Hanks. 1966. Evaluation of the evaporation zone in soil by measurement of heat flux, Soil Sci. Soc. Am. Proc. 30:425-428.

Ham, J.M., and E.J. Benson. 2004. On the construction of dual-probe heat-capacity sensors, Soil Sci. Soc. Am. J. 68:1185-1190.

Heitman, J.L., R. Horton, T.J. Sauer, and T.M. DeSutter. 2008. Sensible heat observations reveal soil water evaporation dynamics, J. Hydrometeor. 9:165-171.

Jury, W.A., and B. Bellantouni. 1976. A background temperature correction for thermal conductivity probes, Soil Sci. Soc. Am. J. 40:608-610.

Knight, J.H., and G.J. Kluitenberg. 2004. Simplified computational approach for the dual-probe heat-pulse method, Soil Sci. Soc. Am. J. 68:447-449.

Kondo, J., N. Saigusa, and T. Sato. 1990. A parameterization of evaporation from bare soil surfaces, J. Appl. Meteor. 29:385-389.

Lemon, E.R. 1956. The potentialities for decreasing soil moisture evaporation loss, Soil Sci. Soc. Am. Proc. 20:120-125.

Mahrt, L., and H. Pan. 1984. A two-layer model of soil hydrology, Bound. Layer Meteor. 29:1-20.

Mayocchi, C.L., and K.L. Bristow.1995. Soil surface heat flux: Some general questions and comments on measurements, Agric. Forest Meteor. 75:43-50.

Nassar, I.N., and R. Horton. 1997. Heat, water, and solute transfer in unsaturated porous media: I. Theory development and transport coefficient evaluation, Transpor. Porous Media, 27:17-38.

Ochsner, T.E., T.J. Sauer, and R. Horton. 2007. Soil heat capacity and heat storage measurements in energy balance studies, Agron. J. 99:311-319.

Ochsner, T.E., T.J. Sauer, and R. Horton.2006. Field tests of the soil heat flux plate method and some alternatives. Agron. J. 98:1005-1014.

Prat, M. 2007. On the influence of pore shape, contact angle, and film flows on drying of capillary porous media, Int. J. Heat Mass Transfer, 50:1455-1468.

Sauer, T.J., and R. Horton. 2005. Soil heat flux, in Micrometeorology in Agricultural Systems. Agron. Monogr., No. 47, edited by J. L. Hatfield and J. M. Baker, Am. Soc. Agron., Madison, WI.

Sauer, T.J., P.A. Moore, Jr., J.M. Ham, W.L. Bland, J.H. Prueger, and C.P. West 2002. Seasonal water balance of an Ozark hillslope, Agric. Water Manage. 55:71-82.

Segura L.A. and P.G. Toledo. 2005. Pore-level modeling of isothermal drying of pore networks: Effects of gravity and pore shape and size distributions on saturation and transport parameters, Chem. Eng. J. 111:237-252.

Wetzel, P.J., and J.T. Chang. 1987. Concerning the relationship between evapotranspiration and soil moisture. J. Climate Appl. Meteor. 26:18-27.

Yamanaka, T., and T. Yonetani.1999. Dynamics of the evaporation zone in dry sandy soils, J. Hydrol. 217:135-148.

Yamanaka, T., A. Takeda, and J. Shimada. 1998. Evaporation beneath the soil surface: Some observational evidence and numerical experiments, Hydrologic Processes. 12:2193-2203.

Figure Captions

Figure 1. Conceptual model of the heat balance for a soil layer (see Eq. 3). G_1 and G_2 are sensible heat flux density at two depths; ΔS and LE are the change in sensible heat storage and the latent heat flux, respectively.

Figure 2. Heat-pulse sensor measurements for implementing Eq. (3). Temperature, temperature gradient, volumetric heat capacity, and thermal conductivity are represented as T, dT/dz, C, and λ, respectively. The sensor is not drawn to scale.

Figure 3. Measurements obtained with a heat-pulse sensor for computing Eq. (3): A. soil temperature (T), B. volumetric heat capacity (C) and thermal conductivity (λ), C. temperature gradient (dT/dz), and D. heat flux densities (G_1 and G_2) and change in sensible heat storage (ΔS). Data were collected from the Been field following rainfall on day of year 172.

Figure 4. Comparison of heat-pulse measured heat flux density for the 3-mm soil depth (G_1) and independent measurements of latent heat flux density (LE) and surface soil heat flux (G) obtained with the Bowen ratio energy balance measurement station at the Been Field.

Figure 5. Evaporation determined by heat balance (Eq. 3) using heat-pulse sensors. Data were collected from the Been Field following rainfall on day of year 172.

Figure 6. Comparison of daily evaporation obtained by the heat balance and two independent methods (Bowen ratio and microlysimeters). Data included in the figure

were obtained 3 or more days after rainfall events. Data from DOY 177 at the Been field have been omitted.

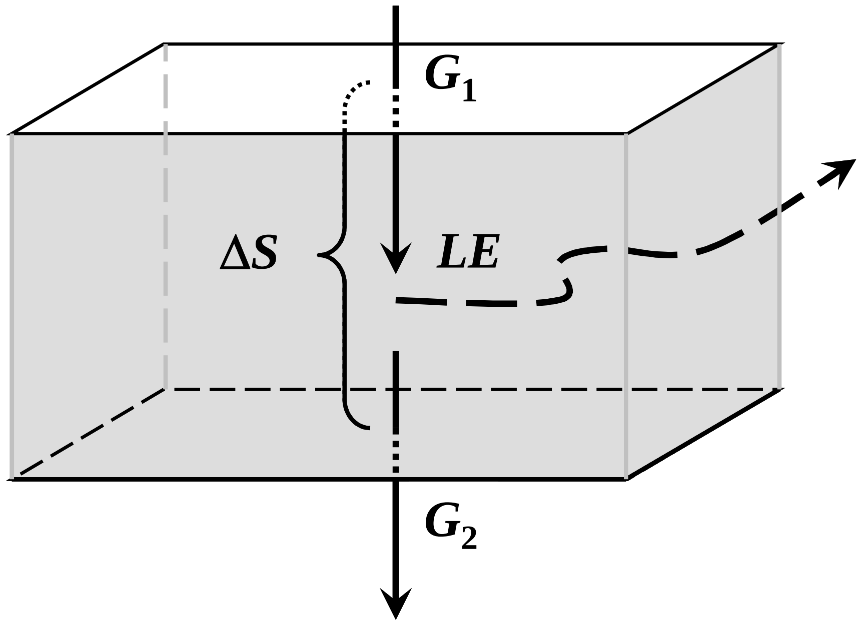

Figure 1. Conceptual model of the heat balance for a soil layer (see Eq. 3). G_1 and G_2 are sensible heat flux density at two depths; ΔS and LE are the change in sensible heat storage and the latent heat flux, respectively.

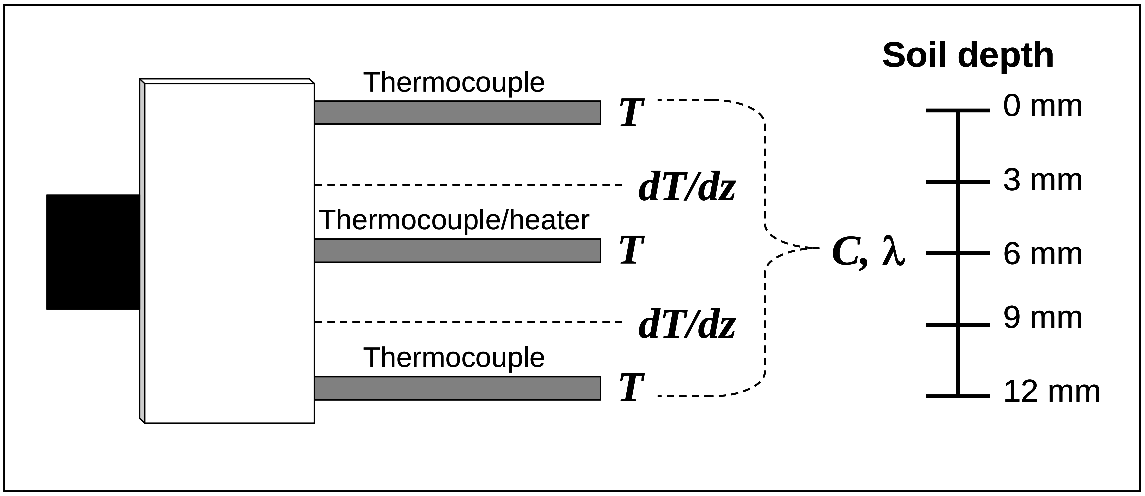

Figure 2. Heat-pulse sensor measurements for implementing Eq. (3). Temperature, temperature gradient, volumetric heat capacity, and thermal conductivity are represented as *T*, *dT*/*dz*, *C*, and λ, respectively. The sensor is not drawn to scale.

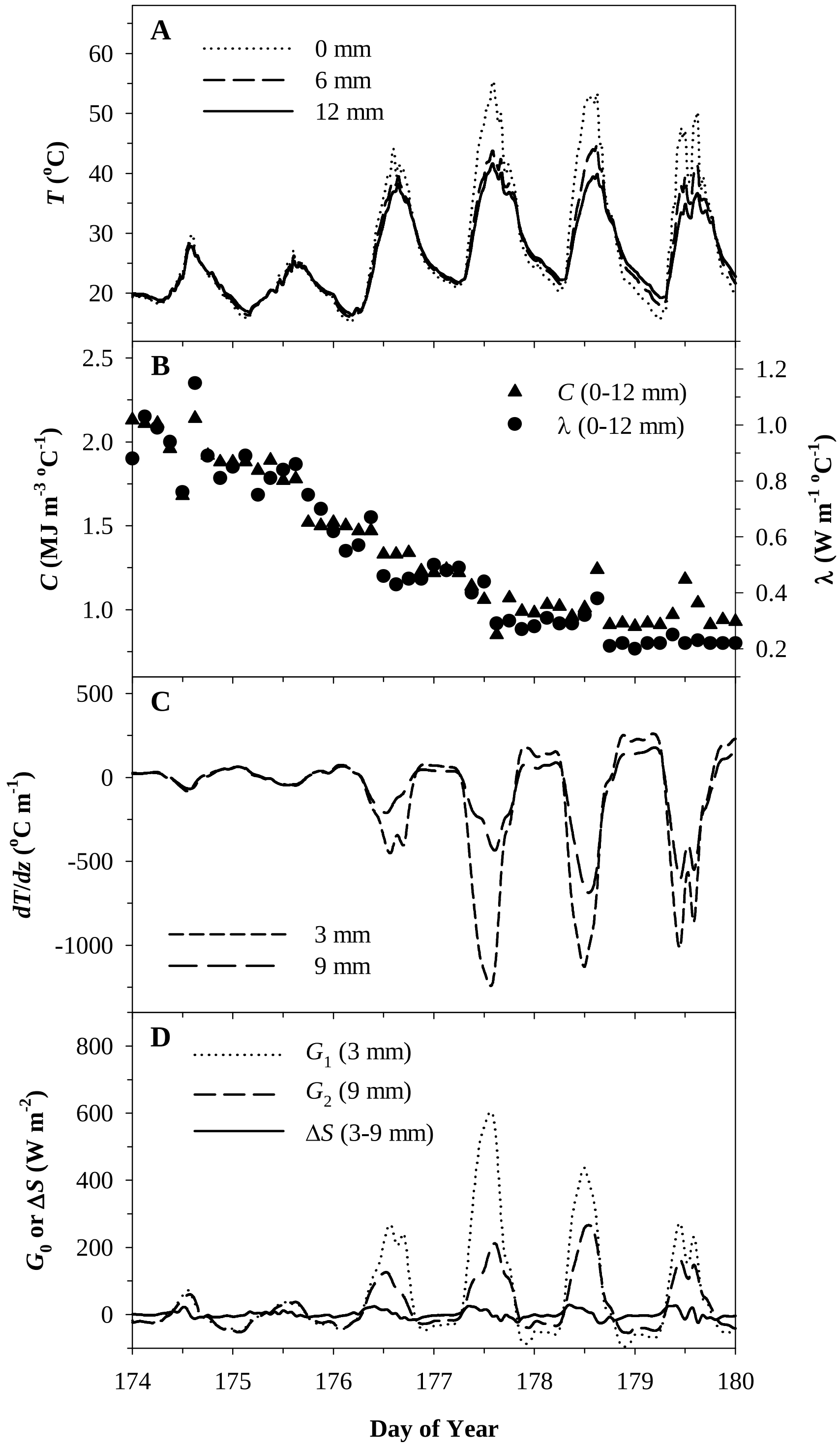

Figure 3. Measurements obtained with a heat-pulse sensor for computing Eq. (3): A. soil temperature (T), B. volumetric heat capacity (C) and thermal conductivity (λ), C.

temperature gradient (dT/dz), and D. heat flux densities (G_1 and G_2) and change in sensible heat storage (ΔS). Data were collected from the Been field following rainfall on day of year 172.

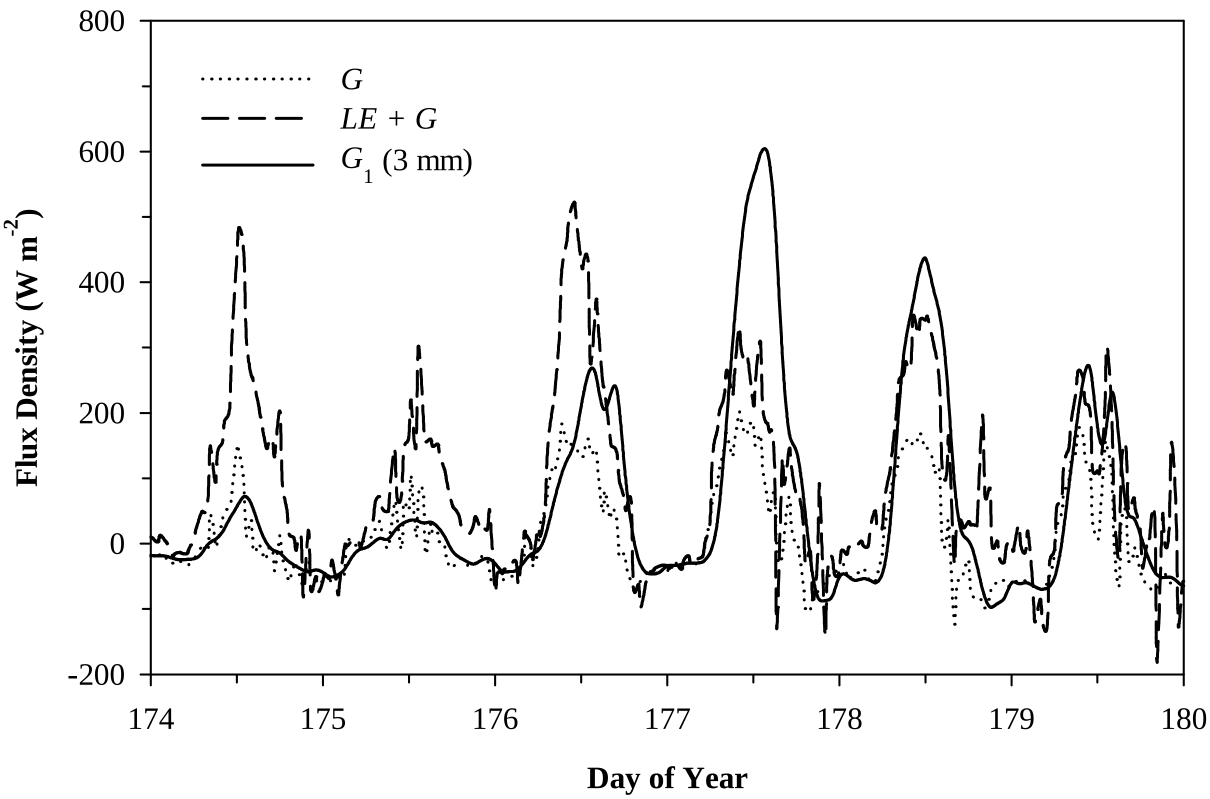

Figure 4. Comparison of heat-pulse measured heat flux density for the 3-mm soil depth (G_1) and independent measurements of latent heat flux density (*LE*) and surface soil heat flux (*G*) obtained with the Bowen ratio energy balance measurement station at the Been Field.

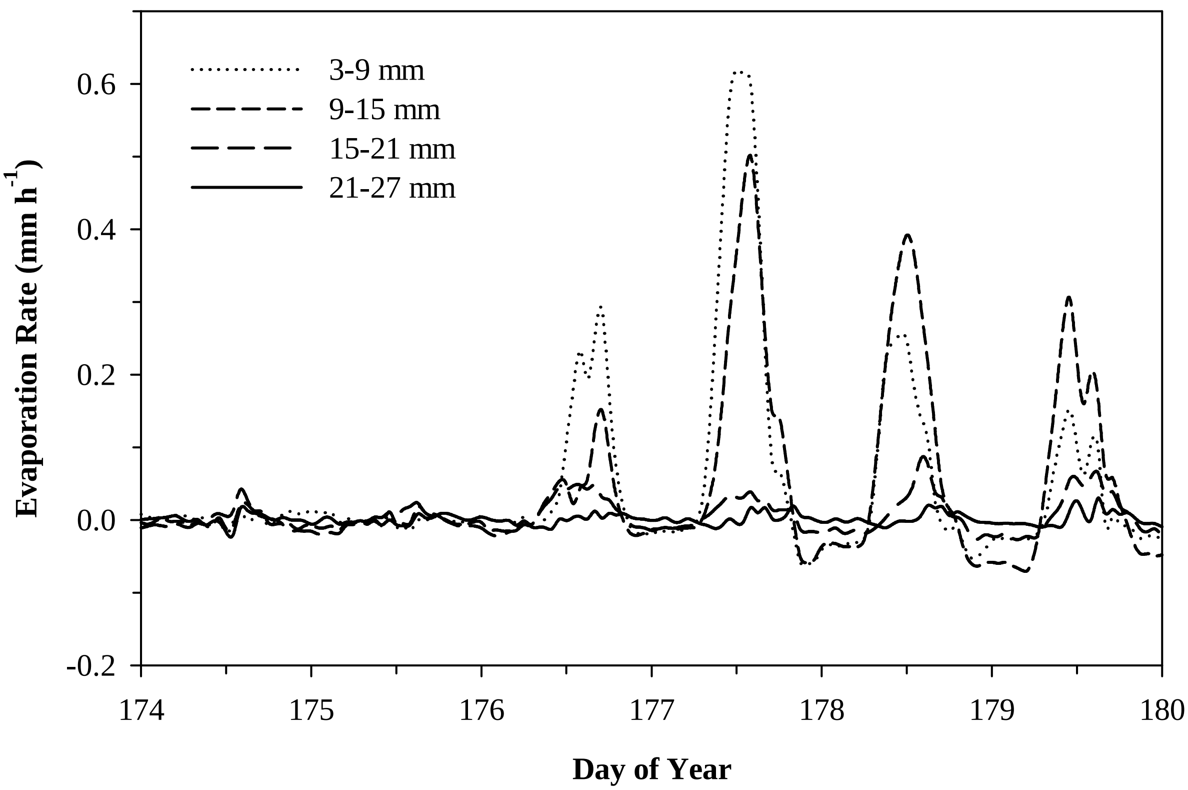

Figure 5. Evaporation determined by heat balance (Eq. 3) using heat-pulse sensors. Data were collected from the Been Field following rainfall on day of year 172.

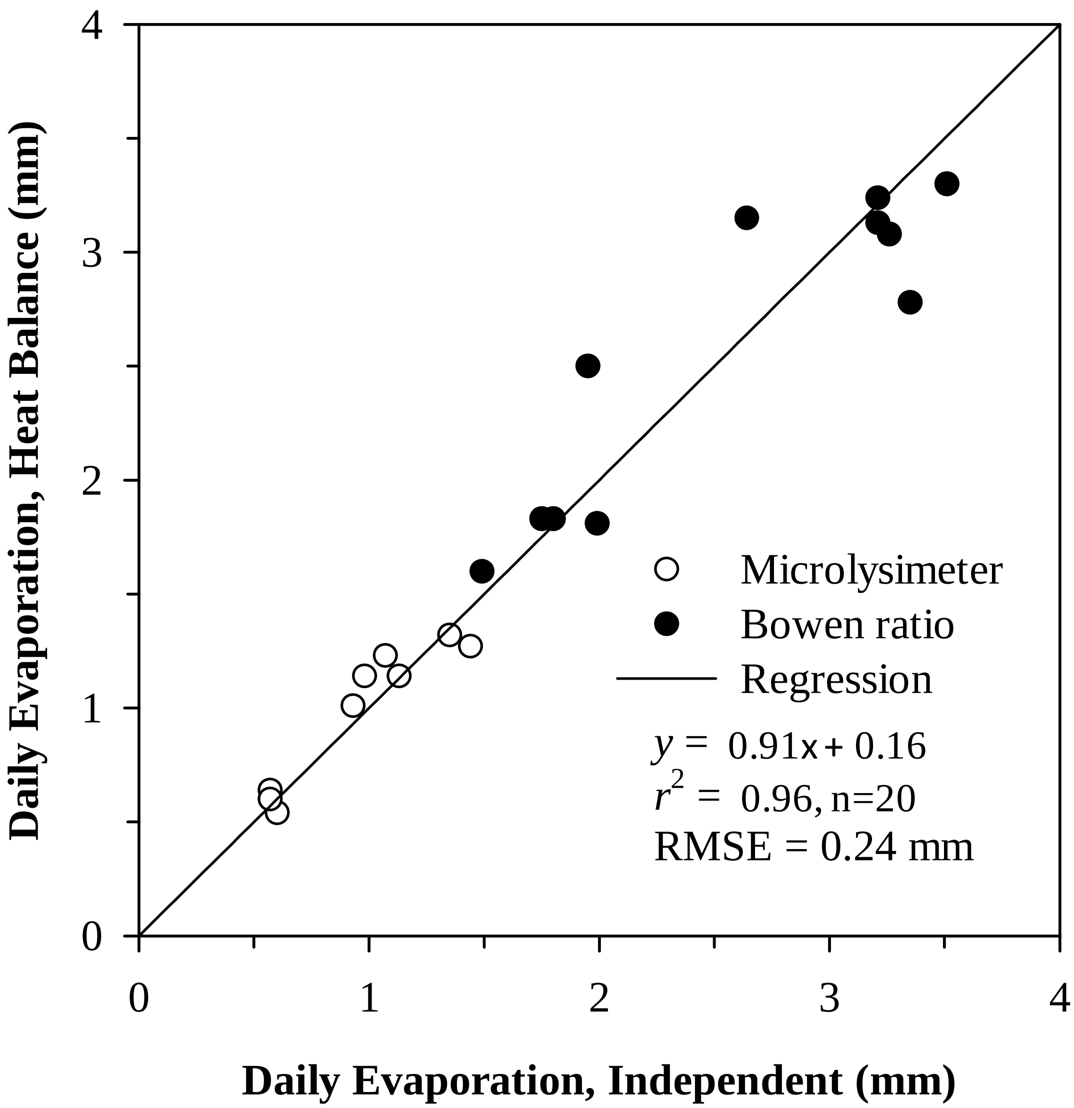

Figure 6. Comparison of daily evaporation obtained by the heat balance and two independent methods (Bowen ratio and microlysimeters). Data included in the figure were obtained 3 or more days after rainfall events. Data from DOY 177 at the Been field have been omitted.

Chapter 3 Cumulative soil water evaporation as a function of depth and time

A paper published in the Vadose Zone Journal

X. Xiao, R. Horton, T.J. Sauer, J.L. Heitman and T. Ren

Abstract

Soil water evaporation is an important component of the surface water balance and the surface energy balance. Accurate and dynamic measurements of soil water evaporation enhance the understanding of water and energy partitioning at the land-atmosphere interface. The objective of this study is to measure the cumulative soil water evaporation with time and depth in a bare field. Cumulative water evaporation at the soil surface was measured by the Bowen ratio method. Subsurface cumulative soil water evaporation was determined with the heat pulse method at fine scale depth increments. Following rainfall, the subsurface cumulative evaporation curves followed a pattern similar to the surface cumulative evaporation curve, with approximately a 2-d lag before evaporation was indicated at the 3 and 9 mm soil depths, and several more days delay in deeper soil layers. For a 21-d period in 2007, the cumulative evaporation totals at soil depths of 0, 3, 9, 15 and 21 mm were 60, 44, 29, 13, and 8 mm, respectively. For a 16-d period in 2008, the cumulative evaporation totals at soil depths of 0, 3, 9, 15, and 21 mm were 32, 25, 16, 10, and 5 mm, respectively. Cumulative evaporation results from the Bowen ratio and heat pulse methods indicated a consistent dynamic pattern for surface and subsurface water evaporation with both time and depth. These findings suggest that heat pulse sensors can accurately measure subsurface soil water evaporation over several wetting-drying cycles.

Introduction

As a key component of both the surface water balance and the surface energy balance, soil water evaporation impacts water and energy distributions at the land-atmosphere interface. Soil water evaporation is a dynamic process. However, many scientists have divided the process into three major stages (Hide, 1954; Lemon, 1956; Idso et al, 1974). The first stage is evaporation at the wet soil surface being controlled by atmospheric demand; the second stage is evaporation extending from the drying surface to subsurface soil being controlled by upward water movement toward the soil surface; and the third stage is evaporation occurring below the surface where water vapor must diffuse through a dry surface layer to the atmosphere. The techniques for measuring soil water evaporation include energy balance (micrometeorology) and water balance approaches (Hanks and Ashcroft, 1980; Hillel, 1980). Bowen ratio (Fritschen and Fritschen, 2005) and eddy covariance (Meyers and Baldocchi, 2005; Moncrieff et al., 1997) are widely used micrometeorological methods for estimating surface soil water evaporation over an adequate fetch area. The automatic weighing lysimeter method (van Bavel, 1961; Robins, 1965; Tanner, 1967), the manual weighing micro-lysimeter method (Boast and Roberson, 1982), and the soil water depletion method (Böhm et al., 1977) are established ways to determine evaporation by measuring changes in soil water storage and other components of the water balance. However, none of the methods can accurately measure dynamic soil water evaporation with time and depth in the field, especially at shallow depths near the soil surface. The reason they cannot measure soil water evaporation with depth and time is because they do not measure the mm-scale soil water moving up to the zone of evaporation. Based on sensible heat balance theory, Gardner and Hanks (1966), Heitman et al. (2008a, 2008b) developed a new heat pulse method to measure subsurface (3-mm depth and below) soil water evaporation with time at fine-scale depth increments in a bare field over an hourly time period. They reported that daily soil water evaporation from the heat pulse method agreed with Bowen ratio and micro-lysimeter results. However, comparisons of soil water evaporation among the three methods have been limited to daily evaporation for a few discrete days. It is not yet known if the heat pulse method can be used to accurately measure evaporation with depth and time over an entire drying period following a rainfall event. There is a need to evaluate the ability of the heat pulse method to estimate soil water evaporation over consecutive days that represent wetting-drying sequences.

The objective of this study is to measure the surface and subsurface cumulative soil water evaporation with depth and time in a bare field including wetting-drying sequences. The cumulative evaporation from the soil surface is measured with the Bowen ratio method. The subsurface cumulative soil water evaporation is determined at fine scale depth increments with the heat pulse method. The cumulative evaporation measurements are used to examine the development of a soil water evaporation zone with time and depth for natural wetting-drying processes in a bare field.

Materials and Methods

Experiment location description

The study was performed during the summers of 2007 and 2008 in a bare field (125 m × 125 m) located near Ames, Iowa (41.98°N, 93.68°W). The soil at the site was Canisteo clay loam (fine-loamy, mixed, superactive, calcareous, mesic Typic

Endoaquolls). The surface soil bulk density was 1.15 Mg m^{-3}. The soil consisted of 44% sand, 30% silt and 26% clay, and the topography was relatively flat (slope < 2%). This field was tilled each year and kept bare by spraying herbicides for weed control. Three-needle heat pulse sensors were installed to measure subsurface cumulative soil water evaporation at several depth increments. About 20 m away from the heat pulse sensors, a Bowen ratio energy balance (BREB) measurement system was installed in this bare field to measure surface cumulative soil water evaporation. The BREB system was positioned toward the northeast part of the field in order to optimize the fetch for the prevailing southwesterly winds. This provided fetch of approximately 100 m to the south, 130 m to the southwest, and 90 m to the west. The lower sensor was at 25 cm (top at 125 cm). Thus, fetch to upper sensor height ratios were approximately 80:1, 104:1, and 72:1 for wind from the south, southwest, and west, respectively.

Instrument description and installation

Heat pulse sensors used in this study are identical to those used by Ren et al. (2003) and Heitman et al. (2008a, 2008b), which consisted of three parallel stainless steel needles (1.3-mm diameter, 40-mm length) with about 6 mm spacing between the needles. Each needle contained a chromel–constantan thermocouple for measuring temperature. In the middle needle there was also a resistance heater wire, through which a small current could be applied to generate a heat pulse, leading to temperature increases at the outer needles. The distances between neighboring needles were determined from heat pulse measurements made in agar-stabilized water (6 g L^{-1}) before experiments (Campbell et al., 1991).

Ten sensors at each of two locations were installed in the bare field each year, to measure in situ subsurface cumulative soil water evaporation at several depths (Fig. 1). The two locations were within 20 m of each other. At each location a narrow trench was dug, and the sensors were inserted at multiple depths into the undisturbed 0 to 40 mm soil layer. Heitman et al. (2008a and 2008b) reported that evaporation was not detected at depths below 30 mm. The trench was carefully back filled with soil. The heat pulse sensors were installed individually in 2007. To improve the accuracy of sensor placement depths, three sensors were glued together before installation in 2008. The thermocouples and heater wires of the heat pulse sensors were connected to multiplexers (AM16/32 and AM416, Campbell Scientific, Inc., Logan, UT), which were controlled by a Campbell CR10X data-logger. On the data-logger, the thermocouple reference was connected to single-ended channel 1 (1H), excitation channel 3 (E3) and analog ground (AG). The data-logger was powered by a 12-volt battery, which was recharged by a solar panel. Soil thermal diffusivity and volumetric heat capacity measurements were performed every 4 h. The measurement sequence for each heat pulse sensor consisted of 30 s background temperature measurement, 8 s heating duration at the middle needle, and 72 s temperature measurements after heating. So the temperature response of a total time of 110 s with a 2-Hz sensing interval at the two outer needles and the power applied to the middle needle during the 8 s heating period were recorded in the sequence. The 30 s background temperatures were used to correct for temperature drift (Ochsner et al., 2006). In addition, ambient soil temperature at each needle position was measured and recorded every 1-h.

The BREB system used in this study was the same as that of Heitman et al. (2008b), and was similar to those of Bland et al. (1996) and Sauer et al. (2002). On a tripod, two air temperature/relative humidity probes (Model HMP45C, Vaisala Inc., Woburn, MA) with thermistor circuits were installed to measure vapor pressure and air temperature. The sensors were mounted in aspirated radiation shields with a vertical separation of 1 m. Sensor elevation positions were exchanged every 5 min. On another tripod, a net radiometer (Model Q*7, Radiation and Energy Balance Systems (REBR), Seattle, WA) was installed at a height of 2 m. Soil heat flux was measured with two heat flux plates (Model HFT3.1, REBR) at a depth of 60 mm. Soil temperatures at 15-and 45-mm depths, adjacent to each plate, were measured with type T (copper-constantan) thermocouples. The measured soil temperature and estimated volumetric soil water content were used to determine energy storage changes in soil above the flux plates (Sauer and Horton, 2005). All of the sensors were connected to a Campbell CR500 data-logger, and data were collected at a 5-s interval and the 5-min averages computed. The BREB system provided estimates of net radiation, latent heat flux, sensible heat flux and soil heat flux. A tipping bucket rain gage was used to record rainfall.

Basic theory of heat pulse method

The theory for measuring soil water evaporation is based upon the sensible heat balance of a soil layer (Gardner and Hanks, 1966; Heitman et al., 2008a and 2008b). A heat pulse sensor can be used to measure the sensible heat balance terms, for a soil layer, e.g., sensible heat in, sensible heat out and change in sensible heat storage (Fig. 2).

$$\left(H_u - H_l\right) - \Delta S = LE \qquad [1]$$

where H_u and H_l are soil sensible heat fluxes (W m^{-2}) at upper and lower boundaries, respectively, of a specified soil layer; ΔS (W m^{-2}) is the change in sensible heat storage of the soil layer; L (J m^{-3}) is the volumetric latent heat of vaporization and E is evaporation rate (m s^{-1}). For a specific soil layer, we assume that the difference between the net sensible heat transferred and the change in sensible heat storage is equal to the latent heat. If the difference is positive, then some of the soil layer sensible heat is being partitioned to latent heat indicating that some of the water in the soil layer is evaporating. If the difference is zero, then all of the soil layer sensible heat is accounted for indicating that no water is evaporating and no water is condensing in the soil layer. If the difference is negative, then some of the soil layer sensible heat must be deriving from latent heat as water vapor condenses and latent heat becomes sensible heat in the soil layer. Heat pulse measurements in conjuction with Eq. (1) are used to calculate soil water evaporation, similar to the approach presented by Heitman et al. (2008a, 2008b).

The temperature response with time at the outer needles of a heat pulse sensor to the heat pulse from the middle needle was used to determine soil thermal diffusivity and soil volumetric heat capacity.

Soil thermal diffusivity (α, m^2 s^{-1}) was computed as (Bristow et al., 1994):

$$\alpha = \frac{r^2}{4t_m}\left(\frac{t_0}{t_m - t_0}\right) / \left[\ln\left(\frac{t_0}{t_m - t_0}\right)\right] \qquad [2]$$

where for a given sensor, r (m) is the spacing between the middle and outer needle, t_0 is the heating duration (8 s), and t_m (s) is the time from the beginning of heating to when the maximum temperature occurred. Thermal diffusivities for soil between the middle needle and the upper needle (α_u) and for soil between the middle needle and the lower needle

(α_l) were obtained from the outer needle temperature responses to middle needle heat inputs for each heat pulse sensor.

Soil volumetric heat capacity (C, J m^{-3} °C^{-1}) was computed using the following equation (Knight and Kluitenberg, 2004):

$$C = \frac{q' t_0}{e\pi r^2 T_m}\left(1 - \frac{1}{24}\varepsilon^2 - \frac{1}{24}\varepsilon^3 - \frac{5}{128}\varepsilon^4 - \frac{1}{192}\varepsilon^5\right) \qquad [3]$$

where T_m is the maximum temperature increase (°C), q' the applied heating power per unit length of heater (W m^{-1}), and ε the ratio of heating duration to the time corresponding to the maximum temperature increase ($\varepsilon = t_0 / t_m$). The soil volumetric heat capacities for soil between the middle needle and the upper needle (C_u) and for soil between the middle needle and the lower needle (C_l) were obtained from the outer needle temperature responses to middle needle heat inputs for each heat pulse sensor.

Accordingly, soil thermal conductivities (W m^{-1} °C^{-1}) from the middle needle to the upper needle (λ_u) and from the middle needle to the lower needle (λ_l) were computed as the product of α and C:

$$\lambda_u = \alpha_u C_u \ , \qquad \lambda_l = \alpha_l C_l \qquad [4]$$

The temperature gradients (°C m^{-1}) dT_u/dz_u and dT_l/dz_l at soil layer boundaries were determined from the measured ambient temperatures (T_1, T_2, T_3, °C) and the calibrated distances (or depths; z, m) between the needles. Using λ_u and λ_l together with thermal gradients, the sensible heat fluxes (W m^{-2}), H_u and H_l , at the mid-depths of the adjacent needles were calculated with Fourier's law,

$$H_u = -\lambda_u \frac{dT_u}{dz_u}, \qquad\qquad H_l = -\lambda_l \frac{dT_l}{dz_l} \qquad [5]$$

The change of sensible heat storage ΔS was calculated from the value of C (C was the average of C_u and C_l) and the middle needle temperature changes with time ($\Delta T_2/\Delta t$, °C s^{-1}) for a given soil layer with thickness, Δz (m) (Ochsner et al. 2007):

$$\Delta S = C \; \frac{\Delta T_2}{\Delta t} \Delta z \qquad [6]$$

Latent heat of vaporization L for a given soil layer was calculated as a function of the middle needle temperature T_2 (Forsythe 1964)

$$L = 2.49463 \times 10^9 - 2.247 \times 10^6 T_2 \qquad [7]$$

Soil thermal properties were calculated using Eqs. [2-4], and sensible heat fluxes, changes in sensible heat storage, and latent heat distributions were calculated using Eqs. [5-7]. Soil water evaporation rates were determined using Eq. [1]. In 2007 individual heat pulse sensors were installed in the soil to determine soil water evaporation rates in the 3-9, 9-15, 15-21, 21-27 mm soil layers (see Fig. 3). In 2007, the soil water evaporation was calculated for each separate sensor. In 2008, in order to improve sensor depth accuracy, the heat pulse sensors were glued together before field installation. The 2008 heat pulse sensors were used to determine the soil water evaporation rates in the 3-9, 9-15, 15-21, 21-27 mm soil layers (see Fig. 3). Heat pulse measurements represented identical soil layers in 2007 and 2008. Reported values of evaporation for each soil layer represent the average of replicated heat pulse measurements.

Evaporation rates are integrated over time to determine cumulative evaporation for specific depths. The cumulative evaporation at a specific depth is the sum of evaporation rates for all of the soil layers below that depth, integrated in time. For example, the evaporation rate at the 3-mm depth is the sum of evaporation from the 3-9, 9-15, 15-21 and 21-27 mm soil layers, and the cumulative evaporation is determined by integrating the evaporation rates over time.

Results

Cumulative soil water evaporation with depth and time

We obtained consecutive measurements for 21-d in 2007 and for 16-d in 2008. Figure 4 shows the volumetric soil water content (m^3 m^{-3}) for the 0-60 mm soil layer, the daily net radiation (MJ m^{-2}), the net cumulative evaporation (mm) at 0-, 3-, 9-, 15-, and 21-mm soil depths, and the daily rainfall (mm) for the 2007 measurement period. Water content for the 0-60 mm soil layer represents the average water content of several soil layers measured by the heat pulse sensors. Since all of the measurements were made in a bare field, the cumulative evaporation from the Bowen ratio measurements included the net soil water evaporation occurring at and below the soil surface (0-mm depth). The cumulative evaporations at 3-, 9-, 15- and 21-mm soil depths were measured by heat pulse sensors. During the measurement period, there were two rainfall events, day of year (DOY) 172 through 173 and DOY 190.

Surface cumulative evaporation from the Bowen ratio method increased continuously over the 21-d measurement period. Following the first rainfall event (20-mm) on DOY 172 through DOY 173, cumulative evaporation at subsurface depths did not increase for

2 days. On the third day (DOY 176), the cumulative evaporation curve at the 3-mm depth began to increase. One day later, the cumulative evaporation curve at the 3-mm depth began to parallel the surface cumulative evaporation curve until the next rainfall event on DOY 190. The cumulative evaporation curves at the 9-, 15-, and 21-mm depths behaved similarly to the curve at the 3-mm depth, with a time lag of one day at the 9-mm depth and several days at the 15- and 21-mm depths. Cumulative evaporation curves at the various soil depths indicated the development of soil water evaporation zones with time and depth following a natural drying process in the bare field. In wet soil, soil water evaporation occurred at the soil surface and from the surface to a depth of 3-mm within two days after the rainfall event (i.e., first stage evaporation). The zone of evaporation shifted downward to the 3- and 9-mm soil depths several days later, and even later to the 15- and 21-mm soil depths (i.e., second and third stages of evaporation). Our results indicate that following rainfall, soil water evaporation is a continuous process not necessarily identified as having three separate stages.

In the summer of 2008, three rainfall events occurred in a 16-d period: DOY 240 through 241, DOY 248 through 249, and DOY 252 (Fig. 5). Surface cumulative evaporation from the Bowen ratio method increased continuously throughout the measurement period.

Following the first rainfall event (21 mm) on DOY 240 through DOY 241, cumulative evaporation at depths of 3, 9, 15, and 21 mm, with a time-lag pattern similar to the results from 2007, increased with time until the start of the second rainfall event (DOY 248). After DOY 243, the cumulative evaporation curve for the 3-mm depth began to parallel the surface cumulative evaporation curve until the second rainfall event from DOY 248 through 249. The cumulative evaporation curve of the 9-mm depth was further delayed to DOY 244 before it began to parallel the cumulative evaporation curves of the soil surface and 3-mm depth. The cumulative evaporation curves of the 15-and 21-mm depths behaved similarly, with only a few days delay. Since there were only two days between the second and the third rainfall events, no obvious increase in subsurface cumulative evaporation curves was noticed following the second rainfall event, indicating that the depth of evaporation shifted back to the soil surface. Similar to 2007, the cumulative evaporation at various soil depths in 2008 indicated the development of a soil water evaporation zone with time and depth. When the soil was wet following a rainfall, evaporation occurred first at the soil surface and then advanced from the surface to the shallow subsurface. When the soil surface started to dry, the evaporation zone shifted downward.

Cumulative evaporation curves from the soil surface for the Bowen ratio measurements and the subsurface from the heat pulse measurements were consistent from year to year and depth to depth, in both magnitude and time. This finding is particularly interesting because the measurement scales for Bowen ratio and heat pulse methods differ considerably. Although both involve one-dimensional approximations, the Bowen ratio measurements occur above the ground surface and may be influenced by a land area of several hundred square meters, while the heat pulse sensors are buried below the soil surface and are influenced by the surrounding soil at mm- to cm-scale. The data obtained from the independent techniques of different scales is surprising consistent for 2007 and 2008. For a 21-d period in 2007, the subsurface cumulative evaporation at soil depths of 3, 9, 15 and 21 mm from the heat pulse method was 44, 29, 13, and 8 mm, accounting for

73%, 48%, 21% and 13%, respectively, of the Bowen ratio surface cumulative evaporation (60 mm). For a 16-d period in 2008, the subsurface cumulative evaporation at soil depths of 3-, 9-, 15- and 21-mm was 25-, 16-, 10-, and 5-mm from the heat pulse method, accounting for 74%, 50%, 30% and 16%, respectively, of the Bowen ratio result (32 mm). In both years, the results showed that the rate of cumulative evaporation decreased gradually from shallow to deeper soil.

Comparison between years

The 2007 and 2008 measurement periods had similar amounts of rainfall (21 mm in 2007 and 22 mm in 2008). In the same bare field, however, the development of the soil water evaporation from the soil surface to the subsurface occurred differently in 2007 and 2008. Part of the difference was associated with the temporal distribution of the rainfall and net radiation, and part was due to the differences in initial soil water content. Other weather factors (such as air temperature and wind speed) were similar during the two measurement periods (data not shown).

For soil water evaporation, soil water is the source of water and net radiation is the main energy available for evaporation. In the days following rainfall events, initial soil water content and net radiation at the soil surface differed significantly between 2007 and 2008 (Figs 4. 5). The initial water contents of the 0-60 mm soil layers were about 0.21 (m^3m^{-3}) and 0.17 (m^3m^{-3}) prior to the first rainfall events in 2007 and 2008, respectively. The difference in initial soil water content was caused by the difference in timing and amount of rainfall prior to the first measurement period-rainfall event. The greater initial soil water content in 2007 than that in 2008 was likely part of the reason for the larger evaporation rate in 2007 than in 2008. The mean daily surface evaporation for 7 days following the initial rainfall event was 2.8 mm in 2007 and 1.6 mm in 2008.

The first rainfall event in 2007 was 20 mm on DOY 172 through 173, and the daily net radiation totals for the following two days (DOY 174 and 175) were 9.5 and 4.5 MJ m^{-2}. The first rainfall event in 2008 was 22 mm on DOY 240 through 241, and the daily net radiation totals the following two days (242 and 243) were 11.5 and 9.9 MJ m^{-2}, respectively. For the days following rainfall, the daily total net radiation was larger in 2008 than in 2007. Following the first rainfall event in 2007, there was almost no subsurface cumulative evaporation increase for the two days (174 and 175). Cumulative evaporation began to increase on DOY 176 at the 3-mm depth. In 2008, however, subsurface cumulative evaporation showed some increase shortly after the rain. These data indicate that net radiation affects the time lag of evaporation shifting from the surface to the subsurface following a rainfall event, which is physically consistent with more energy available for depletion (evaporation) of soil water.

Additional future data observations may lead to the development of a quantitative expression of the time series of soil water evaporation following rainfall.

Conclusions

Bowen ratio and heat pulse measurements of cumulative water evaporation from bare soil were consistent in magnitude and time. The cumulative evaporation clearly followed rainfall events with the zone of soil water evaporation shifting from the surface downwards. Cumulative evaporation over time showed the development of a soil water evaporation zone, revealing the time and depth dynamics of bare-field evaporation. The rates and the time lag of evaporation with depth were influenced by initial water content and net radiation. The heat pulse method enabled the determination of cumulative evaporation over consecutive days and wetting-drying periods, and the heat pulse cumulative evaporation values were consistent with the Bowen ratio results.

Acknowledgments

This work was supported by the National Science Foundation under Grant 0809656, by ConocoPhillips Company, by the Chinese Academy of Sciences Visiting Professorship for Senior International Scientists (Grant Number 2009Z2-37),and by Hatch Act, State of Iowa, and State of North Carolina funds. We gratefully acknowledge Dr. Sally Logsdon for providing the soil texture data.

References

Bland, W.L., J.T. Loew and J. M.Norman. 1996. Evaporation from cranberry. Agric. For. Meteorol. 81:1– 12.

Boast, C.W. and T.M. Roberson. 1982. A “Micro-lysimeter” method for determining evaporation from bare soil: description and laboratory evaluation. Soil Sci. Soc. Am. J. 46:689-696.

Böhm, W., H. Maduakor and H.M. Taylor. 1977. Comparison of five methods for characterizing soybean rooting density and development. Agron. J. 69:415–419.

Bristow, K.L., G.J. Kluitenberg and R. Horton, 1994. Measurement of soil thermal properties with a dual-probe heat-pulse technique. Soil Sci. Soc. Am. J. 58:1288-1294.

Campbell, G.S., C. Calissendorff and J. H. Williams. 1991. Probe for measuring soil specific heat using a heat-pulse method, Soil Sci. Soc. Amer. J. 55:291-293.

Forsythe, W.E. 1964. Smithsonian Physical Tables. Smithsonian Inst. Publ. 4169. Washington, DC, USA.

Fritschen, L.J. and C.L. Fritschen. 2005. Bowen ratio energy balance method. *In* J.L.Hatfield and J.M. Baker (eds.) Micrometeorology in Agricultural Systems. Agron. Monogr., Am. Soc. Agron. 47:397-405.

Gardner, H.R. and R.J. Hanks. 1966. Evaluation of the evaporation zone in soil by measurement of heat flux. Soil Sci. Soc. Am. J. 30:425– 428.

Hanks, R.J. and G.L. Ashcroft. 1980. Applied Soil Physics. Springer Verlag, New York.

Heitman, J.L., R. Horton, T.J. Sauer and T.M. DeSutter. 2008a. Sensible heat observations reveal soil water evaporation dynamics. J. Hydrometeor. 9:165-171.

Heitman, J.L., X. Xiao, R. Horton and T.J. Sauer. 2008b. Sensible heat measurements indicating depth and magnitude of subsurface soil water evaporation. Water Resour. Res., 44, W00D05.

Hide, J.C., 1954. Observations on factors influencing the evaporation of soil moisture. Soil Sci. Soc. Am. J. 18:234-239.

Hillel, D. 1980. Introduction to Soil Physics, Academic Press, London.

Idso, S.B., R. J. Reginato, R.D. Jackson, B.A. Kimball and F.S. Nakayamaz. 1974. The three stages of drying of a field soil. Soil Sci. Soc. Am. J. 38:831-837.

Knight, J.H. and G.J. Kluitenberg. 2004. Simplified computational approach for the dual-probe heat-pulse method. Soil Sci. Soc. Am. J. 68:447-449.

Lemon, E.R. 1956. The potentialities for decreasing soil moisture evaporation loss. Soil Sci. Soc. Am. J. 20:120-125.

Meyers, T.P. and D.D. Baldocchi. 2005. Current micrometeorological flux methodologies with applications in agriculture. *In*: J. L. Hatfield and J. M. Baker (ed.) Micrometeorology in Agricultural Systems. Agron. Monogr. Am. Soc. of Agron. 47:381-396.

Moncrieff. J, R.Valentini, S. Greco, G. Seufert and P. Ciccioli. 1997. Trace gas exchange over terrestrial ecosystems: methods and perspectives in micrometeorology. J. Exper. Botany. 48:1133-1142.

Ochsner, T.E., T.J. Sauer and R. Horton. 2006. Field tests of soil heat flux plates and some alternatives. Agron. J. 98:1005-1014.

Ochsner, T.E., T.J. Sauer and R. Horton. 2007. Soil heat storage measurements in energy balance studies. Agron. J. 99:311-319.

Ren, T., T.E. Ochsner and R. Horton. 2003. Development of thermo-time domain reflectometry for vadose zone measurements. Vadose Zone J. 2:544-551.

Robins, J.S. 1965. Evapotranspiration. *In* C.A. Black et al. Methods of Soil Analysis. Agron. I, Am. Soc. Agron. 9:286-298.

Sauer, T.J., and R. Horton. 2005. Soil heat flux. *In* J.L. Hatfield and J.M. Baker (eds.) Micrometeorology in Agricultural Systems, Agron. Monogr. Am. Soc. Agron. 47:131-154.

Sauer, T.J., P.A. Moore, J.M. Ham, W.L. Bland, J.H. Prueger and C.P. West. 2002. Seasonal water balance of an Ozark hillslope. Agric. Water Manage. 55:71– 82.

Tanner, C.B. 1967. Measurement of evaporation. *In* R.M. Hagen et al. (ed.) Irrigation of Agricultural Lands. Agron.Π, Am. Soc. Agron. 11:534-574.

van Bavel, C.H.M. 1961. Lysimetric measurements of evapotranspiration rates in the eastern United States. Soil Sci. Soc. Am. Proc. 25:138-141.

Figure Captions

Figure 1: A cross-sectional view of the heat pulse sensor installation designs in 2007 and 2008. White rectangles are the sensor bodies for heat-pulse sensors; dark-colored circles within rectangles indicate the position of sensor needles. Numbers beside each sensor indicate the middle needle depth (mm).

Figure 2: Diagram of heat pulse sensor measurements applied to determine sensible and latent heat of a soil layer, where H is sensible heat flux, ΔS is change in sensible heat storage, LE is latent heat, T is temperature, z is depth, λ is thermal conductivity, C is volumetric heat capacity, and the subscripts u and l represent upper and lower, respectively**.**

Figure 3: Diagram indicating the 2007 and 2008 heat pulse sensor placements used to calculate LE (latent heat). Each rectangular shape represents a 3-needle heat pulse sensor, and the solid circles in the rectangles indicate the needle positions. In 2007, individual heat pulse sensors were inserted into the soil, and in 2008, in order to improve depth placement accuracy, heat pulse sensors were glued together before being inserted into soil. The numeric subscripts indicate soil depth or soil layer (mm). The exact same depths and layers were represented in 2007 and 2008. The symbols in the diagrams refer to temperature (T), depth (z), volumetric heat capacity (C), thermal conductivity (λ), sensible heat flux (H), and change of sensible heat storage (ΔS).

Figure 4: 2007 values of average soil water content (0 – 60 mm), daily net radiation, cumulative evaporation for the surface and for various subsurface soil depths, and daily rainfall.

Figure 5: 2008 values of average soil water content (0 – 60 mm), daily net radiation, cumulative evaporation for the surface and for various subsurface soil depths, and daily rainfall.

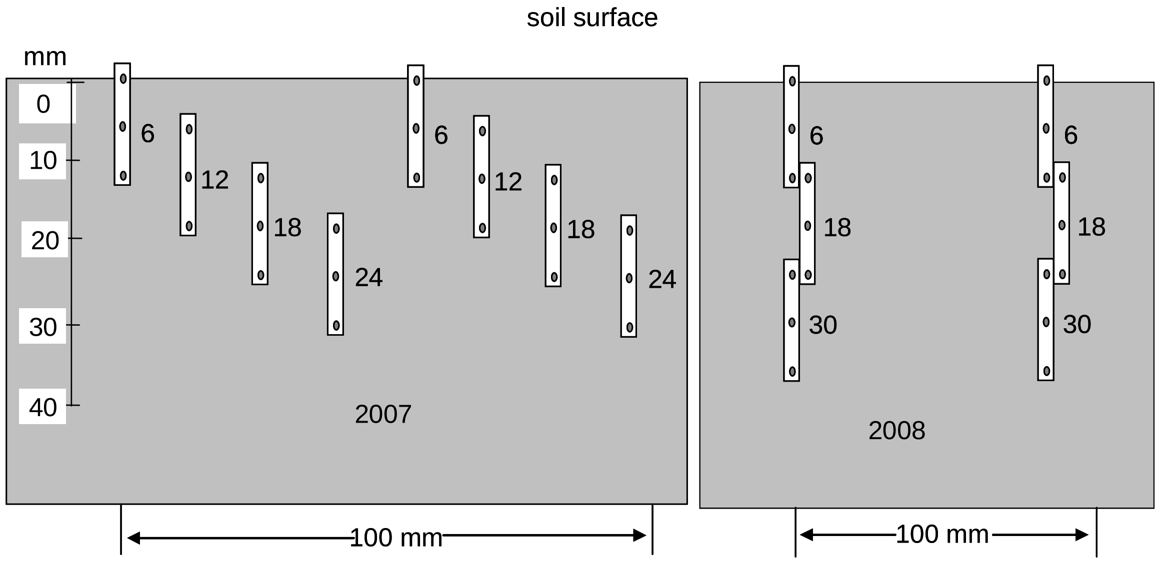

Figure 1: A cross-sectional view of the heat pulse sensor installation designs in 2007 and 2008. White rectangles are the sensor bodies for heat-pulse sensors; dark-colored circles within rectangles indicate the position of sensor needles. Numbers beside each sensor indicate the middle needle depth (mm).

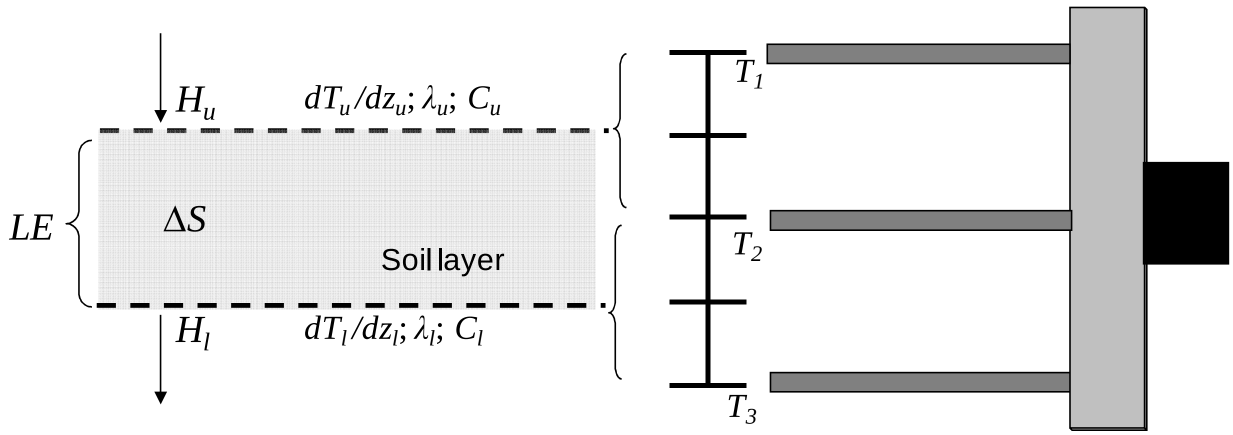

Figure 2: Diagram of heat pulse sensor measurements applied to determine sensible and latent heat of a soil layer, where *H* is sensible heat flux, Δ*S* is change in sensible heat storage, *LE* is latent heat, *T* is temperature, *z* is depth, λ is thermal conductivity, *C* is volumetric heat capacity, and the subscripts *u* and l represent upper and lower, respectively**.**

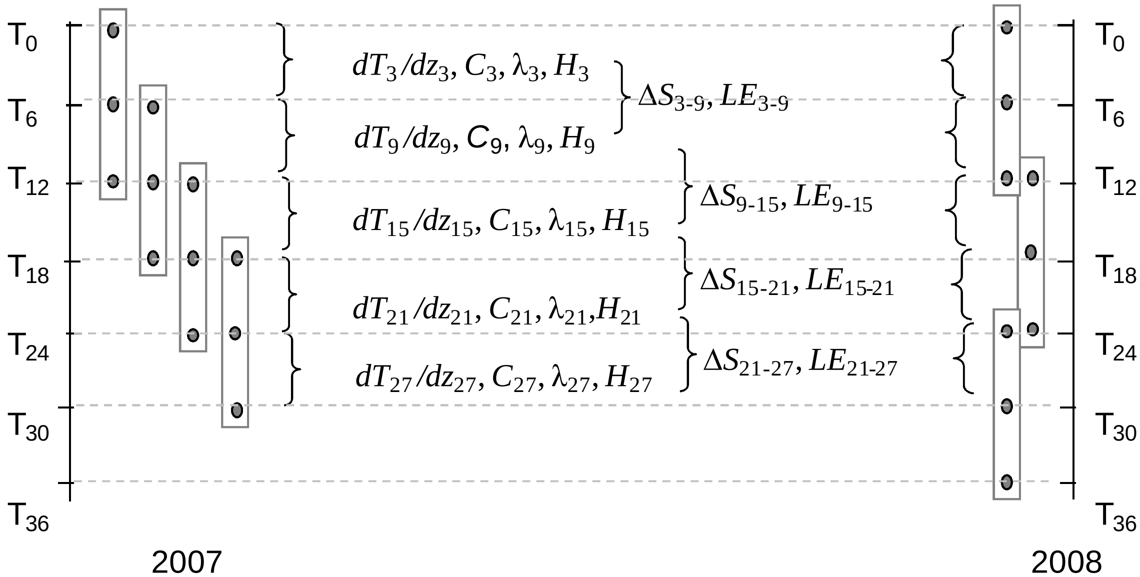

Figure 3: Diagram indicating the 2007 and 2008 heat pulse sensor placements used to calculate *LE* (latent heat). Each rectangular shape represents a 3-needle heat pulse sensor, and the solid circles in the rectangles indicate the needle positions. In 2007, individual heat pulse sensors were inserted into the soil, and in 2008, in order to improve depth placement accuracy, heat pulse sensors were glued together before being inserted into soil. The numeric subscripts indicate soil depth or soil layer (mm). The exact same depths and layers were represented in 2007 and 2008. The symbols in the diagrams refer to temperature (T), depth (z), volumetric heat capacity (*C*), thermal conductivity (λ), sensible heat flux (*H*), and change of sensible heat storage (Δ*S*).

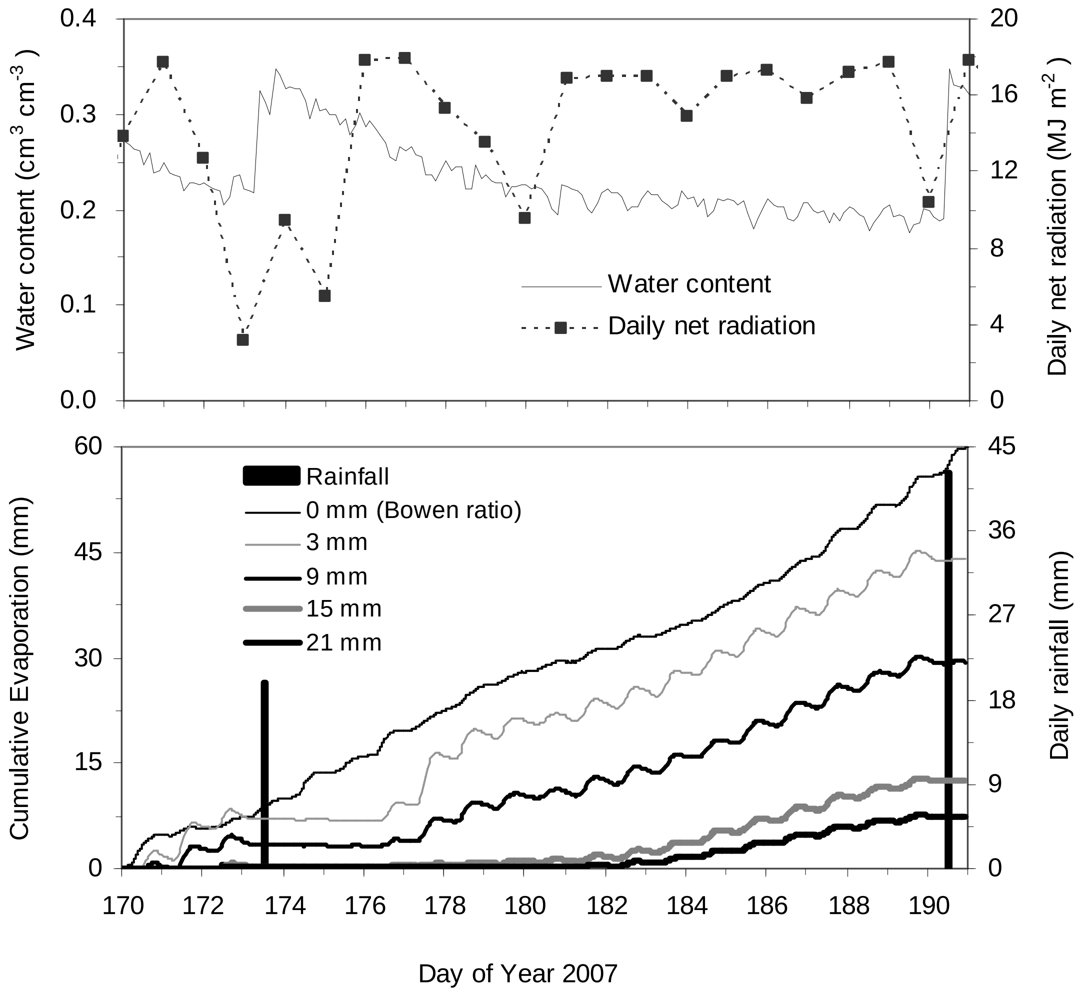

Figure 4: 2007 values of average soil water content (0 – 60 mm), daily net radiation, cumulative evaporation for the surface and for various subsurface soil depths, and daily rainfall.

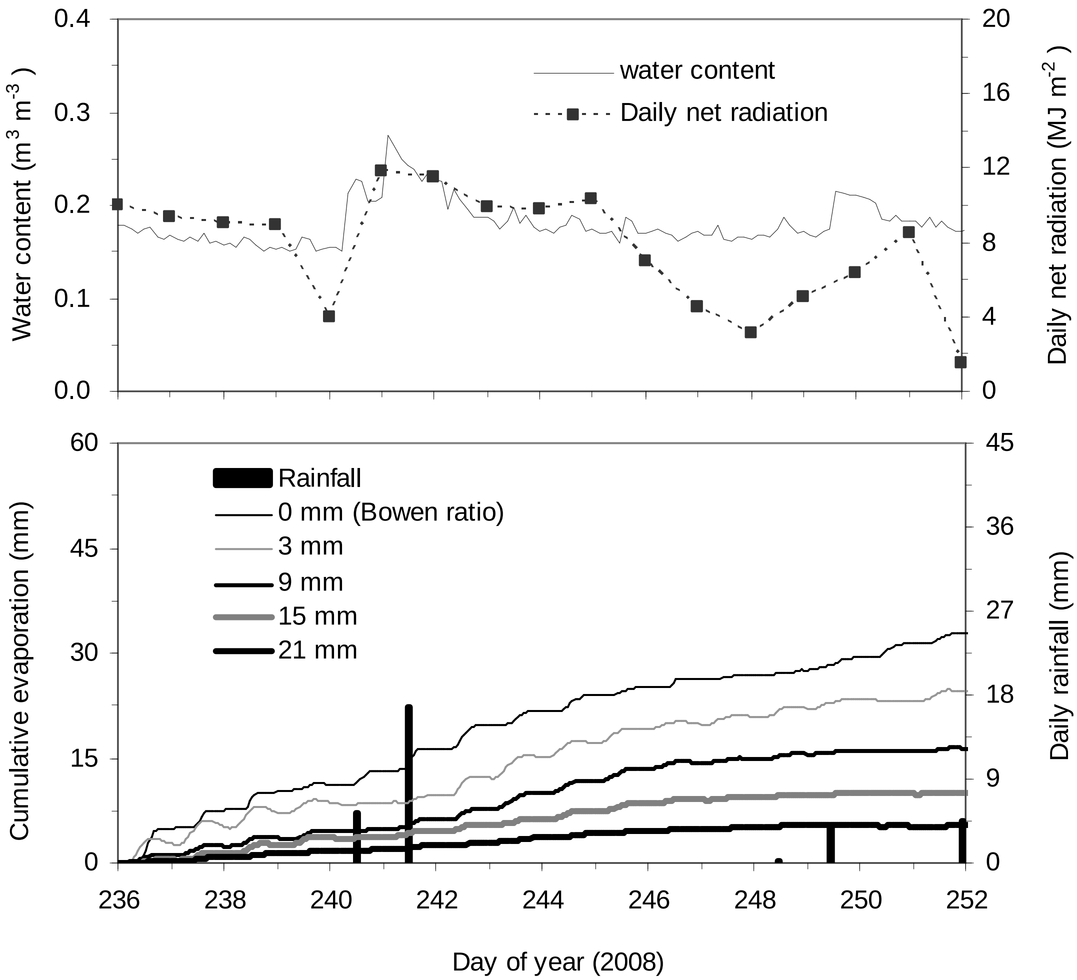

Figure 5: 2008 values of average soil water content (0 – 60 mm), daily net radiation, cumulative evaporation for the surface and for various subsurface soil depths, and daily rainfall.

Chapter 4 Heat pulse sensor measurements of soil water evaporation in a corn field

X. Xiao, R. Horton, T.J. Sauer, J.L. Heitman and T. Ren

A paper submitted in the Soil Science Society of America Journal

Abstract

Latent heat fluxes from cropped fields consist of soil water evaporation and plant transpiration. Accurate measurement of soil water evaporation in a cropped field is challenging. Heat pulse sensors have been used to measure subsurface (3 mm and below soil surface) soil water evaporation from bare fields, however, the applicability of heat pulse sensors to measure soil water evaporation in the 0-3 mm soil layer and the applicability of the heat pulse sensors in a cropped field are still uncertain. In this study, we used 11-needle heat pulse sensors to determine transient soil water evaporation at the surface and the subsurface in a corn (*Zea mays* L.) field. Soil water evaporation fluxes were measured during natural soil wetting and drying periods in the summer of 2009 at the following locations within the corn field: within-row (ROW), between-rows with roots (BR), and between-rows without roots (BRNR). In addition to the heat pulse sensor measurements, micro-lysimeters were used to measure daily soil water evaporation at ROW and BR locations. During the rainy days, there was no obvious net soil water evaporation detected at the three locations. Following rains, the majority of net soil water evaporation occurred in the 0-3 mm soil layer for about 9 days, before the soil water evaporation noticeably shifted to deeper soil layers. The heat pulse sensor measurements provided realistic estimates of

the soil water evaporation dynamics at the various locations. The cumulative soil water evaporation at the BRNR location was slightly larger than at the ROW and BR locations which were very similar. Soil water evaporation estimates from heat pulse and micro-lysimeter methods were similar, with the total differences in 9 days cumulative for evaporation being 0.5 mm out of 5.4 mm and 0.8 mm out of 5.9 mm at the ROW and BR corn field locations, respectively. Thus, the heat-pulse method is a promising approach for measuring soil water evaporation at different management zones in cropped fields.

Introduction

Soil water evaporation is a significant component of the surface water balance and the surface energy balance. Soil water evaporation occurs at the soil surface when soil is wet, but as soil dries the evaporation rate declines and shifts its location downward being limited by water flow rates from deeper soil toward the soil surface (Jury and Horton, 2004). Soil water evaporation is a transient process and it varies with time and depth. The most common techniques for measuring soil water evaporation include water balance and energy balance (micrometeorology) approaches (Hanks and Ashcroft, 1980; Hillel, 1980). Evaporation pans, lysimeters (van Bavel, 1961; Robins, 1965; Tanner, 1967; Boast and Roberson, 1982), and soil moisture depletion (Böhm et al., 1977) are long-established methods to determine evaporation directly. Eddy covariance (Meyers and Baldocchi, 2005; Moncrieff et al., 1997) and Bowen ratio energy balance (Fritschen and Fritschen, 2005) are widely used micrometeorological methods for estimating evaporation over an adequately fetched area by using meteorological sensors mounted above the surface.

However, none of the methods are able to measure transient soil evaporation rates with time and depth. In cropped fields, furthermore, soil water evaporation is often combined with plant transpiration in a measurement of evapotranspiration (Petersen, et al., 2010).

The heat pulse method has been introduced as a means to measure subsurface soil water evaporation in bare fields over time and depth with minimal disturbance to the soil. Heitman et al. (2008a, 2008b) and Xiao et al. (2011) reported that bare field soil water evaporation determined by 3-needle sensors agreed well with daily evaporation values determined by micro-lysimeters and Bowen ratio energy balance techniques. Based on numerical simulations of bare soil conditions, Sakai et al. (2011) reported that the Heitman et al. (2008a, 2008b) heat pulse method could accurately estimate subsurface soil water evaporation. Thus, there exists a limited amount of observational and numerical evidence indicating that the heat pulse method can determine subsurface evaporation in bare field conditions.

However, soil surface layer soil water evaporation (0-3 mm soil layer) has not been measured with heat pulse sensors, and heat pulse sensors have not been used to determine evaporation at different soil management locations in cropped fields. Thus the objectives of this study are 1) to extend the heat pulse method to the soil surface by measuring soil water evaporation from the 0-3 mm soil layer with an 11-needle heat pulse sensor, and 2) to compare heat pulse daily soil water evaporation values with micro-lysimeter daily soil water evaporation values measured in a corn field.

Materials and Methods

Experiment location description

The study was performed in a corn field located near Ames (41.98°N, 93.68°W), Iowa during the summer of 2009. This field had been planted in a corn-soybean rotation for many years. The soil at the site was Canisteo clay loam (fine-loamy, mixed, superactive, calcareous, mesic Typic Endoaquolls). The surface soil bulk density was 1.2 Mg m^{-3}. The soil consisted of 44% sand, 30% silt and 26% clay, and the topography was relatively flat (slope < 2%).

Heat pulse sensors were installed at within-row (ROW), between-rows with roots (BR), and between-rows without roots (BRNR) in the field (see Fig. 1). The BRNR location was a small area of 2 m × 0.45 m in between-rows (0.75 m row spacing). On each side of this area, 0.5-m deep narrow trenches were dug with a chain saw. Plastic sheets were placed in each trench before back-filling the trenches with soil. This was done when the corn leaf area index was approximately 2. The plastic sheets served as barriers to prevent roots from growing into the BRNR area. In the same corn field close to the three locations, there was a weather station tower, which measured and recorded the rainfall, net radiation, air temperature, air humidity, atmospheric pressure and wind speed.

Instrument description and installation

To improve measurement resolution of in situ soil water evaporation, 11-needle heat pulse sensors (Zhang et al., 20012) were used in this study (Fig. 2). The sensors were a modification of the 3-needle heat pulse sensors used by Ren et al. (2003). Each sensor consisted of four long parallel stainless steel needles (1.3 mm diameter, 40 mm length) and seven short parallel stainless steel needles (1.3 mm diameter, 20 mm length). Two short needles were off-set from the top short needle in a ‘T’ shape with a vertical spacing of 1 mm between each of the top 3 needles. The four long needles and the other five short needles alternated in a straight line in an epoxy body, with about 6 mm spacing between the adjacent needles.

Each needle contained a chromel–constantan (type E) thermocouple for measuring temperature. In each long needle there was also a resistance heater wire, through which a small current could be applied to generate a heat pulse, leading to temperature increases at the adjacent short needles. The precise distances between neighboring needles were determined from heat pulse measurements made in agar-stabilized water (6 g L^{-1}) before installation in the field (Ren et al. 2003).

Two 11-needle heat pulse sensors were installed at each of the three locations: ROW, BR, and BRNR. To install each sensor, a narrow trench was dug and a sensor was inserted vertically into the undisturbed soil profile with the top sensor needle at the soil surface and the bottom sensor needle at a depth of 48 mm. The trench was then carefully back-filled with soil. The thermocouples and heater wires of two heat pulse sensors were connected to one Campbell AM16/32 multiplexer and one AM416 multiplexer, respectively (Campbell Scientific Inc., Logan, Utah). Both multiplexers were controlled by a Campbell CR10X data-logger. The data-logger was powered by a 12-volt power supply.

Heat pulse sensor measurements of soil thermal diffusivity and volumetric heat capacity were performed with each heating needle every 8 hours. The heating sequence for the pair of heat pulse sensors at each location was to apply a heat pulse at hours 1, 3, 5, and 7 from top to bottom to individual heater needles of one heat pulse sensor, and at hours 2, 4, 6, and 8 from top to bottom to individual heater needles of the other heat pulse sensor. The sequence for each heat pulse measurement consisted of 30 s background temperature measurement, 8-s heating duration at the heater needle, and 72-s temperature measurements after heating. Thus, the temperature response at the adjacent thermocouple needles during heat pulse measurements was recorded for a total time of 110 s with a 2-Hz sensing interval. The 30-s background temperatures were used to correct for temperature drift (Ochsner et al., 2006). In addition, ambient soil temperature at each needle position was measured and recorded every hour (before initiating heat pulses).

Heat pulse measurements were made for 21 consecutive days. During the measurement period micro-lysimeters were used to measure daily soil water evaporation at the ROW and BR locations for 9 days (DOY 235 to 236, and 241 to 247). There were no micro-lysimeter measurements made at the BRNR location because of the limited area for BRNR treatment (0.9 m^2). The micro-lysimeters were the same type used by Singer et al. (2010). They were white polyvinyl chloride cylinders 100 mm long by 76 mm inner diameter, and wall thickness of 3 mm. Before rainfall events, micro-lysimeters were tapped into soil with a hammer at the three locations with the top rim level with the soil surface. One day after a rainfall event, five of the micro-lysimeters were dug out from the soil at each location to measure the mass of each micro-lysimeter in the morning around 8:00 am. Each micro-lysimeter was cleaned of soil on the outside, trimmed even at the bottom, sealed on the bottom end with a thin plastic sheet, and then weighed with a balance. The micro-lysimeters were then put back in their original positions and the surrounding soil was carefully packed around them. Twenty-four hours later, the micro-lysimeters, with ends still sealed, were removed from the ground and reweighed. Each micro-lysimeter was used for two consecutive days and then discarded. The difference in mass for consecutive days was assumed to be the daily water loss due to evaporation.

The daily soil water evaporation (mm) from the micro-lysimeters was the ratio of the difference of mass (g) of two consecutive days divided by liquid density (g mm^{-3}), divided by the cross-sectional area (mm^2) of the micro-lysimeters.

Based on energy conservation principles, the net heat entering or leaving a soil layer through conduction, through liquid water flow, through water evaporation or condensation, and the change in water content (including heat associate with plant water uptake) should equal to the change in heat storage of the soil layer. Our calculations indicate that the net sensible heat flux (ΔH) is much larger than the change in sensible heat storage (ΔS) of a soil layer. The change in sensible heat storage due to soil water flow and plant water uptake is even less than ΔS. Thus, in this study our analysis of the heat pulse measurements assumes that the effects of soil water flow and root water uptake on the heat balance method are negligible.

Soil water evaporation at the three corn field locations was determined from the net sensible heat fluxes, and ΔS of specific soil layers was measured by 11-needle heat pulse sensors based on sensible heat balance (Heitman et al., 2008a and 2008b, Xiao et al., 2011, Zhang et al., 2012). With an 11-needle heat pulse sensor installed vertically from the surface to a depth of 48 mm, latent heat for soil water evaporation was determined for specific soil layers (3-9, 9-15, 15-21, 21-27, 27-33, 33-39 and 39-45 mm) according to measured temperature and thermal properties from the 11-needle heat pulse sensors.

Soil latent heat flux (*LE*) for soil water evaporation at the soil surface was obtained based on surface energy balance:

$$LE = R_n - G - H \tag{8}$$

where R_n is surface net radiation measured by a tube net radiometer (TRL, Delta-T Devices, Burwell, Cambridge, UK) installed 15 cm above the soil surface in the corn field, G is the soil surface heat flux and H is sensible heat flux.

G was calculated from the soil heat flux at the 3 mm depth (G_3) and the heat storage change in the 0-3 mm soil layer ($\Delta S_{0\text{-}3}$), where G_3 and $\Delta S_{0\text{-}3}$ were determined from the soil temperature at 0-, 1-, 2- and 6-mm depths and soil thermal properties at 3 mm depths measured by heat pulse sensors (Xiao et al., 2011).

$$G = G_3 + \Delta S_{0-3} \tag{9}$$

H is sensible heat flux calculated as sensible heat flux transport between soil and atmosphere (Campbell and Norman, 1998).

$$H = -g_{Ha}\, C_p\, \left(T_s - T_a\right) \tag{10}$$

where g_{Ha} is heat conductance (mol $m^{-2}s^{-1}$) between the soil surface and a height z of 5 cm above the soil surface, C_p is specific heat of air (29.3 $Jmol^{-1}°C^{-1}$), and T_s and T_a are soil surface temperature and air temperature (°C) measured with chromel-constantan thermocouples 6 cm above the soil surface.

$$g_{Ha} = \frac{0.4^2 \hat{\rho}\, u(z)}{\left[\ln\left(\frac{z-d}{z_M}\right) + \Psi_M\right]\left[\ln\left(\frac{z-d}{z_H}\right) + \Psi_H\right]} \qquad [11]$$

We assumed stable flow (momentum and heat correction factors equal to zero ($\Psi_M = \Psi_H = 0$), zero plane displacement d=0, molar density of air $\hat{\rho}$ (44.6 mol m^{-3}), roughness length for momentum at soil surface z_M=0.4 cm, and roughness length for heat z_H=0.2 (z_M) (Hansen 1993)

Wind speed at the soil surface u(z=0) was corrected from wind speed above the canopy u(h=3 m) with the attenuation coefficient (a) equal to 2.0 (from Cionco, 1972) in the corn field:

$$u(z=0) = u(h)\exp\left[a\left(\frac{z}{h} - 1\right)\right] \qquad [12]$$

Similar to earlier studies (Heitman et al. 2008a; Heitman et al., 2008b), in this study evaporation was not detected at depths below 27 mm. Reported values of evaporation rates for each soil layer represented the average of two replicated heat pulse measurements. The cumulative evaporation at a specific soil depth was the sum of evaporation rates for all of the soil layers below that depth, integrated over time. For example, the cumulative evaporation at the soil surface was the sum of evaporation from the 0-3, 3-9, 9-15, 15-21 and 21-27 mm soil layers.

The evaporation in the 0-3 mm soil layer was estimated from the difference of the surface soil water evaporation determined with Eq. 8 and the sum of heat pulse subsurface soil water evaporation at 3-9, 9-15, 15-21 and 21-27 mm soil layers.

Results

Soil water evaporation rates in the 0-3, 3-9, 9-15 15-21 and 21-27 mm soil layers were estimated using 11-needle heat pulse sensors at ROW, BR and BRNR locations in a corn field. The heat pulse sensor measurement period consisted of 21 consecutive days during natural soil wetting and drying periods from day of year (DOY) 233 to 253 in the summer of 2009. Micro-lysimeter measurements were made for 9 days (DOY 235 to 236, and 241 to 247) at the ROW and BR locations. A rainfall event (33 mm) occurred from DOY 230 through 233 just before starting the measurements, and a rainfall event (30 mm) occurred from DOY 237 through 239 during the measurement period.

Dynamic soil water evaporation

Figure 3 shows the observed soil temperature values at various depths at ROW, BR, and BRNR locations within the corn field. The diurnal temperature fluctuations at different depths were similar at the three locations. Soil temperatures ranged from 10 to 25 ºC at ROW and BR locations and ranged from 10 to 24 ºC at BRNR location. The differences in soil temperature amplitude between the surface and the 6 mm depth were about 2 ºC, and amplitude differences were relatively small among the 12 mm to 36 mm depths at the three locations.

Using the measured ambient soil temperatures with depth and time, and soil layer thermal properties determined by heat-pulse measurements, soil water evaporation rates were calculated with time and depth for different soil layers at each of the three locations (Fig. 5).

During the rainfall event (DOY 237 through 239), there was no obvious net soil water evaporation observed at the three locations. The largest soil water evaporation occurred in the 0-3 mm soil layer and a relatively small amount of soil water evaporation was observed in the soil layers below a depth of 3 mm on the days between the two rainfall events (DOY 234 to 236) at each of the three locations. Following the second rain event, soil water evaporation occurred mostly in the 0-3 mm soil layer with a relatively small amount of soil water evaporation in the soil layers below the 3 mm depth for a week before large increases in evaporation occurred for soil layers below the 3 mm depth. Diurnal variations including positive and negative soil water evaporation rates were detected in all of the soil layers, which indicated that both evaporation and condensation occurred.

ROW and BR locations had similar soil water evaporation patterns. The daily net evaporation increased rapidly in the 0-3 mm soil layer but slowly in the 3-9 and 9-15 mm soil layers for one week after the second rain event. At both locations, the major net soil water evaporation occurred in the 0-3, 3-9 and 9-15 mm soil layers, and the evaporation rate in the 0-3 mm soil layer was larger than in the 3-9 and 9-15 mm soil layers early in the measurement period. The 11-needle heat pulse sensors combined with above ground measurements, were able to detect the development of water evaporation zones at the

ROW and BR locations. Soil water evaporation was small during the rainy days, and increased rapidly in the 0-3 mm soil layer and increased slowly in the soil layers below a depth of 3 mm for about a week after rainfall, and then the evaporation zone shifted to the 3-9 and 9-15 mm soil layers. The soil water evaporation at the BRNR location was similar to that at the ROW and BR locations with the main difference being that the daytime evaporation and nighttime water condensation in the soil layers below the 3 mm soil depth occurred several days earlier than at the BRNR location, and little water condensation was observed in the 0-3 mm soil layer after DOY 248. A possible reason for this difference was that there were no plant roots to take up water at the BRNR location. Thus, the soil was slightly wetter at the BRNR location than at the ROW and BR locations which resulted in slightly larger evaporation occurring in the 0-3 mm soil layer.

Compared with the soil water evaporation in a bare field reported by (Heitman et al., 2008b), the soil water evaporation rates within the corn field were much smaller and the evaporation zone shifted downward more slowly. A main reason for the difference was that bare field had much larger net radiation than did corn field.

Overall the heat pulse sensor measurements provided the development of soil water evaporation dynamics at the ROW, BR and BRNR locations within the corn field. There was no obvious net soil water evaporation during rainy days. Relatively large early soil water evaporation occurred in the 0-3 mm soil layer and relatively small amounts of soil water evaporation were observed in the soil layers below the 3 mm depth for up to a week.

Cumulative soil water evaporation

Cumulative soil water evaporation with time for the ROW, BR and BRNR locations in the corn field is shown in Fig. 6. The amounts of cumulative soil evaporation during the measurement period were 10, 10 and 14 mm at the ROW, BR and BRNR locations, respectively. The BRNR location had cumulative evaporation comparable to the ROW and BR locations when the soil was relatively wet before DOY 246, but BRNR had larger cumulative evaporation than the ROW and BR locations as the soil dried after DOY 246. The BRNR location did not have root water uptake so it had more available water for evaporation than did the ROW and BR locations.

Cumulative soil water evaporation at various soil depths (0, 3, 9, 15, 21 mm) of the ROW, BR and BRNR locations of the corn field are shown in Fig. 7. Large cumulative evaporation differences were observed at 0 and 3 mm, and soil water evaporation occurring in the 0-3 mm soil layer accounted for larger portions at the BRNR location than at the ROW and BR locations. The ROW and BR locations might be subjected to more root water uptake leading to slightly smaller soil water evaporation than at the BRNR location. The cumulative evaporation differences at 3 and 9 mm (soil water evaporation occurring in the 3-9 mm soil layer) and 9 and 15 mm (soil water evaporation occurring in the 9-15 mm soil layer) were small compared with the difference at 0 and 3 mm, and even smaller cumulative evaporation differences were observed for deeper soil depths at the three locations.

C***omparison of heat pulse and micro-lysimeter daily soil water evaporation***

A comparison was made between heat pulse and micro-lysimeter estimates of daily soil water evaporation at the ROW and BR locations for 9 days (DOY 235 to 236, and 241 to 247) (Table 1 and Fig. 8).

Heat pulse estimates of daily evaporation ranged from 0.1 to 0.9 mm and 0.2 to 1.1 mm at the ROW and BR locations, respectively. Micro-lysimeter estimates of daily evaporation ranged from 0.1 to 1.0 mm at the ROW and BR locations. Heat pulse estimates of daily water evaporation were similar to the micro-lysimeter estimates at the ROW and BR locations, with the total differences in cumulative evaporation for 9 days of measurements being 0.5 mm out of 5.4 mm and 0.8 mm out of 5.9 mm at the ROW and BR corn field locations, respectively.

The differences between heat pulse and micrio-lysimeter estimates of daily water evaporation varied each day during the measurement period, but the differences were within 0.4 mm at both ROW and BR locations. The BR location had slightly larger heat-pulse and micro-lysimeter evaporation than the ROW location.

Comparisons were made between the heat pulse and micro-lysimeter daily soil water evaporation at ROW and BR in the corn field, and for the corn field data combined with bare field data reported by Heitman et al. (2008b) (see Fig. 9). The heat pulse and micro-lysimeter daily soil water evaporation at ROW and BR in the corn field showed a linear trend, with R^2=0.50 and slope=0.74, but the relatively small daily evaporation values had noticeable day to day variations within the small range of values. When the corn field results were combined with bare field results, a relatively large range of daily evaporation values existed, and a favorable linear comparison was found for heat pulse daily evaporation and micro-lysimeter and Bowen ratio values, with R^2=0.96 and slope=0.93. Thus, the heat-pulse method appears to be a promising way to accurately measure diurnal water evaporation in bare and cropped soils.

Conclusions

Soil water evaporation estimated with heat pulse sensors revealed the dynamics of the development of evaporation during natural soil drying and wetting periods at the ROW, BR and BRNR corn field locations. During rainy days, there was no obvious net soil water evaporation detected at the three locations within the corn field. A major portion of the soil water evaporation originated in the 0-3 mm soil layer for a week before evaporation shifted to deeper soil layers. Soil water evaporation rates were similar at ROW and BR location beneath the corn crop canopy. The soil water evaporation at the BRNR location was slightly larger than at the ROW and BR locations. Soil water evaporation estimates from heat pulse and micro-lysimeter methods were consistent with the total daily soil water evaporation being within 0.5 mm and 0.8 mm for a 9 day period at the ROW and BR corn field locations, respectively. The heat pulse sensors provided an accurate representation of soil water evaporation in the corn field.

Acknowledgments

This work was supported by the National Science Foundation under Grant 0809656, by ConocoPhillips Company, and by the Hatch Act, State of Iowa, and State of North Carolina funds.

References

Boast, C.W. and T. M. Roberson. 1982. A “Micro-lysimeter” method for determining evaporation from bare soil: description and laboratory evaluation. Soil Sci. Soc. Am. J. 46:689-696.

Böhm, W., H. Maduakor and H.M. Taylor. 1977. Comparison of five methods for characterizing soybean rooting density and development. Agron. J. 69:415–419.

Bristow, K.L., G.J. Kluitenberg and R. Horton. 1994. Measurement of soil thermal properties with a dual-probe heat-pulse technique. Soil Sci. Soc. Am. J. 58:1288-1294.

Campbell G.S. and J.M. Norman. 1998. An introduction to environmental biophysics. Second edition. Spring Press.

Cionco, R.M. 1972. A wind-profile index for canopy flow. Boundary-layer Meteorol. 3:255-263.

Forsythe, W.E. 1964. Smithsonian Physical Tables. Smithsonian Inst. Publ. 4169. Washington, DC, USA.

Fritschen, L.J. and C.L. Fritschen. 2005. Bowen ratio energy balance method. *In* J.L.Hatfield and J.M. Baker (eds.) Micrometeorology in Agricultural Systems. Agron. Monogr. 47:397-405.

Gardner, H.R., and R.J. Hanks. 1966. Evaluation of the evaporation zone in soil by measurement of heat flux. Soil Sci. Soc. Am. J. 30:425-428.

Hanks, R.J. and G.L. Ashcroft. 1980. Applied Soil Physics. Springer Verlag, New York.

Hansen, F.V. 1993. Surface roughness lengths. ARL technical report, U.S. Army, White Sands Missile Range, NM 88002-5501.

Heitman, J.L., R. Horton, T.J. Sauer and T.M. DeSutter. 2008a. Sensible heat observations reveal soil water evaporation dynamics. J. Hydrometeor. 9:165-171.

Heitman, J.L., X. Xiao, R. Horton and T. J. Sauer. 2008b. Sensible heat measurements indicating depth and magnitude of subsurface soil water evaporation. Water Resour. Res. 44, W00D05.

Hillel, D. 1980. Introduction to Soil Physics. Academic Press, London.

Jury, W. and R. Horton. 2004. Soil Physics. 6th ed., John Wiley, Hoboken,N. J.

Knight, J.H. and G.J. Kluitenberg. 2004. Simplified computational approach for the dual-probe heat-pulse method. Soil Sci. Soc. Am. J. 68:447-449.

Meyers, T.P. and D.D. Baldocchi. 2005. Current micrometeorological flux methodologies with applications in agriculture. *In*: J. L. Hatfield and J. M. Baker (ed.) Micrometeorology in Agricultural Systems. Agron. Monogr. Am. Soc. of Agron. 47:381-396.

Moncrieff. J, R.Valentini, S. Greco, G. Seufert and P. Ciccioli. 1997. Trace gas exchange over terrestrial ecosystems: methods and perspectives in micrometeorology. J. of Exper. Botany. 48:1133-1142.

Novak, M.D. 2010. Dynamics of the near-surface evaporation zone and corresponding effects on the surface energy balance of a drying bare soil. Agric Forest Meteorol. 150(10):1358-1365.

Ochsner, T.E., T.J. Sauer and R. Horton. 2007. Soil heat storage measurements in energy balance studies. Agron. J. 99:311-319.

Ochsner, T.E., T.J. Sauer, and R. Horton. 2006. Field tests of the soil heat flux plate method and some alternatives. Agron. J. 98:1005-1014.

Petersen, J.F., D. Sack, and R.E. Gabler. 2010. Fundamentals of physical geography, International Edition, Brooks/Cole Pub Co. P:199.

Ren, T., T.E. Ochsner and R. Horton. 2003. Development of thermo-time domain reflectometry for vadose zone measurements. Vadose Zone J. 2:544-551.

Robins, J. S., 1965. Evapotranspiration. *In* C.A. Black et al. Methods of Soil Analysis, Agron. Am. Soc. Agron. 9:286-298.

Sakai, M., S.B. Jones, and M. Tuller. 2011. Numerical evaluation of subsurface soil water evaporation derived from sensible heat balance, Water Resour. Res. 47, W02547, doi:10.1029/2010WR009866.

Singer, J.W., J.L Heitman, G. Hernandez Ramirez, T.J. Sauer, J.H. Prueger, and J.L. Hatfield. 2010. Contrasting methods for estimating evapotranspiration in soybean. Agric. Water Manage. 98(1):157-163.

Tanner, C.B. 1967. Measurement of evaporation. *In* R.M. Hagen et al. (ed.) Irrigation of Agricultural Lands. Agron.11, Am. Soc. Agron. 11:534-574.

van Bavel, C.H.M, 1961. Lysimetric measurements of evapotranspiration rates in the eastern United States. Soil Sci. Soc. Am. J. 25:138-141.

Xiao,X., R. Horton, T.J. Sauer, J.L. Heitman and T. Ren. 2011. Cumulative evaporation as a function of depth and time. Vadose Zone J. 10:1016-1022.

Zhang, X., S. Lu, J.L. Heitman, R. Horton and T. Ren. 2012. Subsurface soil-water evaporation with an improved heat-pulse probe. Soil Sci. Soc. Am. J. 76: 3:876-879.

Figure Captions

Table 1: Daily and cumulative soil water evaporation from heat pulse (HP) and micro-lysimeter (ML) methods from DOY 236 to 237, and 241 to 247. HP-ML was the difference of daily evaporation between the heat pulse and micro-lysimeter methods.

Figure 1: Heat pulse sensor installation at the ROW, BR and BRNR locations.

Figure 2: Photo and side view configuration of an 11-needle heat pulse sensor (photo courtesy of Pukhraj Deol).

Figure 3: Soil temperature (°C) with time of various depths (soil temperatures at 6, 18, 24 and 36 mm not shown here) at the ROW, BR, and BRNR locations in the corn field.

Figure 4: Soil water content (m^3 m^{-3}) (0-30 mm soil layer) measured by heat pulse sensors at the ROW, BR, and BRNR locations (Fig.4A); net radiation Rn (W m^{-2}) below the canopy (Fig.4B).

Figure 5: Soil water evaporation dynamics (0-3, 3-9, 9-15, 15-21, 21-27-mm soil depth) at the ROW, BR and BRNR locations in the corn field.

Fig 6: Cumulative surface soil water evaporation at the ROW, BR and BRNR locations in the corn field.

Figure 7: Cumulative soil water evaporation at various soil depths at the ROW, BR and BRNR locations in the corn field.

Fig. 8: Daily surface soil water evaporation from heat pulse and micro-lysimeter methods at the ROW and BR locations in the corn field. (error bars represent standard deviation of the micro-lysimeter measurement).

Fig.9: Comparison of heat pulse daily soil water evaporation estimates with micro-lysimeter and Bowen ratio daily soil water evaporation estimates. Bare field measurement data are from Heitman et al. (2008b).

Table 1: Daily and total soil water evaporation from heat pulse (HP) and micro-lysimeter (ML) methods from DOY 236 to 237, and 241 to 247. HP-ML was the difference of daily evaporation between the heat pulse and micro-lysimeter methods.

		Daily evaporation E (mm)									Toatal E (mm)
		Day of year 2009									
Location	Method	236	237	241	242	243	244	245	246	247	
ROW	HP	0.8	0.1	0.8	0.3	0.6	0.7	0.9	0.9	0.6	5.7
	ML	0.7	0.1	1.0	0.5	0.7	0.6	0.6	0.5	0.4	5.2
	HP-ML	0.1	0.0	-0.2	-0.2	-0.1	0.1	0.3	0.4	0.2	0.5
	Difference %	12	32	27	44	13	17	44	50	36	9
BR	HP	1.1	0.2	0.9	0.4	0.6	0.6	0.9	1.0	0.7	6.3
	ML	0.7	0.1	1.0	0.5	0.8	0.6	0.6	0.6	0.6	5.5
	HP-ML	0.4	0.1	-0.1	-0.1	-0.2	0.0	0.3	0.3	0.2	0.8
	Difference %	48	46	15	23	29	4	34	42	28	14

Note: difference %* : The ratio of the absolute daily evaporation difference from heat pulse and micro-lysimeter methods and the average daily evaporation from the two methods.

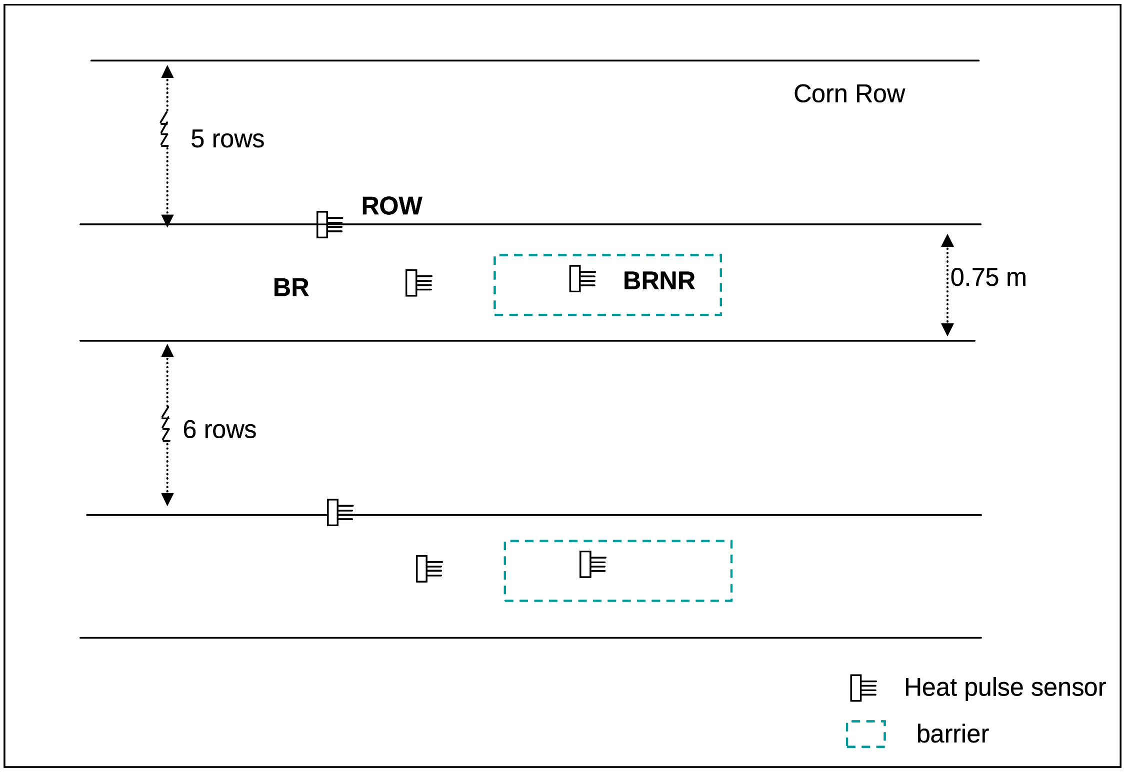

Figure 1: Heat pulse sensor installation at the ROW, BR and BRNR locations.

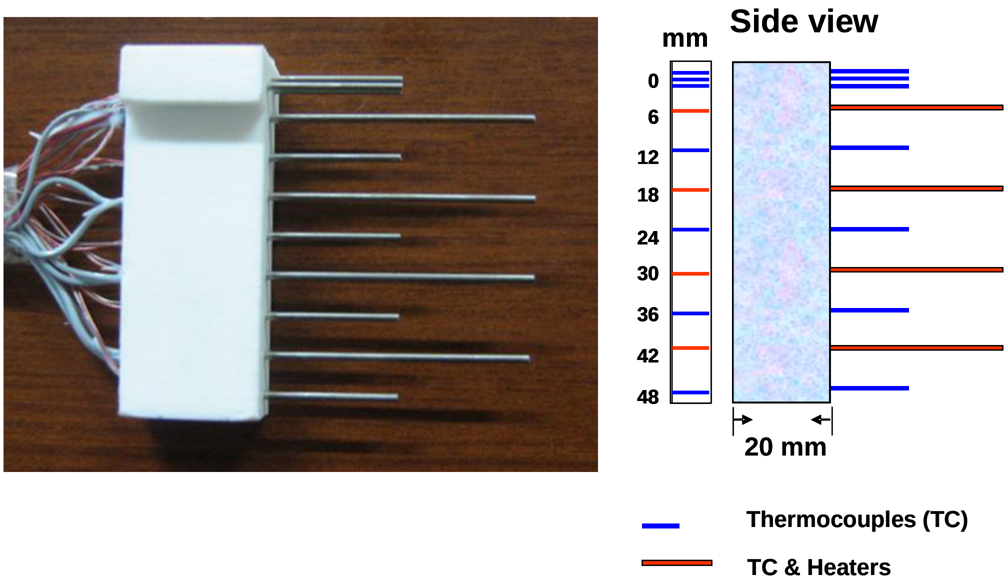

Figure 2: Photo and side view configuration of an 11-needle heat pulse sensor (photo courtesy of Pukhraj Deol).

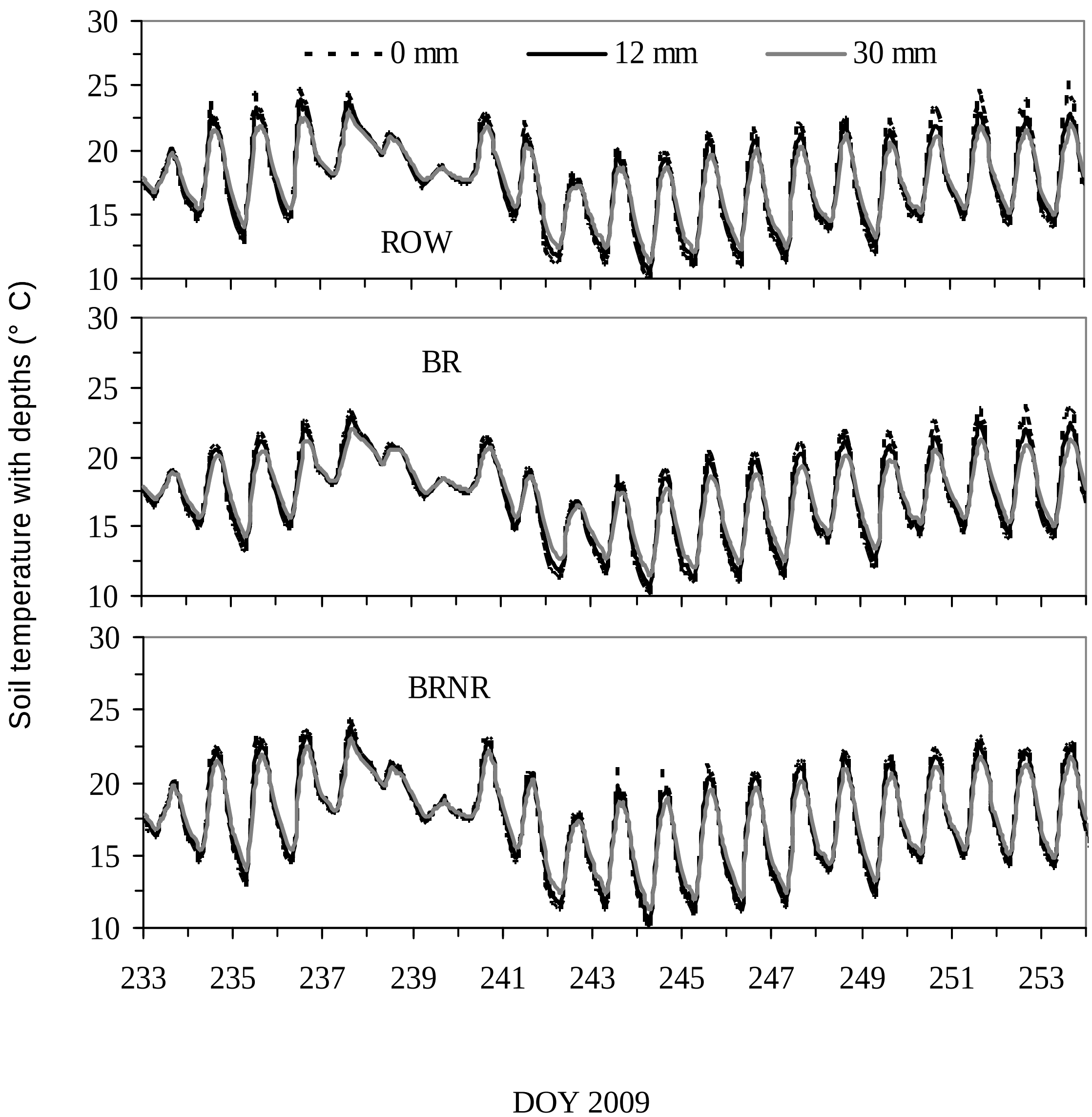

Figure 3: Soil temperature (°C) with time of various depths (soil temperatures at 6, 18, 24 and 36 mm not shown here) at the ROW, BR, and BRNR locations in the corn field.

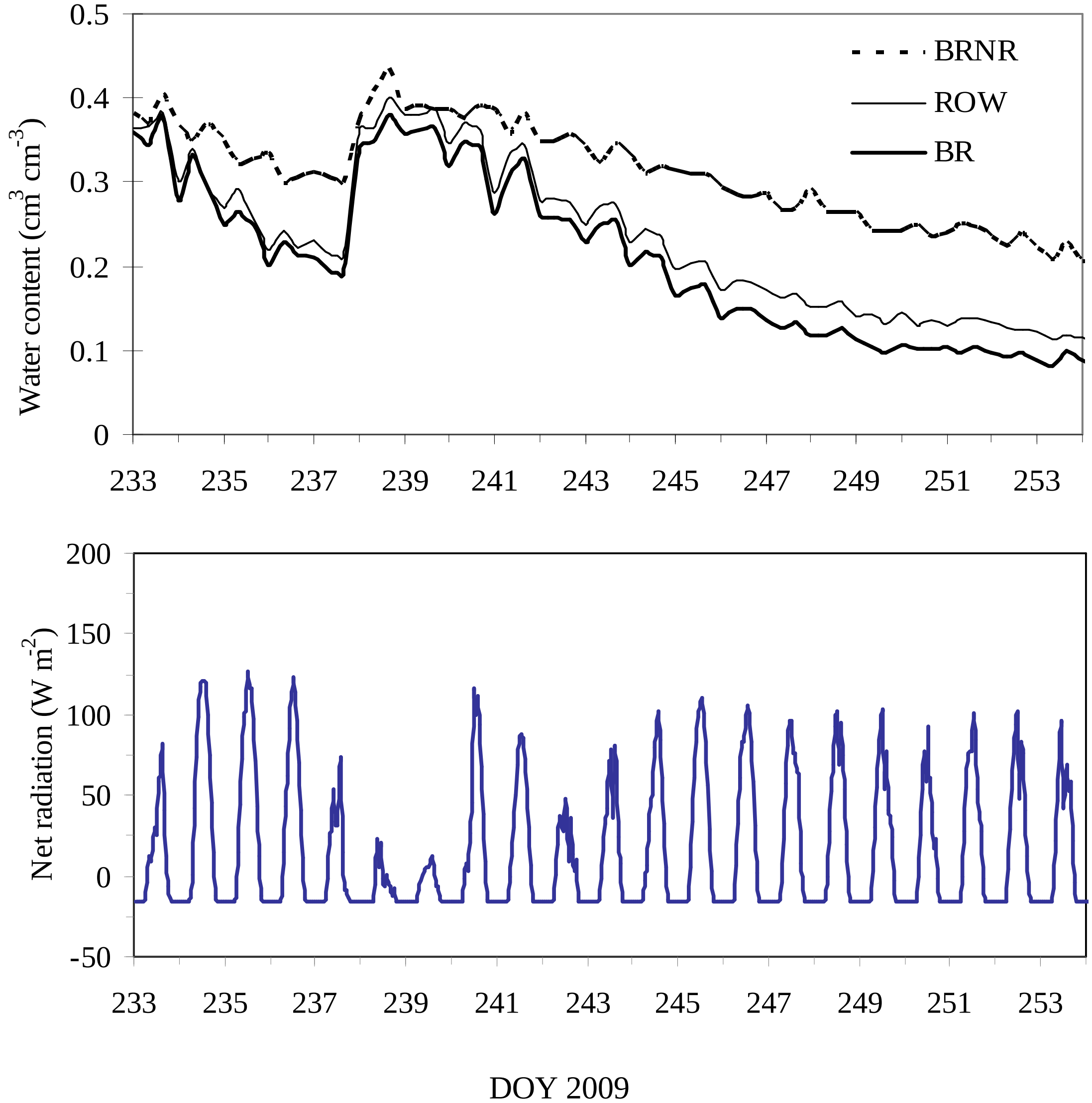

Figure 4: Soil water content (m^3 m^{-3}) (0-30 mm soil layer) measured by heat pulse sensors at the ROW, BR, and BRNR locations (Fig.4A); net radiation Rn (W m^{-2}) below the canopy (Fig.4B).

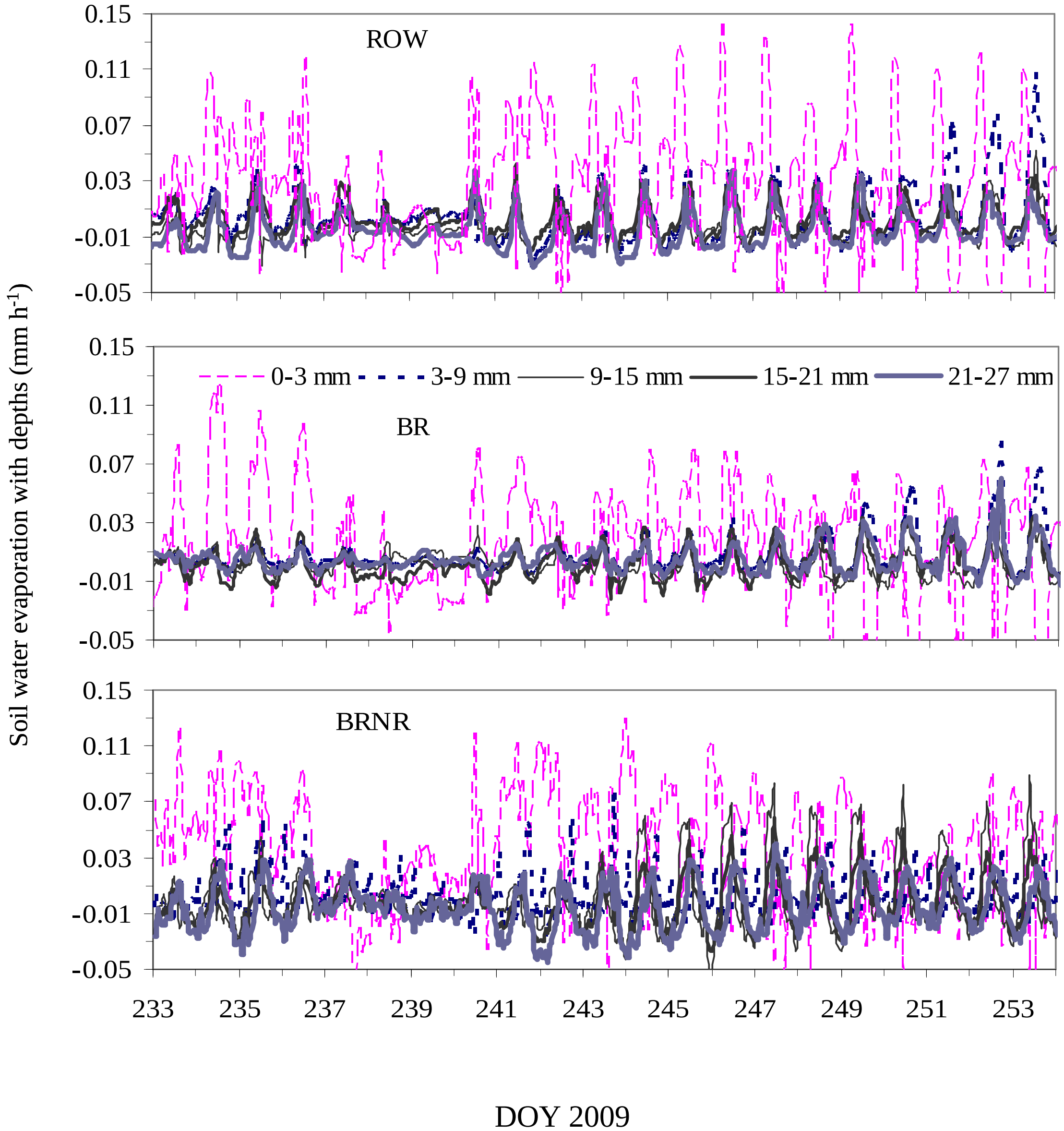

Figure 5: Soil water evaporation dynamics (0-3, 3-9, 9-15, 15-21, 21-27-mm soil depths) at the ROW, BR and BRNR locations in the corn field.

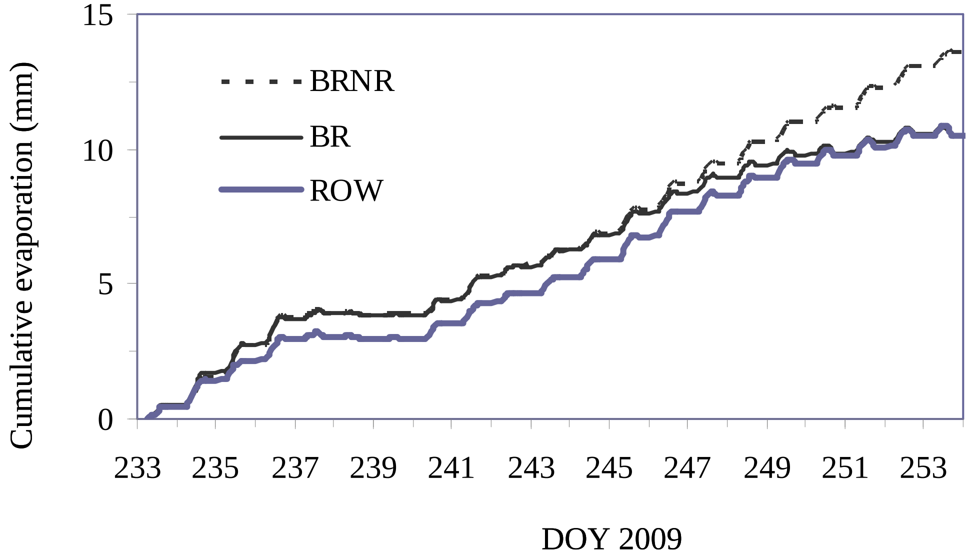

Fig 6: Cumulative surface soil water evaporation at the ROW, BR and BRNR locations in the corn field.

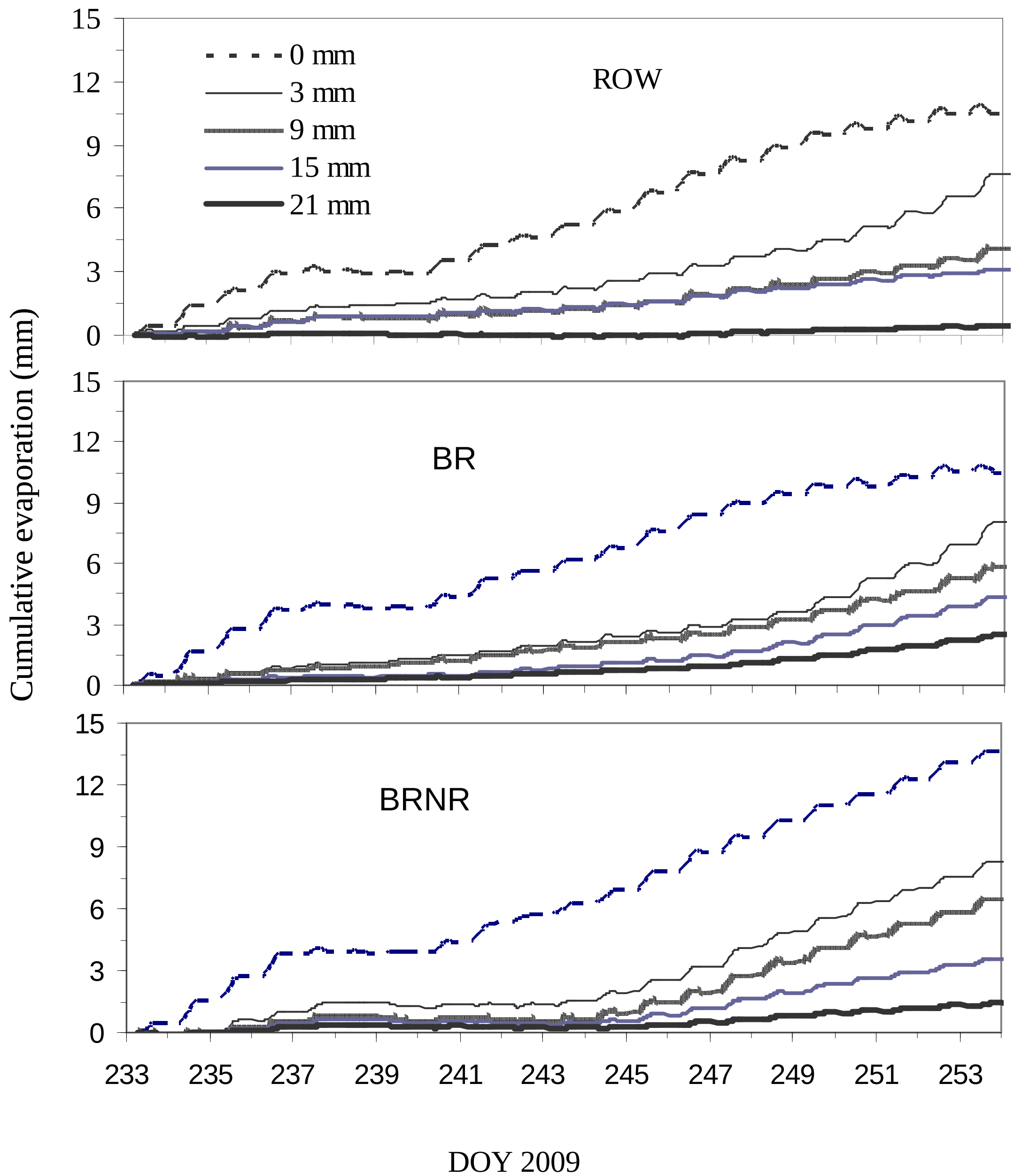

Figure 7: Cumulative soil water evaporation at various soil depths at the ROW, BR and BRNR locations in the corn field.

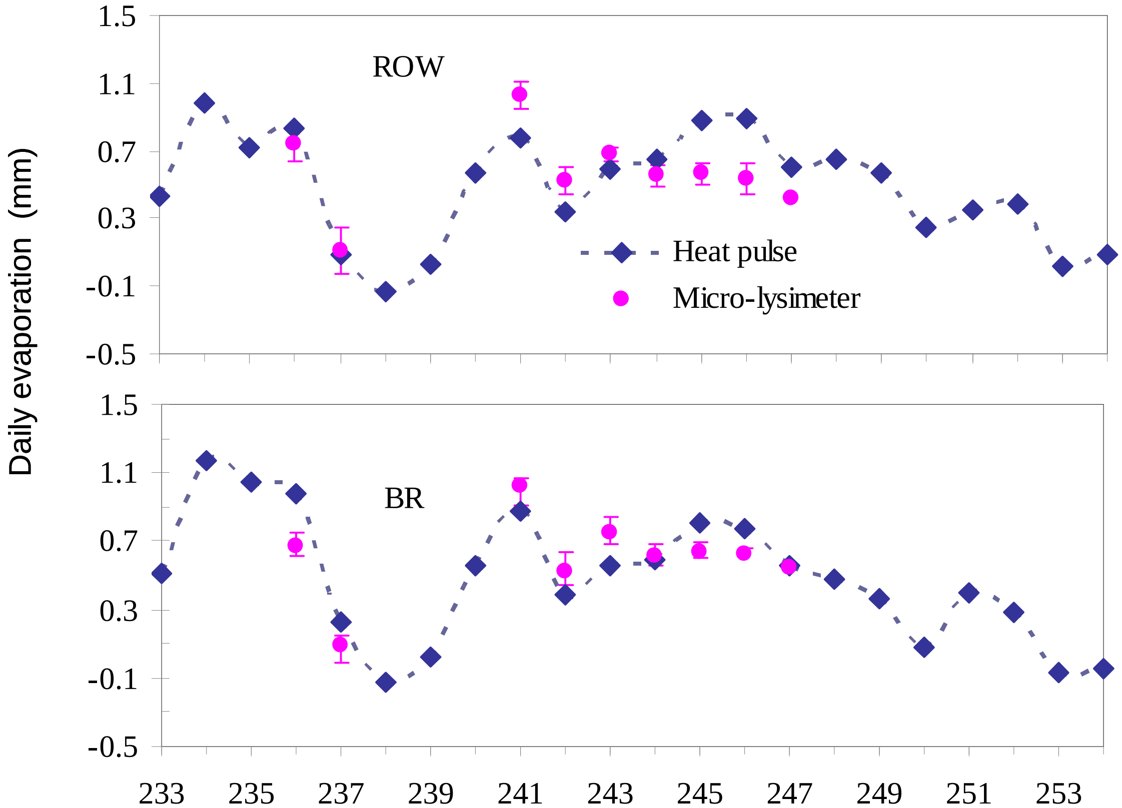

Fig. 8: Daily surface soil water evaporation from heat pulse and micro-lysimeter methods at the ROW and BR locations in the corn field. (error bars represent standard deviation of the micro-lysimeter measurement).

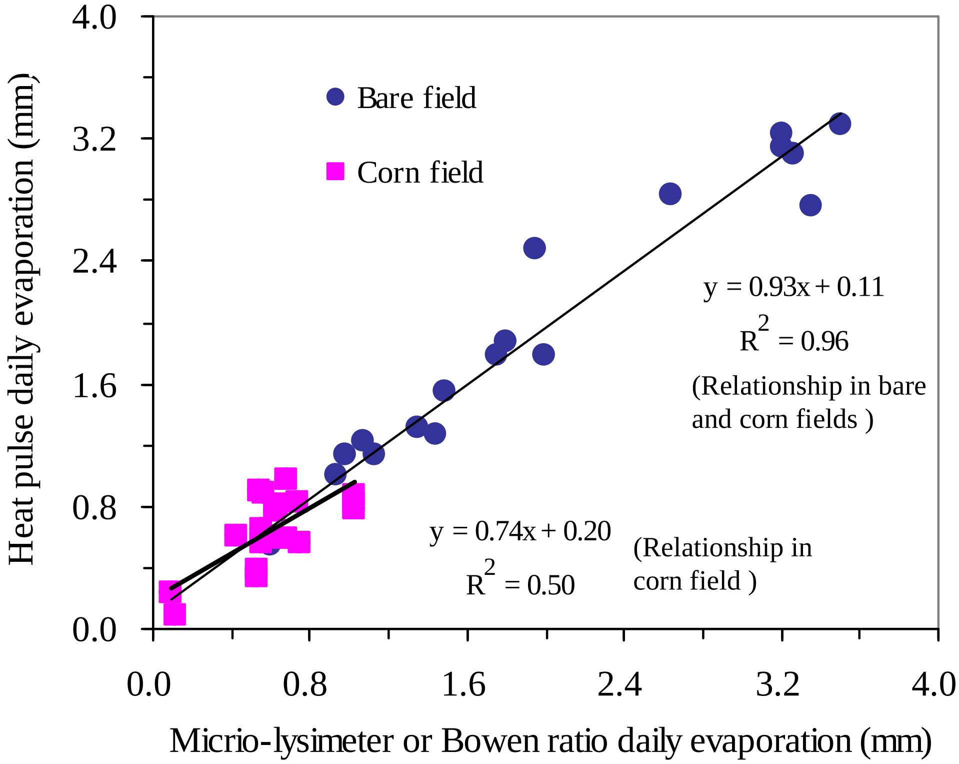

Fig.9: Comparison of heat pulse daily soil water evaporation estimates with micro-lysimeter and Bowen ratio daily soil water evaporation estimates. Bare field measurement data are from Heitman et al. (2008b).

Chapter 5 Partitioning evaporation and transpiration in a corn field

A paper to be submitted in the Agronomy Journal

X. Xiao, T.J. Sauer, J.W. Singer, R. Horton, J.L. Heitman and T. Ren

Abstract

Evapotranspiration (ET) is a major component of the hydrological cycle. It consists of soil water evaporation (E) and plant transpiration (T). Accurate partitioning of ET into E and T is challenging but can improve water balance determination at the field and regional scales and help quantify components of the hydrological cycle. In this study, we measured soil water E using heat pulse sensors, T using stem flow gauges, and ET using an eddy covariance system in a corn (*Zea mays L.*) field. Potential evapotranspiration ET_0 was also calculated with the Penman-Monteith equation. During a 12-day measurement period, ET was estimated from the sum of individually measured heat pulse E and stem flow T, eddy covariance measurements, and from Penman-Monteith calculations. All three estimates of ET had similar trends, with large ET values on sunny days, and small ET values on rainy days or with relatively small net radiation. ET_0 was larger than the individually measured E+T and eddy covariance ET. Eddy covariance ET was consistently lower than the individually measured E+T and the potential ET_0 during the measurement period. E, T, E+T and eddy covariance ET accounted for 13%, 77%, 90% and 61% of ET_0, respectively during the 12-day period. The three ways for estimating ET tracked similar in time but compared to the other two methods the eddy covariance measurements consistently underestimated ET.

Introduction

Evapotranspiration (ET) is the sum of soil water evaporation (E) and plant transpiration (T). E and T processes occur simultaneously, and it is very challenging to distinguish these fluxes. The common approach for partitioning ET is to measure ET and its components. Measurements of ET and one of the ET components are enough to partition ET. The lysimeter method (van Bavel, 1961) is a direct way to measure soil water E by measuring the water loss of lysimeters buried in the soil. The heat pulse method has been used recently as a means to measure soil water E over time and depth with minimum disturbance to soil based on sensible heat balance (Heitman et al., 2008a, Heitman et al., 2008b, Xiao et al., 2011). Sap flow gauges use heat as a tracer for sap movement to determine plant T based on heat balance (Sakuratani 1981; Heilman and Ham, 1990; Steinberg et al., 1990). Eddy covariance and Bowen ratio are widely used micrometeorological approaches for estimating ET (Wolf et al., 2008). Stable isotopes have been used to measure ET components by collecting samples of soil water, plant water and vapor at different depths and tracing the isotopic compositions of soil water E and plant T at steady state conditions (Williams et al., 2004; Rothfuss et al., 2010).

Several studies in various locations have been performed to partition ET into E and T. Tuzet et al. (1997) partitioned ET in a sparse canopy by measuring ET with eddy covariance and T with the sap flow method. They found that the partitioning of ET varies considerably with soil surface water availability. Jara et al. (1998) measured ET and its components in a corn field and found low agreement between E estimates from micro-lysimeters and E from the difference between Bowen ratio ET and sap flow T. Compared with eddy covariance and sap flow, Williams et al. (2004) found that stable isotopes were able to partition ET into E and T in an irrigated olive orchard. Singer et al. (2010) measured soil water E from micro-lysimeters and leaf T from the portable open path infrared gas analyzer (IRGA) in a soybean field. They reported that the sum of E and T did not agree well with eddy covariance ET.

Most efforts to partition ET only included measurements of two of the three values ET, E and T, with the third value being calculated from the two measured values. Such an approach does not provide enough information to fully evaluate the methods. In this study, we measured ET and its components E, T during wetting-drying periods in a corn field. We measured soil water E with heat pulse sensors, T with stem flow gauges, ET with an eddy covariance system, and we estimated potential ET_0 with the Penman-Monteith equation. Our objectives were to measure ET and its components and evaluate the consistency of the measurements.

Materials and Methods

The study was performed in a corn field with area 800 m by 1000 m located near Ames, Iowa (41.98°N, 93.68°W) during the summer of 2009. The field had been planted in a corn-soybean rotation for several years. The soil at the site was Canisteo clay loam (fine-loamy, mixed, superactive, calcareous, mesic Typic Endoaquolls). The surface soil bulk density was 1.2 Mg m^{-3}. The soil consisted of 44% sand, 30% silt and 26% clay, and the topography was relatively flat (slope < 2%).

Heat pulse sensor measurements

Based on sensible heat balance, the heat pulse method determines latent heat for soil water evaporation by measuring the net soil sensible heat flux and the heat storage change of selected soil layers. Soil sensible heat fluxes at the boundaries and the heat storage of a soil layer are determined from the soil thermal properties and the ambient soil temperature measured by heat pulse sensors (Heitman et al., 2008a and 2008b; Zhang et al., 2012; Xiao et al., 2012).

Eleven-needle heat pulse sensors were installed at both InRow (within rows) and BwRow (between rows) locations with the top sensor needle at the soil surface and the bottom sensor needle at a depth of 48 mm. The 11-needle heat pulse sensors used in this study were the same as those reported by Xiao et al. (2012). The heat pulse sensor consisted of four long parallel stainless steel needles (1.3 mm diameter, 40 mm length) (at soil depths: 6, 18, 30, 42 mm) and seven short parallel stainless steel needles (1.3 mm diameter, 20 mm length) (at soil depths: 0, 1, 2, 12, 24, 36, 48 mm).There was a chromel–constantan thermocouple in each needle for measuring ambient temperature at various depths. In each long needle there was also a resistance heater wire, through which a small current could be applied to generate a heat pulse, leading to temperature increases at the adjacent short needles. The temperature increases with time at the adjacent short needles were used to determine the thermal properties between the heat needle and the short needles (0-6, 1-6, 2-6, 6-12, 12-18, 18-24, 24-30, 30-36, 36-42, 42-48 mm). Using the measured ambient soil temperatures with depth and time and soil layer thermal properties determined by heat-pulse measurements, soil water evaporation rates were determined with time and depth for selected soil layers (3-9, 9-15, 15-21, 21-27, 27-33, 33-39 and 39-45 mm). The soil water evaporation in the 0-3 mm was estimated from net radiation, sensible heat flux and soil heat flux at the soil surface based on energy balance calculations (Xiao et al., 2012).

The heat pulse E used in this study was the average of E at InRow and BwRow locations. E was not detected at depths below 27 mm, so the E at each location was the sum of E from the 0-3, 3-9, 9-15, 15-21, 21-27 mm soil layers.

Stem flow gauge measurements

Whole-plant transpiration was measured from R1 (Ritchie et al., 1993) to physiological maturity (R6) using 19 mm Dynagage Sap Flow Sensors (Dynamax Inc., Houston, TX, USA). Sensors were installed on six consecutive maize plants approximately 0.3 m above the soil surface. Lower maize leaves and sheaths were removed to enhance sensor placement on the maize stem. Sensors were insulated with foam and covered with foil to minimize environmental fluctuations. Input voltage was set at 4.5 V for all sensors. Stem diameter was determined by averaging two measurements on opposite sides of the stem with electronic calipers approximately 0.3 m above the soil surface. Sap flow was measured using an energy balance method determined by a constant heat source (Sakuratani, 1981). Sap flow was measured every 60 s and averaged every 12 min with a CR5000 datalogger (Campbell Scientific, Inc.). Data collected from 0700 to 1900 h were used to calculate daily plant T. Sensors were moved two times during the measurement period to refresh the plants and to increase the number of plants involved in the study. The sensors were always deployed on six consecutive plants. A total of 18 plants were measured during the field study. Data were converted from g day^{-1} to mm water depth by multiplying by the plant density (average = 6.7 plants m^{-2}).

Eddy covariance system

An eddy-covariance flux station was positioned in the field 1.6 m above the soil surface or 1 m above the canopy when the canopy height was > 0.6 m. This station consisted of a fast-response open path H_2O vapor analyzer (LI-7500, LICOR Biosciences Inc., Lincoln, NE), a three-dimensional sonic anemometer (CSAT, Campbell Scientific, Inc., Logan, UT), a net radiometer (CNR 1, Kipp and Zonen, Delft, The Netherlands), and two soil heat flux plates (HFT-3, Radiation and Energy Balance Systems, Seattle, WA) 0.1 m below the soil surface. Pairs of soil thermocouples (copper-constantan) were placed 2 and 8 cm below the surface near each soil heat flux plate. Soil water content in the top 0.1 m at each site was measured with a soil moisture sensor (ML2X, Delta-T Devices, Burwell, Cambridge, UK). Signals from all sensors were recorded at 10 Hz, and 15-min averages stored in a datalogger (CR 5000, Campbell Scientific Inc., Logan, UT). Turbulent fluxes were corrected following the density correction of Webb–Pearman–Leuning (Webb et al., 1980). Soil heat flux plate data were corrected for heat storage in the surface soil layer using measured soil temperature and water content (Sauer, 2002).

Data were screened for anomalous values beyond pre-selected ranges. With the exception of rainy periods, intervals of missing data were gap filled using an iterative interpolation technique (Hernandez-Ramirez et al., 2009). The energy balance was forced closed following Twine et al. (2000)

Penman-Monteith equation predicted potential ET

Potential ET_0 could be estimated from Penman-Monteith method (Allen et al., 1998).

$$ET_0 = \frac{0.408\Delta\left(R_n - G_0\right) + \gamma \frac{900}{T + 273} U_2\left(e_s - e_a\right)}{\Delta + \gamma\left(1 + 0.34 U_2\right)}$$

where *R*n is the net radiation at the crop surface (W m^{-2}), *G* is the soil heat flux density (W m^{-2}), *T* is the air temperature at 2 m height (°C), u_2 is the wind speed at 2 m height (m s^{-1}), e_s is the saturation vapor pressure (kPa), e_a is the actual vapor pressure (kPa), Δ is the slope of the relationship between saturation vapor pressure and air temperature (kPa K^{-1}) and γ is the psychrometric constant (0.067 kPa C^{-1}).

Results and Discussion

Measurements were performed in 12 consecutive days (DOY 233 to 245) in the summer of when corn leaf area index (LAI) values were between 4.0 and 4.3. Daily values of the measurements used in this study included the sum of daytime values from 7:00 to 19:00 each day. Two rainfall events occurred during the measurement period: DOY 230 to 233 (33 mm), and DOY 237 to 239 (30 mm).

ET partitioning into E and T

E obtained from the heat pulse sensor measurements agreed well with E from micro-lysimeters methods in the corn field (Xiao, et al., 2012). Values of daily heat pulse E, stem flow T, E+T, percentage ET components, rain, and net radiation over the canopy are shown at Table 1. During the measurement period, E accounted for a small portion of the total E+T. E ranged from 0.01 to 1.08 mm with an average daily value of 0.56 mm, and stem flow T ranged from 0.29 to 5.29 mm with an average daily value of 3.34. E and T accounted for 1-18% and 82-99% of the total measured E+T, respectively. E and T were relatively small (Fig. 2) when the net radiation was relatively small (≤10 MJ m^{-2}, e.g., DOY 233, 237 to 239 and 242) and E and T were relatively larger when the net radiation was relative large (e.g., DOY 234 to 236, 240 to 241, and 243 to 245) (Fig. 1A). The increase of T was larger than E when the net radiation increased. The T-fraction was larger at large net radiation than at low net radiation. The fractions of E and T to ET vary with crop system, crop growth stages, surface soil condition, and climatic and environmental conditions. When the available net radiation was small ((≤8 MJ m^{-2}), the fraction of E (E%) was small (≤11%) even when the soil was wet on DOY 237 to 239 and 242. The fraction of E (E%) was large (between 13 and 18%) when the net radiation was large (Rn ≥8 MJ m^{-2}). Jara et al. (1998) reported comparable partitioning results when the leaf area index was 3.9 in a corn field. They reported that E was <25% of ET as determined with micro-lysimeters and Bowen ratio measurements.

Comparison of ET estimates from different methods

ET estimates were obtained in three ways, the individually measured E+T, the eddy covariance measurements of ET and the potential ET_0 calculated from the Penman-Monteith equation.

The diurnal ET estimates from the three methods are shown in Fig. 3. All three estimates of ET had similar trends, with large ET values on sunny days, and small ET values for rainy days or for low net radiation days. The ET estimates for the rainy days (DOY 233, 237, 238, 239) were lower than those for the sunny days during the measurement period. Although no rain occurred on DOY 242, the ET estimates were relatively small because the Rn (8 MJ m^{-2}) relatively was small (Fig. 1A). Zhang et al. (2011) found that daily sap flow T increased linearly with solar radiation in a vineyard.

Slightly different daily ET values were obtained for each day. Individually measured daily E+T ranged from 0.32 to 6.18 mm with an average daily value of 3.90 mm, eddy covariance ranged from 0.06 to 4.60 mm with an average daily value of 2.63 mm, and potential ET_0 from the Penman-Monteith equation ranged from 1.12 to 6.10 mm with an average daily value of 4.32 mm. Potential ET_0 represents the ET rate of a short green crop, completely shading the ground, with uniform height and adequate water status in the soil profile. Thus, it was reasonable for ET_0 values to be larger than the individually measured E+T and eddy covariance ET. During the measurement period, individually measured E+T and eddy covariance ET accounted for 90% and 61% of ET_0 (Fig. 5). Individually measured E+T was close to ET_0 on rainy days or on low net radiation days, and the difference between E+T and ET_0 increased with increasing net radiation and soil drying (Fig. 3 and Fig. 4). Eddy covariance ET was consistently lower than individually measured E+T and potential ET_0. The disparities between eddy covariance ET and the other two ET measurements may be due to combination of factors. One possible reason was difference in spatial scales among the methods. Individual measurements of E+T from heat pulse and stem flow methods represent a meter scale while eddy covariance ET and potential ET_0 estimation represent hundreds of m scale. Individual measurements of E and T at a small spatial scale may not represent all of the corn plants within the footprint of the eddy covariance flux measurements. Indeed, in the corn field we observed variation in LAI. Corn plants close to the heat pulse sensors and stem flow gauges had LAI of 4.1 while LAI at the other field locations was only 3.7. Thus, the corn samples we chose for stem flow gauge measurement of T may not fully represent the entire area sampled by the eddy covariance system. Eddy covariance measurements may underestimate ET, or individual component measurements of E and T may overestimate ET due to measurement errors or bias that we have not yet discovered. During the measurement period, the soil was wet and there was little water stress in the soil-plant system, but the ET estimates from the eddy covariance measurements were consistently lower than the ET_0. The cumulative ET was 61% of ET_0. Eddy covariance ET also was consistently lower than individually measured E+T, and the cumulative ET was 68% of E+T during the measurement period. These are evidences that the eddy covariance tended to underestimate ET. Singer et al. (2010) reported that eddy covariance ET underestimated individually measured E from micro-lysimeters and T from the portable open path IRGA method.

Although the disparities existed among the three methods, the individually measured E+T was highly correlated with eddy covariance ET and with ET_0 (Fig. 6). Eddy covariance ET was lower than the individually measured E+T with R^2=0.95, slope=0.79 and intercept=-0.47 mm. And ET_0 was slightly larger than the individually measured E+T with R^2=0.95, slope=0.97 and intercept= 0.52 mm.

Conclusions

E accounted for a small portion of the individually measured E+T (1-18%) values while T accounted for a large portion of E+T (82-99%) during the measurement period. The trends of eddy covariance ET, individually measured E+T and ET_0 were similar, with small ET estimates observed on the rainy days and on low net radiation days, and large ET estimates observed on sunny days. The eddy covariance ET was consistently smaller than the individually measured E+T and both were smaller than ET_0 from the Penman-Monteith equation. Individually measured E+T and eddy covariance ET accounted for 90% and 61%, respectively, of ET_0 during the measurement period. The measured E and T accounted for 14% and 86%, respectively, of the sum of the total measured E+T. Thus, we concluded that the three methods for ET estimations tracked similar with time, but the eddy covariance measurements consistently underestimated ET.

Acknowledgments

This work was supported by the National Science Foundation under Grant 0809656, by ConocoPhillips Company, and by the Hatch Act, State of Iowa, and State of North Carolina funds.

References

Allen, R.G., L.S. Pereira, D. Raes, D., and M. Smith. 1998. Crop evapotranspiration, guidelines for computing crop water requirements. FAO Irrig. and Drain. Paper 56, Food and Agric. Orgn. of the United Nations, Rome, Italy. 300 pp.

Heilman, J.L. and J.M. Ham. 1990. Measurement of mass flow rate of sap in ligustrum japonicum. Amer. Soc. Hort. Sci. 25:465-467.

Heitman, J.L., R. Horton, T.J. Sauer and T.M. DeSutter. 2008a. Sensible heat observations reveal soil water evaporation dynamics. J. Hydrometeor. 9: 165-171.

Heitman, J.L., X. Xiao, R. Horton and T.J. Sauer. 2008b. Sensible heat measurements indicating depth and magnitude of subsurface soil water evaporation. Water Resour. Res. 44, W00D05

Hernandez-Ramirez, G., J.L. Hatfield, T.B. Parkin, J.H. Prueger, and T.J. Sauer. 2009. Energy balance and turbulent flux partitioning in a corn-soybean rotation in the Midwestern U. S. Theor. Appl. Climatol. DOI:10.1007/s00704-009-0169-y.

Jara, J., C.O. Stockle, and J. Kjelgaard. 1998. Measurement of evapotranspiration and its components in acorn (ZeaMaysL.) field. Agric. For. Meteorol. 92 (2):131–145.

Ritchie, S.W., J.J. Hanwayand and G.O. Benson 1993. How a corn plant develops. Spec. Rep. 48. Iowa State Univ. Coop. Ext. Serv., Ames, IA.

Rothfuss, Y., P. Biron, I. Braud, L.Canale, J. Durand, J. Gaudet, P. Richard, M.Vauclin and T. Bariac. 2010. Partitioning evapotranspiration fluxes into soil evaporation and plant transpiration using water stable isotopes under controlled conditions. Hydrol. Process. 24:3177–3194.

Sakuratani, T. 1981. A heat balance method for measuring water flux in the stem of intact plants. Agric. Meteorol. 37:9-17.

Sauer, T.J. 2002. Heat flux density. pp. 1233-1248, In: Dane, J. D. and G. C. Topp, (ed.) Methods of Soil Analysis – Part 1, Physical and Mineralogical Methods. Amer. Soc. of Agron. Madison, WI.

Singer, J.W., J.L Heitman, G. Hernandez Ramirez, T.J. Sauer, J.H. Prueger, and J.L. Hatfield. 2010. Contrasting methods for estimating evapotranspiration in soybean. Agric. Water Manage. 98(1):157-163.

Steinber, S., C.H.M. van Bavel, and M.J. Mcfarland. 1988. A gauge to measure mass flow rate of sap in stems and trunks of woody plants. Amer. Soc. Hort. Sci. J. 114:466-472.

Tuzet, A., J. Castell, A. Perrier, O. Zurfluh. 1997. Flux heterogeneity and evapotranspiration partitioning in a sparse canopy: the fallow savanna. J. Hydrol. Volumes 188–189, P 482–493.

Twine, T.E., W.P. Kustas, J.M. Norman, D.R. Cook, P.R. Houser, T.P. Meyers, J.H. Prueger, P.J. Starks, and M.L.Wesely. 2000. Correcting eddy-covariance flux underestimates over a grassland. Agric. For. Meteorol. 103:279–300.

van Bavel, C.H.M, 1961. Lysimetric measurements of evapotranspiration rates in the eastern United States, Soil Sci. Soc. Am. J. 25:138-141.

Webb, E.K., G.I. Pearman, and R. Leuning. 1980. Correction of flux measurements for density effects due to heat and water vapor transfer. Quart. J. Royal Meteorol. Soc. 106:85-100.

Williams, DG., W. Cable, K. Hultine, J.C.B. Hoedjes, E.A. Yepez , V. Simonneaux, S. Er-Raki, G. Boulet, H.A.R. de Bruin, A. Chehbouni, O.K. Hartogensis, and F. Timouk. 2004. Evapotranspiration components determined by stable isotope, sap flow and eddy covariance techniques. Agric. For. Meteorol. 125:241–258.

Wolf, A., S. Nick, A. Kanat, A. J. Douglas, and L.Emilio. 2008. Effects of different eddy covariance correction schemes on energy balance closure and comparisons with the modified Bowen ratio system. Agric. For. Meteorol. 148:942–952.

X. Xiao, R. Horton, T.J. Sauer, J.L. Heitman and T. Ren. 2011. Cumulative evaporation as a function of depth and time. Vadose Zone J. 10:1016-1022.

X. Xiao, R. Horton, T.J. Sauer, J.L. Heitman and T. Ren. 2012. Heat pulse sensor measurements of soil water evaporation in a corn field (in review).

Zhang, Y., S. Kang, E.J. Ward, R. Ding, X. Zhang, and R. Zheng. 2011. Evapotranspiration components determined by sap flow and microlysimetry techniques of a vineyard in northwest China: Dynamics and influential factors. Agric. Water Manag. 98 (8):1207–1214.

Zhang, X., S. Lu, J.L. Heitman, R. Horton and T. Ren. 2012. Subsurface soil-water evaporation with an improved heat-pulse probe. Soil Sci. Soc. Am. J. 76: 3:876-879.

Figure Captions

Table 1: Heat pulse daily soil water evaporation E, stem flow daily transpiration T, E+T (mm), percentage of E and T of E+T (E%, T%), daily rain(mm) and daily net radiation (MJ m^{-2}) from day of year, DOY 233 to 245.

Fig. 1 A: daily net radiation (Rn, MJ m^{-2}) and daily rain (mm), B: soil water content at 0-30 mm (cm^3 cm^{-3}), and C: air temperature (°C) and VPD (vapor pressure difference, kPa)

Fig. 2: Measured heat pulse E and stem flow T, T accounted for a major portion while E accounted for a minor portion.

Fig. 3: Diurnal ET estimates (mm h^{-1}) from the sum (E+T) of measured heat pulse E and stem flow T, eddy covariance ET and potential ET_0 from Penman-Monteith method.

Fig. 4: Daily ET estimates (mm) from the sum of individually measured E+T from heat pulse sensors and stem flow gauges, Eddy covariance ET and potential ET_0 from the Penman-Monteith equation.

Fig. 5: Cumulative ET (mm) components during measurement period (E from heat pulse sensors, T from stem flow gauges, ET from eddy covariance system, E +T is the sum of heat pulse E and stem flow T, potential ET_0 from the Penman-Monteith equation), E, T, E+T accounted for 13%, 61%, 77%, 90% respectively of potential ET_0.

Fig. 6: Relationships between individually measured E +T and eddy covariance ET and between potential ET_0 and E+T (the dash lines are 1:1).

Table 1: Heat pulse daily soil water evaporation E, stem flow daily transpiration T, E+T (mm), percentage of E and T of E+T (E%, T%), daily rain(mm) and daily net radiation (MJ m^{-2}) from day of year, DOY 233 to 245.

	mm			%		mm	MJ m^{-2}
DOY	Heat pulse E	Stem flow T	E+T	E%	T%	Rain	Net radiation
233	0.47	2.61	3.08	15	85	1	10
234	1.08	4.95	6.03	18	82		20
235	0.89	5.29	6.18	14	86		20
236	0.91	4.70	5.60	16	84		20
237	0.16	2.55	2.70	6	94	1	8
238	0.01	0.86	0.87	1	99	23	4
239	0.02	0.29	0.32	7	93	7	4
240	0.56	3.51	4.07	14	86		14
241	0.83	4.07	4.90	17	83		14
242	0.36	2.84	3.20	11	89		8
243	0.58	4.03	4.61	13	87		13
244	0.62	3.84	4.46	14	86		14
245	0.85	3.82	4.67	18	82		17

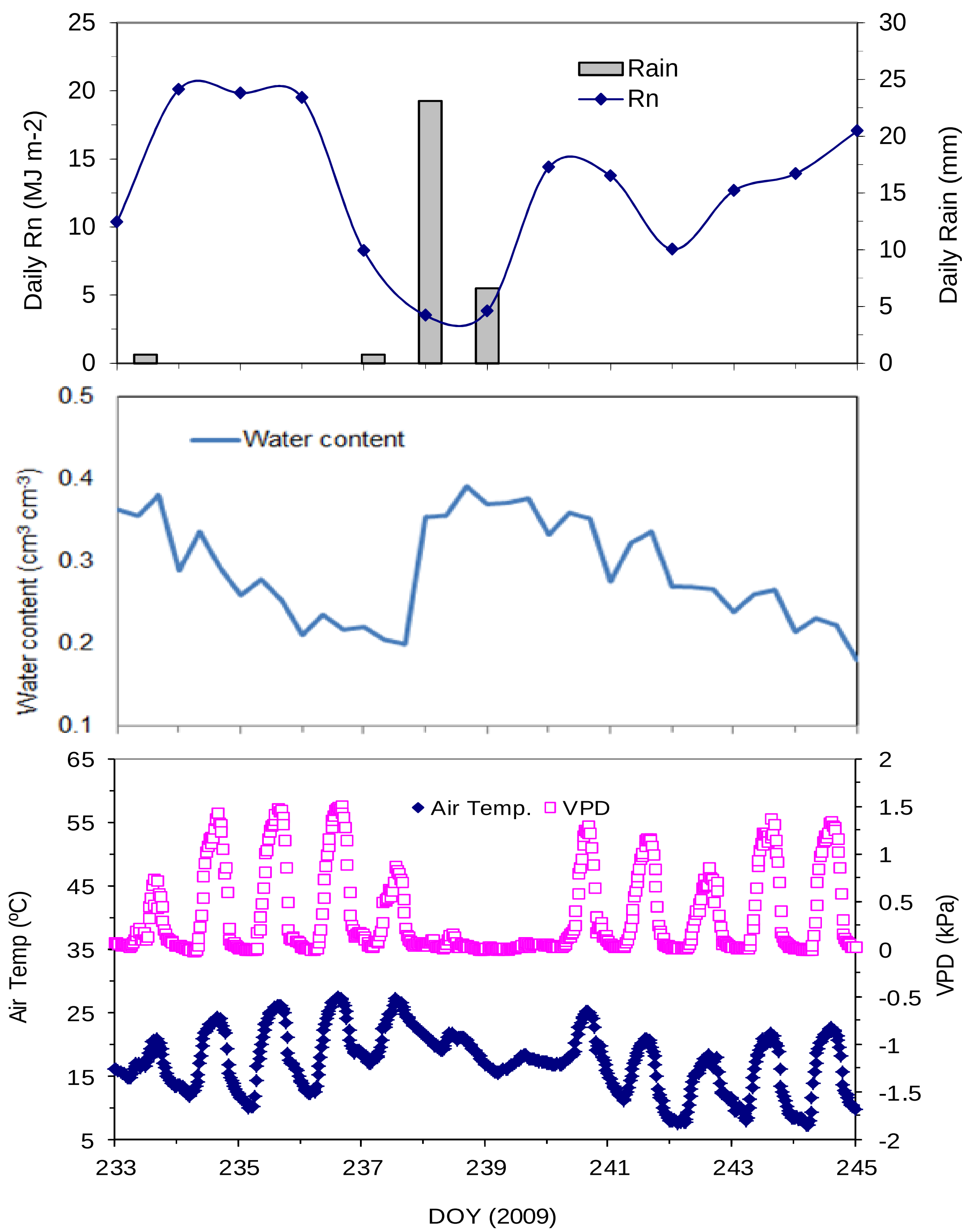

Fig. 1 A: daily net radiation (Rn, MJ m^{-2}) and daily rain (mm), B: soil water content at 0-30 mm (cm^3 cm^{-3}), and C: air temperature (°C) and VPD (vapor pressure difference, kPa)

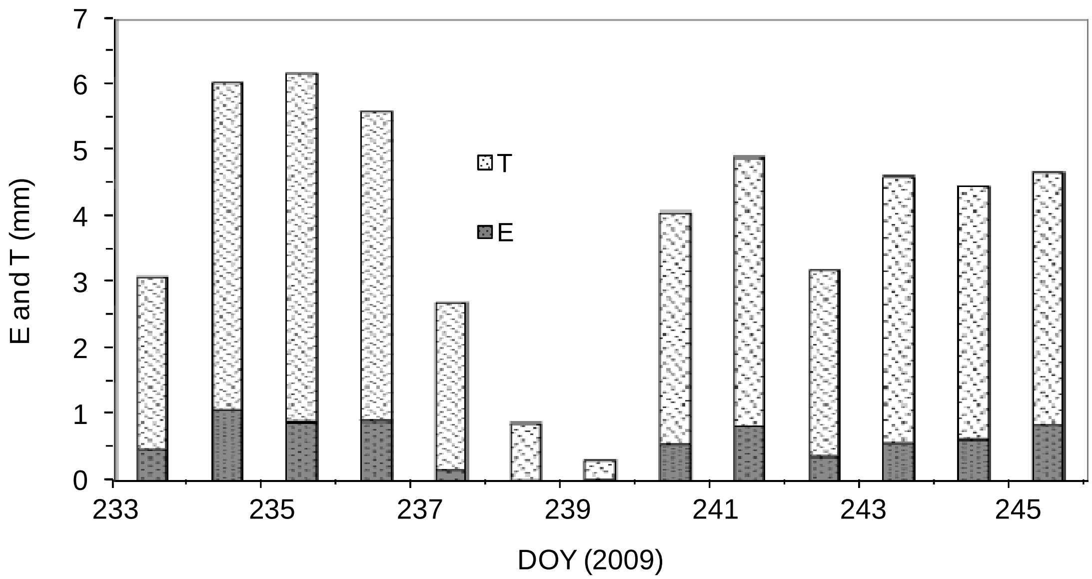

Fig. 2: Measured heat pulse E and stem flow T, T accounted for a major portion while E accounted for a minor portion.

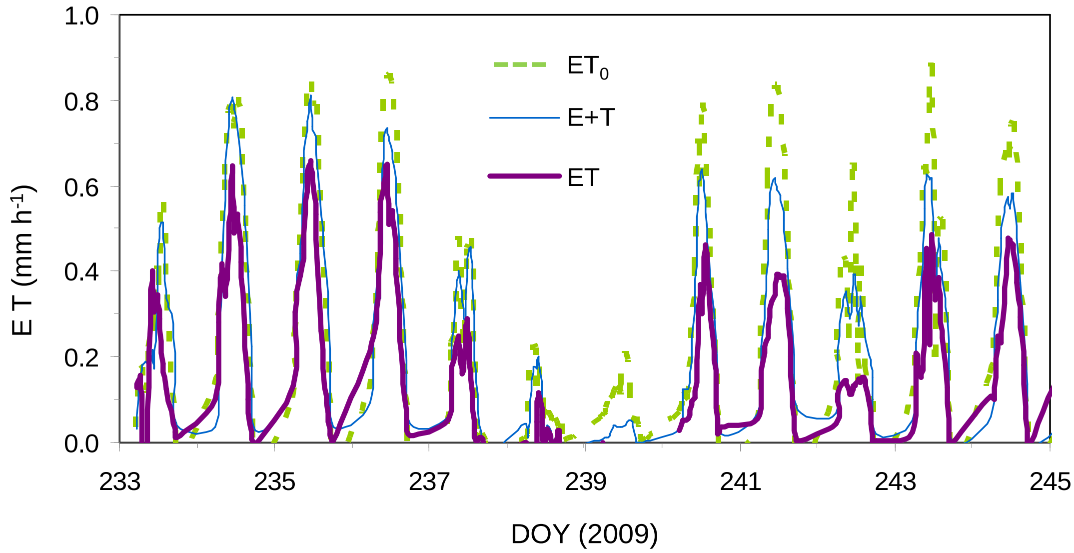

Fig. 3: Diurnal ET estimates (mm h^{-1}) from the sum (E+T) of measured heat pulse E and stem flow T, eddy covariance ET and potential ET_0 from Penman-Monteith method.

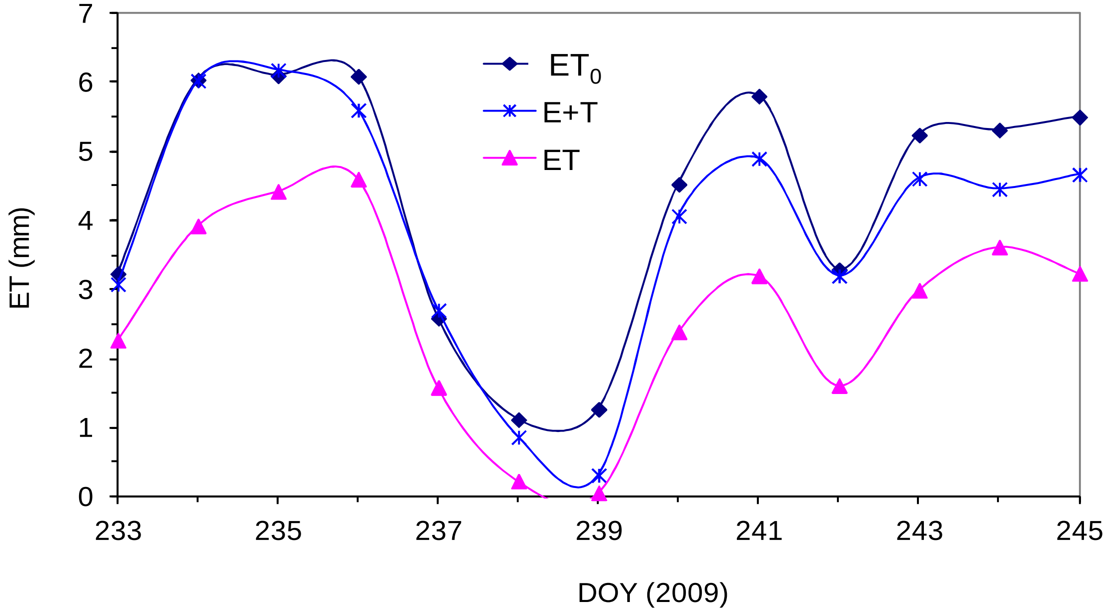

Fig. 4: Daily ET estimates (mm) from the sum of individually measured E+T from heat pulse sensors and stem flow gauges, Eddy covariance ET and potential ET_0 from the Penman-Monteith equation.

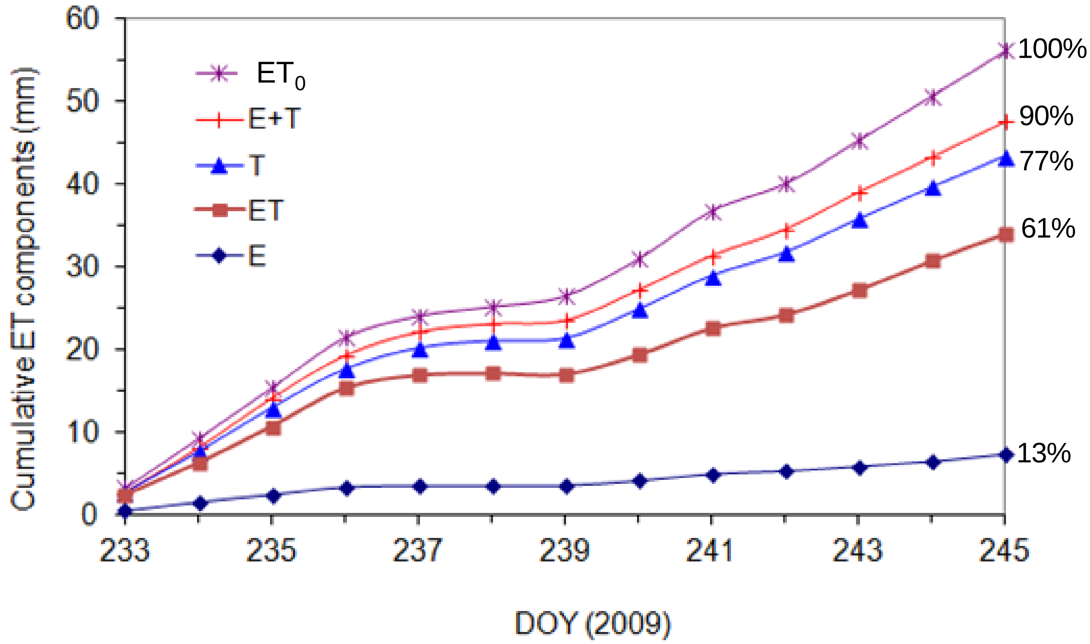

Fig. 5: Cumulative ET (mm) components during measurement period (E from heat pulse sensors, T from stem flow gauges, ET from eddy covariance system, E +T is the sum of heat pulse E and stem flow T, potential ET_0 from the Penman-Monteith equation), E, T, E+T accounted for 13%, 61%, 77%, 90% respectively of potential ET_0.

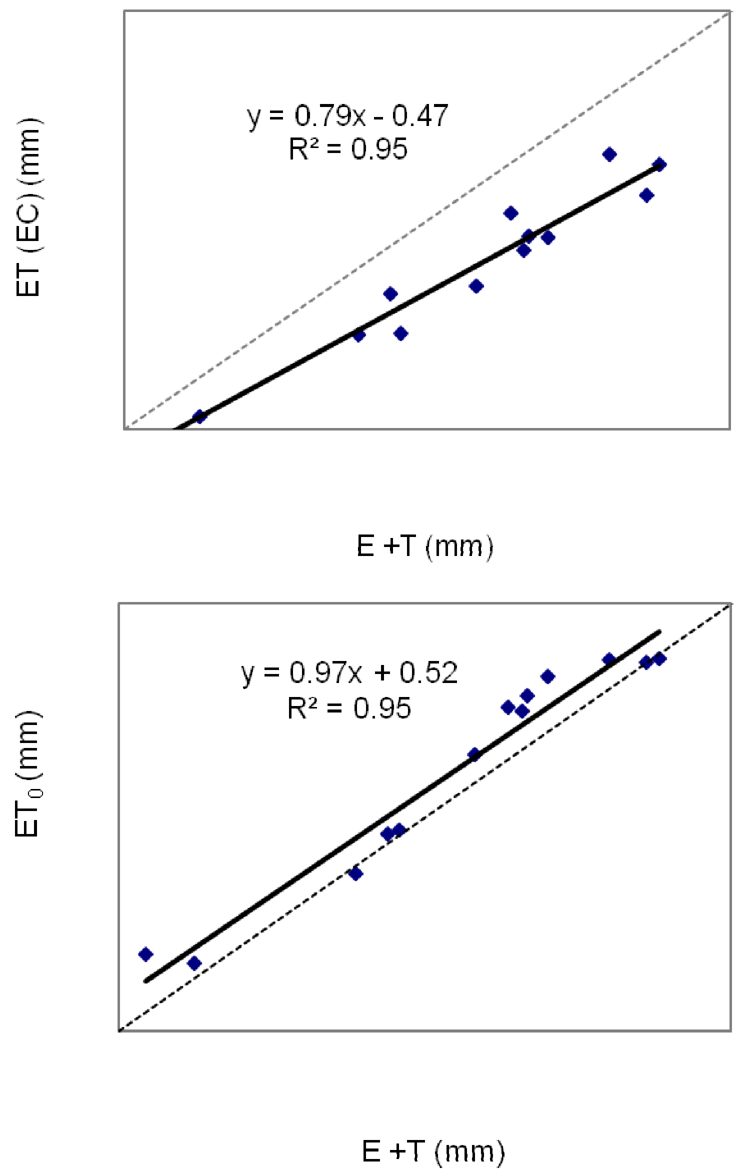

Fig. 6: Relationships between individually measured E +T and eddy covariance ET and between potential ET_0 and E+T (the dash lines are 1:1).

Chapter 6 Soil carbon dioxide fluxes with time and depth in a bare field

A paper to be submitted in the Agricultural and Forest Meteorology Journal

X. Xiao, T.J. Sauer, R. Horton

Abstract

Soil carbon dioxide (CO2) efflux is an important component of the terrestrial carbon cycle, and the amount of CO2 emitted from soil to atmosphere has significant effects on the soil-atmosphere system. The objectives of this study are 1) to determine bare soil CO2 fluxes with time and depth with a concentration gradient method that uses measured soil CO2 concentrations and estimated gas diffusion coefficients, 2) to estimate CO2 production with time and depth in a bare soil, 3) to compare surface CO2 effluxes determined by the gradient method and by a closed-chamber method. Soil CO2 concentrations were measured by solid-state sensors. Observed CO2 concentrations were used with a gradient method to calculate soil CO2 fluxes with time and depth. Surface CO2 fluxes were also measured automatically with long-term chambers. Results showed that soil CO2 concentrations increased with soil depth, while soil CO2 fluxes decreased with soil depth. For a 12 day period, 8% of the cumulative soil CO2 was produced below a depth of 175 mm, 2% was produced in the 100-175 mm soil layer, and 90% was produced in the 0- 100 mm soil layer. The CO2 concentration gradient effluxes and the closed-chamber CO2 effluxes agreed well of the gradient daily mean CO2 fluxes within the range of the closed-chamber measurements on 10 out 12 days. Thus, there is evidence

that the concentration gradient method was able to accurately measure bare field soil CO_2 fluxes and soil production rates with time and depth.

Introduction

Soil CO_2 efflux is an important component of the carbon cycle that influences global climate and soils (Neung et al., 2005). Several methods have been developed for measuring soil CO_2 efflux (Hutchinson and Livingston, 2002). Two common techniques for measuring soil CO_2 fluxes from the soil surface are chamber-based (Pumpanen et al., 2004) and eddy covariance methods (Tang et al., 2003). Chamber-based methods include open-chamber and closed-chamber approaches that can be used to directly measure CO_2 efflux at a small scale (Norman et al., 1992). Recently, long-term chambers have been developed to automatically and continuously measure CO_2 efflux simultaneously at several locations in order to monitor the spatial and temporal variation of CO_2 efflux distribution (Savage and Davidson, 2003; Xu et al., 2010). Eddy covariance can provide continuous measurements of soil CO_2 efflux without disturbing the soil (Law et al., 1999).

Chamber-based measurements and eddy covariance measurements do not provide information on CO_2 fluxes with depth in soil profiles. Soil CO_2 concentration can impact plant growing conditions in agricultural or forest settings, and the CO_2 efflux is generated by a combination of biotic, chemical and physical processes that take place in the soil (Tang, et al. 2003). Soil temperature and soil moisture are two main factors that impact these soil processes and the movement of CO_2 in the soil (Davidson et al., 1998; Treonis et al., 2002).

A concentration gradient method, based on Fick's diffusion law, is able to estimate CO_2 fluxes within the soil profile. Tang et al. (2003), DeSutter et al. (2008) and Turcu et al. (2005) used a concentration gradient method to estimate CO_2 fluxes in the soil profile by measured soil CO_2 concentrations and model estimated gas diffusion coefficients. Tang et al. (2003), DeSutter et al. (2008) and Turcu et al. (2005) only measured CO_2 concentrations at a few soil depths, and the experiments were conducted in a corn-soybean rotation field, in an oak-grass savanna and in a laboratory soil column, respectively. Since CO_2 concentrations at only a few depths were measured, the concentration gradient and gas diffusion coefficient near the soil surface varied largely depending on the methods for estimating them. DeSutter et al. (2008) used six methods to estimate CO_2 concentration gradients and three models to predict diffusion coefficients and found that some gradient method CO_2 fluxes were over a hundred times larger than the CO_2 fluxes measured by an automated sampling chamber.

In order to accurately measure soil CO_2 fluxes and soil CO_2 production rates with time and depth, in this study, the concentration gradient method, detailed below, was used to estimate soil CO_2 fluxes with time and depth in a bare field. We measured soil CO_2 concentration at 13 soil depths, from the surface to a depth of 200-mm during a natural wetting and drying period. In situ measurements of soil water content and soil temperature were also made. The objectives of this study were 1) to determine bare soil CO_2 fluxes with time and depth with a concentration gradient method that used measured soil CO_2 concentrations and estimated gas diffusion coefficients with time and depth, 2) to estimate CO_2 production with time and depth in the soil 3) to compare surface CO_2 effluxes determined by the gradient method with closed-chamber measurements.

Methods and Instruments

Site description

The study was performed in a 125 m by 125 m bare field located near Ames, Iowa (41.98°N, 93.68°W) during the summer of 2008. The soil at the site was a Canisteo clay loam (a fine loamy, mixed, superactive, calcareous, mesic Typic Endoaquoll). The surface soil bulk density was 1.2 Mg m^{-3}. The soil consisted of 44% sand, 30% silt, and 26% clay, and the topography was relatively flat (slope <2%). Prior to this study the field was tilled, and during the study it was kept bare by spraying herbicides to control plant growth.

Gradient method for determining CO2 fluxes

Thirteen solid-state sensors (GMT 222 and GMT 221, Vaisala, Finland) with three measurement ranges (GMT221, 0-1%; GMT221, 0-3%; GMT222, 0-10%) were used to measure CO2 concentration from the soil surface to 200-mm depth. Probes with a range 0-1% were buried at depths of 0- and 3-mm, probes with a range 0-3% were buried at depths of 9-, 15-, 21-, 27-, 33-, 45-, 57- and 75-mm, and probes with a range 0-10% were buried at depths of 100-, 150-, and 200-mm. For probe installation, a narrow trench was dug, a probe was placed horizontally at a selected depth and the probe was covered with soil. A CO2 analyzer (SBA-4, PP Systems, Inc., Amesbury, MA) was used as a standard to calibrate all of the solid-state sensors before installation. Each sensor was calibrated at 5 known CO2 concentrations in a laboratory gas chamber.

The solid-state CO2 sensors consisted of three parts: a remote probe, a transmitter body, and a cable connecting the probe to the transmitter (Fig.1a). Probes are cylindrical with a length of 15.5 cm and a diameter of 1.85 cm. There are 6 narrow slits around the probe to allow CO2 to diffuse into the sensor. To gain more precise measurement in the soil, we covered 4 of the 6 slits with 3M 5413 polyimide film tape (Fig. 1b) (one slit at the bottom view and three slits at the top view of the probe were covered). By keeping only two probe slits open, the vertical sampling thickness for each probe was limited to 5 mm. Each probe was covered with a porous Teflon cap that allowed CO2 gas to move freely into the uncovered probe slits but prevented water from entering into the probe. Probes were connected to a 24v DC power source (two rechargeable batteries connected in series, and each battery recharged by one 12v solar panel) and a data-logger that recorded the CO2 concentrations by measuring the voltage drop of probes. Two 21X data-loggers (Campbell Scientific Inc., Logan, Utah) were used to contact and monitor the 13 buried sensors in this study. To conserve power and avoid heating of the surrounding soil, a relay was used to regulate the 24v DC power source with 10 min on (including 8 min warm up time, and 2 min measurement time) and 50 min off each hour. The average CO2 concentration during the 2 min measurement period for each probe was recorded. The transmitter bodies and data-loggers were protected from environmental conditions by keeping them in a plastic box in the field.

Using measured CO2 concentrations, CO2 fluxes (F_{CO2}) at various soil depths were calculated with Fick's diffusion law (Eq.1):

$$F_{CO2} = -D_s \frac{\Delta C}{\Delta z} \qquad [1]$$

where ΔC and Δz represent the differences in CO2 concentration and differences in soil depth, respectively. Moldrup et al. (2004) analyzed several models for predicting soil gas diffusion coefficients (D_s) and found that Millington and Quirk (1961) model performed best in undisturbed soil. Soil gas diffusion coefficients (D_s) were estimated with the Millington and Quirk (1961) model with a temperature effect included (Eq.2):

$$D_s = (D_a)\frac{\varepsilon^{10/3}}{\Phi^2}\left(\frac{273.15 + T_{field}}{295.15}\right)^{1.75} \qquad [2]$$

$$\Phi = 1 - \frac{\rho_b}{2.65} \qquad [3]$$

$$\varepsilon = \Phi - \theta \qquad [4]$$

where D_a and D_s are CO2 diffusion coefficients in free air (16E-6 m^2s^{-1}) and in soil (m^2 s^{-1}), Φ is total porosity, and ε is air-filled porosity. Φ was calculated from the measured bulk density (ρ_b) (Eq.3), and ε was calculated from volumetric water content (θ) and Φ (Eq.4). ρ_b was measured by oven-drying soil samples collected in the bare field. One meter away from the buried CO2 sensors, heat pulse sensors were installed in the soil to measure soil water evaporation (Xiao et al., 2012). Volumetric heat capacity (C) was determined from heat pulse sensor measurements (Knight and Kluitenberg, 2004), and θ could be calculated from C and ρ_b (Eq.5) (Fig. 2b).

$$\theta = \left(C - 0.85 \text{ x } 10^6 \rho_b\right) / \left(4.17 \times 10^6\right) \qquad [5]$$

T_{field} is soil temperature measured with time and depth (ºC) (Fig. 2a). Soil temperatures between the surface and 48-mm soil depth were measured with chromel-constantan (type E) thermocouples in the heat pulse sensors and the soil temperatures between 48-mm and 200-mm soil depths were measured by chromel-constantan (type E) thermocouples buried in the soil.

CO2 produced in a soil layer (P_{CO2}) can be estimated from the net soil layer CO2 flux (the difference of F_{CO2} at upper and lower boundaries of a soil layer, $(F_{CO2})_1$-$(F_{CO2})_2$) and the storage change of CO2 (ΔS_{CO2}) in the soil layer (Eq. 6).

$$P_{CO2} = \left[(F_{CO2})_1 - (F_{CO2})_2\right] + \Delta S_{CO2} \qquad [6]$$

The amount of CO2 stored in a soil layer is relatively small compared with F_{CO2}, so the P_{CO2} in a soil layer was estimated from the difference in cumulative CO2 emitted at the soil layer boundaries (Risk et al., 2002).

Closed-chambers for measuring CO2 flux

Adjacent to the soil CO2 sensors, eight long-term closed-chambers (LI-8100-104, LI-COR Inc., Nebraska, USA) were installed in a linear transect 3.5 m apart to automatically measure bare soil surface CO2 efflux. The eight closed-chambers were connected to an infrared gas analyzer (LI-8100) system and a multiplexer (LI-8150), which were both powered by a power supply (LI-8150-770) connected to 110 AC power in the field. PVC collars (with a height of 11.4 cm and a diameter of 20.3 cm) were inserted in the soil with 2-4 cm height of each collar above the soil surface (offsets) to allow for a closed system when the chamber moved automatically and covered the top of the collar. The combined

LI-8100 and LI-8150 Multiplexer system controlled the CO_2 flux measurements. The LI-8150 Multiplexer contained a pump-driven circuit that transported the sample gas from each of the 8 chambers to the infrared gas analyzer in the LI-8100. This circuit provided air flow to and from the chamber while maintaining the ambient pressure in the analyzer. The analyzer measured CO_2 concentrations when the chambers were closed, and the concentrations with time were then used to calculate CO_2 flux. Measurements on the eight closed-chambers were performed sequentially for 16 min every hour with 2 min for each chamber (including 25 s deadband time and 45 s purge time).

Results and Discussions

CO_2 concentration measurements in the soil profile

Soil CO_2 concentrations at various depths 200 mm were measured July 28 (DOY 209) to Aug 9 (DOY 224) in the summer of 2008. There were two rainfall events during the measurement period (DOY 209, 23 mm; DOY 211, 14 mm).

Figure 3 shows the measured hourly CO_2 concentrations at various soil depths: the surface and 9-mm soil depth concentrations are in Fig. 3a, the 15- to 45-mm soil depths concentrations are in Fig. 3b, and the concentrations below a depth of 45-mm are in Fig. 3c.

CO_2 concentrations increased with soil depth. The values of CO_2 concentration were less than 0.12% at the 0 and 3 mm soil depths, ranged from 0.02 to 0.2% at the 9 mm soil depth, from 0.1 to 2.1% at soil depths between 15 and 45 mm, from 0.2 to 2.2% at soil depths between 57 and 100 mm, and 0.8 to 2.4% at depths 150 and 200 mm, respectively.

There were no living roots in the bare field, so soil microbial respiration was the main source of CO_2 in this field. Diffusion is a major pathway for CO_2 efflux from the soil. CO_2 diffuses from the soil to the atmosphere along a CO_2 concentration gradient.

Soil CO_2 concentration distribution was influenced by the rainfalls. CO_2 concentrations at all of the soil depths below 3 mm increased immediately after each rainfall event, reached maximum values about one day after a rainfall event, decreased rapidly one day later and then slowly decreased as the soil dried. Rain did not cause CO_2 concentrations to increase at the 0- and 3-mm soil depths due to the proximity of the soil-atmosphere interface. The large increase of soil CO_2 concentration at the 9-mm depth soon after the rainfall events may be caused by surface sealing, by the wet soil surface layer decreasing gas diffusion between soil and atmosphere, and / or by increased CO_2 production due to enhanced microbial activity in the wetted soil (Chen et al., 2005; Jassal et al., 2005; DeSutter et al., 2008). Following the rainfall, CO_2 concentrations at the 9-mm depth and below began to decrease because the soil was drying, which increased the air-filled pore space for CO_2 gas diffusion from deep soil to the surface.

Soil temperature can influence soil CO_2 distribution (Davidson et al., 1998). Soil CO_2 concentrations demonstrated diurnal changes at all soil depths. The patterns of the CO_2 concentrations below the 33-mm soil depth (Fig. 3b and 3c) were similar to the surface soil temperature (Fig. 2a), with the values increasing in the early morning, reaching a maximum value in the early afternoon, and decreasing to a minimum value near midnight. However the pattern of the CO_2 concentrations between 0 and 33 mm (Fig. 3a and 3b) was out of phase with the surface soil temperature, with peak values occurring in the night and low values occurring in the daytime. Relatively large CO2 values observed in the daytime below the 33 mm depth were due to enhanced soil microbial activity with high temperatures. Possible reasons for the low CO2 concentrations peak at daytime and large nighttime CO2 concentrations in the shallow soil may be 1) larger CO2 diffusion in the 0-33 mm soil layer prevented CO2 build-up in the early afternoon. In the early afternoon, the atmospheric CO2 concentrations above the surrounding cropped fields were relatively low due to photosynthesis. Flux tower measurements indicated that the CO2 concentrations at night were sometimes 2 times larger than the CO2 concentration in the afternoon. The atmospheric CO2 concentration above the bare field might be very low also because the atmosphere above the bare field was well mixed with the surrounding atmosphere at high wind speed and resulted in a large concentration gradient early in the afternoon. 2) CO2 production rates may decrease as soil temperature exceeds a certain high temperature. CO2 production rates are sensitive to high soil temperature. The soil surface temperature exceeded 50 °C in the early afternoon, which may decrease CO2 production rates. Tang et al. (2003) observed the similar soil CO2 concentration distribution pattern. They found CO2 concentration at the 80- and 160- mm soil depths had the same diurnal trends with the surface soil temperature while the CO2 concentration at the soil depth 20 mm had a diurnal trend with opposite that of the surface soil temperature.

CO2 fluxes with time and depth

There were no obvious soil CO2 concentration increases observed at the soil surface and a depth of 3 mm, but large CO2 concentration increases were observed at all of the soil depths below 3 mm during the rainfall events and one day after. This indicates that surface sealing and the increase of water content may be the main reasons for increasing the subsurface CO_2 concentrations (Chen et al., 2005; Jassal et al., 2005; DeSutter et al., 2008). Concentration gradient may not be the only driving force for CO2 diffusion from the soil to atmosphere. The simple Fick's diffusion law equation is not able to accurately describe the CO2 movement in the soil during the rainy days. Soil CO2 fluxes during soil drying period (DOY 213 to 224) were estimated from the measured CO2 concentrations and estimated gas diffusion coefficients at different soil depths with a concentration gradient method.

CO2 fluxes at the 1.5-, 4.5-, and 9-mm soil depths are shown in Fig.4a. Fluxes at the 15-, 21-, 30-, 45-, 60-mm soil depths are shown in Fig.4b. Fluxes at the 88-, 100-, 150- and 175- mm soil depths are shown in Fig. 4c. The CO2 fluxes showed diurnal variations in the 0-60 mm soil layer, and the diurnal variations diminished with soil depth. At the 1.5-mm soil depth, large variation in CO2 fluxes were observed and the values ranged from 1-10 $\mu mol\ m^{-2}s^{-1}$. The variation was relatively stable during the measurement period. At soil depths from 4.5 to 21-mm, significant diurnal variations were observed. The values of CO2 flux ranged from -2 to 9 , -1.5 to 5, -1 to 5.5 and -0.5 to 5 $\mu mol\ m^{-2}s^{-1}$ at the soil depths 4.5-, 9-, 15-, and 21-mm, respectively.

At soil depths from 30 to 60 mm, the diurnal fluctuation of CO2 fluxes decreased to a peak value of 1.5 $\mu mol\ m^{-2}s^{-1}$. At a soil depth of 88-mm and below, CO2 fluxes were stable at about 0.6 $\mu mol\ m^{-2}s^{-1}$.

The CO2 flux distributions indicated that CO2 diffused from the soil to the atmosphere and the CO2 production rates varied with soil depth.

CO_2 production with time and depth

Figure 5 shows cumulative CO_2 fluxes emitted at various soil depths during the soil drying period from DOY 213 to 224. During the 12 day soil drying period, the cumulative emitted CO_2 was 3.78 mol m^{-2} at the soil surface from the closed-chamber measurement, and the cumulative emitted CO_2 were 4.44-, 2.91-, 2.04-, 1.69-, 0.65-, 0.44-, and 0.35- mol m^{-2} at soil depths of 1.5-, 4.5-, 15-, 21-, 60-, 100- and 175-mm, respectively, from the concentration gradient method. The cumulative gradient method CO_2 emitted at the 1.5 mm soil depth overestimated the closed-chambers surface CO_2 by 15%.

CO_2 fluxes varied with depth because CO_2 production rates varied with depth. Most of the CO_2 was produced at the shallow soil depths in this bare field. A small portion (8%) of CO_2 was produced below a depth of 175-mm, 2% was produced in the100-175 mm soil layer, and 90% was produced in the 0-100 mm soil layer. Nakadai et al. (2002) reported that 70% of CO_2 was produced in the 0-100 mm soil layer in a bare field in Japan. The reason that Nakadai et al. (2002) had lower CO_2 production in the 0-100 mm soil layer might be that their field was maintained for a longer time (over 20 years) than this bare field (two years).

Comparing concentration gradient and closed-chamber CO_2 effluxes

As soil CO_2 concentrations were being measured, CO_2 effluxes were measured automatically with eight closed-chambers in the bare field from DOY 213 to 224. The concentration gradient method CO_2 flux at the shallowest depth of 1.5 mm was chosen to compare with CO_2 effluxes measured with closed-chamber method.

The gradient method and closed-chambers (average CO_2 effluxes of the eight chambers) CO_2 fluxes are shown in Fig. 6a. The gradient method diurnal fluctuations of CO_2 flux tracked well with most of the closed-chamber method diurnal fluctuations with large peaks occurring early in the afternoon and low peaks occurring during midnight of each day.

We also compared daily average values of CO_2 fluxes calculated from the concentration gradient method with the minimum, and maximum values of the daily average CO_2 flux from the eight closed-chambers (Fig 6b). We observed some variation in the eight closed-chambers, with the standard deviation ranging from 0.61 to 2.52 μmol $m^{-2}s^{-1}$ and the CV ranging from 28 to 52% during the measurement period (Table 1). The values of daily CO_2 flux from the gradient method were generally within the range of the eight closed-chambers (between the minimum and maximum values of daily average CO_2 flux), with only two daily mean gradient values larger than the maximum values of the closed-chamber daily average CO_2 flux.

Conclusions

Soil CO_2 concentrations increased with soil depth. Soil CO_2 concentration increased immediately after rainfall events and decreased during soil drying. Soil CO_2 fluxes decreased with soil depth in the 0 to 90 mm soil layer, and the fluxes were about 0.6 μmol $m^{-2}s^{-1}$ below a depth of 90-mm. The distribution of in situ CO_2 concentrations was useful for computing soil CO_2 fluxes and soil CO_2 production rates with depth.

The diurnal fluctuations of the gradient CO_2 fluxes were similar to the diurnal fluctuations of the chamber fluxes. The gradient method CO_2 efflux agreed well with the surface closed-chamber CO_2 efflux, with 10 days of the daily mean of gradient CO_2 efflux within the range of 12-day of closed-chamber CO_2 effluxes. Thus, the concentration gradient method was able to measure bare field soil CO_2 fluxes and soil CO_2 production with time and depth as the soil dried. Further studies on a range of field moisture and management conditions are needed to evaluate and improve the determination of vertical CO_2 concentration gradient and in situ CO_2 diffusion coefficients at the soil surface.

Acknowledgement

This work was supported by National Science Foundation (Grant No. 0809656), and by the Hatch Act, State of Iowa, and State of North Carolina funds.

References

Bernhardt, E.S., J.J. Barber, J.S. Pippen, L.Taneva, J.A. Andrew, and W.H. Schlesinger. 2006. Long-term effects of free air CO2 enrichment (FACE) on soil respiration. Biogeochemistry. 77:91–116. DOI 10.1007/s10533-005-1062-0.

Chen, D., J.A.E. Molina, C.E. Clapp, R.T. Venterea, and A.J. Palazzo. 2005. Corn root influence on automated measurement of soil carbon dioxide concentrations. Soil Sci. 170:779-787.

Risk, D., L. Kellman, and H. Beltrami. 2002. Soil CO2 production and surface flux at four climate observatories in eastern Canada. Global BiogeiBIOGEOCHEMICAL Biogeochemical Cycles. 16 (4). 1122. doi:10.1029/2001GB001831.

Davidson, E.A., E. Belk, and R.D. Boone. 1998. Soil water content and temperature as independent or confounded factors controlling soil respiration in a temperate mixed hardwood forest. Global Change Biol. 4:217–227.

DeSutter, T.M., T.J. Sauer, T.B. Parkin, and J.L. Heitman. 2008. A subsurface, closed-loop system for soil carbon dioxide and its application to the gradient efflux approach. Soil Sci. Soc. Am. J. 72:126-134.

Hutchinson, G.L., and G.P. Livingston. 2002. Soil-atmosphere gas exchange. p. 1 l59-1182. In J.H. Dane and G.C. Topp (ed.) Methods of soil analysis. Part 4. SSSA Book Ser. 5. SSSA, Madison,WI.

Jassal, R., A. Black, M. Novak, K. Morgenstern, Z. Nesic, and D. Gaumont-Guay. 2005. Relationship between soil CO2 concentrations and forest-floor CO2 effluxes. Agric. For. Meteor. 130:176–192.

Knight, J.H. and G.J. Kluitenberg. 2004. Simplified computational approach for the dual-probe heat-pulse method. Soil Sci. Soc. Am. J. 68:447-449.

Law, B.E., D.D. Baldocchi, and P.M. Anthoni. 1999. Below-canopy and soil CO2 fluxes in a ponderosa pine forest. Agric. For. Meteor. 94:171–188.

Millington, R.J. and J.M. Quirk. 1961. Permeability of porous solids. Trans. Faraday Soc. 57:1200–1207.

Moldrup, P., T. Olesenb, S. Yoshikawac, T. Komatsud and D. E. Rolstone. 2004. Three-porosity model for predicting the gas diffusion coefficient in undisturbed soil. Soil Sci. Soc. Am. J. 68:750-759.

Nakadai, T., M. Yokozawa, H. Ikedaa, and H. Koizumi. 2002. Diurnal changes of carbon dioxide flux from bare soil in agricultural field in Japan. Applied Soil Ecology. 19 (2):161–171.

Nakadai, T., M.Yokozawa, H. Ikeda, and H. Koizumi. 2002. Diurnal changes of carbon dioxide flux from bare soil in agricultural field in Japan. Appl. Soil Ecol., 19:161–171.

Norman, J.M., R. Garcia, and S.B.Verma. 1992. Soil surface CO2 fluxes and the carbon budget of a grassland. J. Geophys. Res. Atmos. 97:18845–18853.

Pumpanen, J., P. Kolari, H. Ilvesniemi, et. al.. 2004. Comparison of different chamber techniques for measuring soil CO2 efflux. Agric. For. Meteor. 123:159–176.

Savage, K.E. and E.A. Davidson. A comparison of manual and automated systems for soil CO2 flux measurements: trade-offs between spatial and temporal resolution. J. Exper. Botany. 54 (384):891-899.

Tang J., D.D. Baldocchi, Y. Qi, and L. Xu. 2003. Assessing soil CO2 efflux using continuous measurements of CO2 profiles in soils with small solid-state sensors. Agric. For. Meteor. 118:207–220.

Treonis, A.M., D.H. Wall, and R.A.Virginia. 2002. Field and microcosm studies of decomposition and soil biota in a cold desert soil. Ecosystems. 5:159–170.

Turcu, V.E., S.B. Jones, and D. Or. 2005. Continuous soil carbon dioxide and oxygen measurements and estimation of gradient-based gaseous flux. Vadose Zone J. 4:1161-1169.

X. Xiao, R. Horton, T.J. Sauer, J.L. Heitman and T. Ren. 2012. Heat pulse sensor measurements of soil water evaporation in a corn field (in review).

Xu, L., R. Madsen, D. McDermitt, D. Scoby, and T. Arkebauer. 2010. Temporal and spatial variations of soil CO2 flux over a soybean field in Nebraska. Geophysi. Res. Abstr. EGU, Vienna, Austria 12: 2010-11487.

Figure Captions

Fig. 1: Configuration of a CO_2 solid sensor, and installations in the ground.

Fig. 2. Soil temperature and water content (θ) at various depths.

Fig. 3. CO_2 concentrations measured at various depths by CO_2 sensors.

Fig. 4. Soil CO_2 fluxes with time and depth.

Fig. 5. Cumulative soil CO_2 emitted with time and depth.

Fig. 6. a: Diurnal CO_2 fluxes (μmol $m^{-2}s^{-1}$) from the gradient and chamber methods.

b: Daily mean CO_2 fluxes from gradient method and maximum and

minimum CO_2 fluxes from eight closed-chambers.

(Gradient method flux was at 1.5 mm soil depth).

Table 1: Descriptive statistics of CO2 flux from eight closed-chambers.

DOY	Mean	Min	Max	SD	CV (%)
	(μmol $m^{-2}s^{-1}$)				
213	3.83	2.00	6.52	1.35	35
214	4.92	2.09	6.75	1.79	36
215	4.85	2.11	9.77	2.52	52
216	3.28	1.91	4.88	1.12	34
217	4.59	2.07	6.86	1.83	40
218	4.10	1.55	6.37	1.70	41
219	3.52	1.60	5.41	1.32	38
220	3.92	1.46	6.46	1.76	45
221	2.84	1.60	4.06	0.80	28
222	3.30	1.44	4.95	1.19	36
223	4.01	1.37	6.14	1.64	41
224	2.05	0.96	2.77	0.61	30

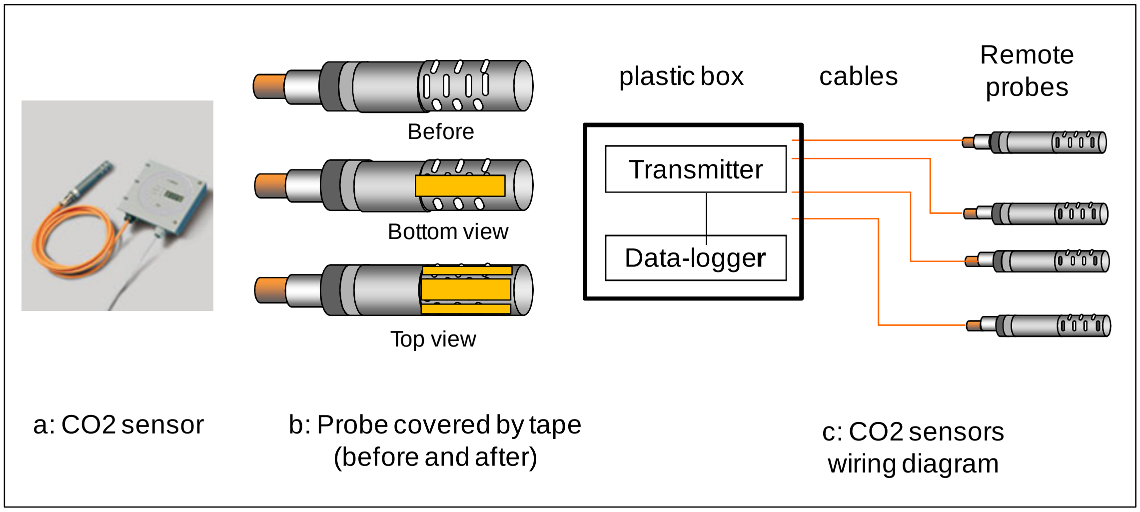

Fig. 1: Configuration of a CO2 solid sensor, and installations in the ground.

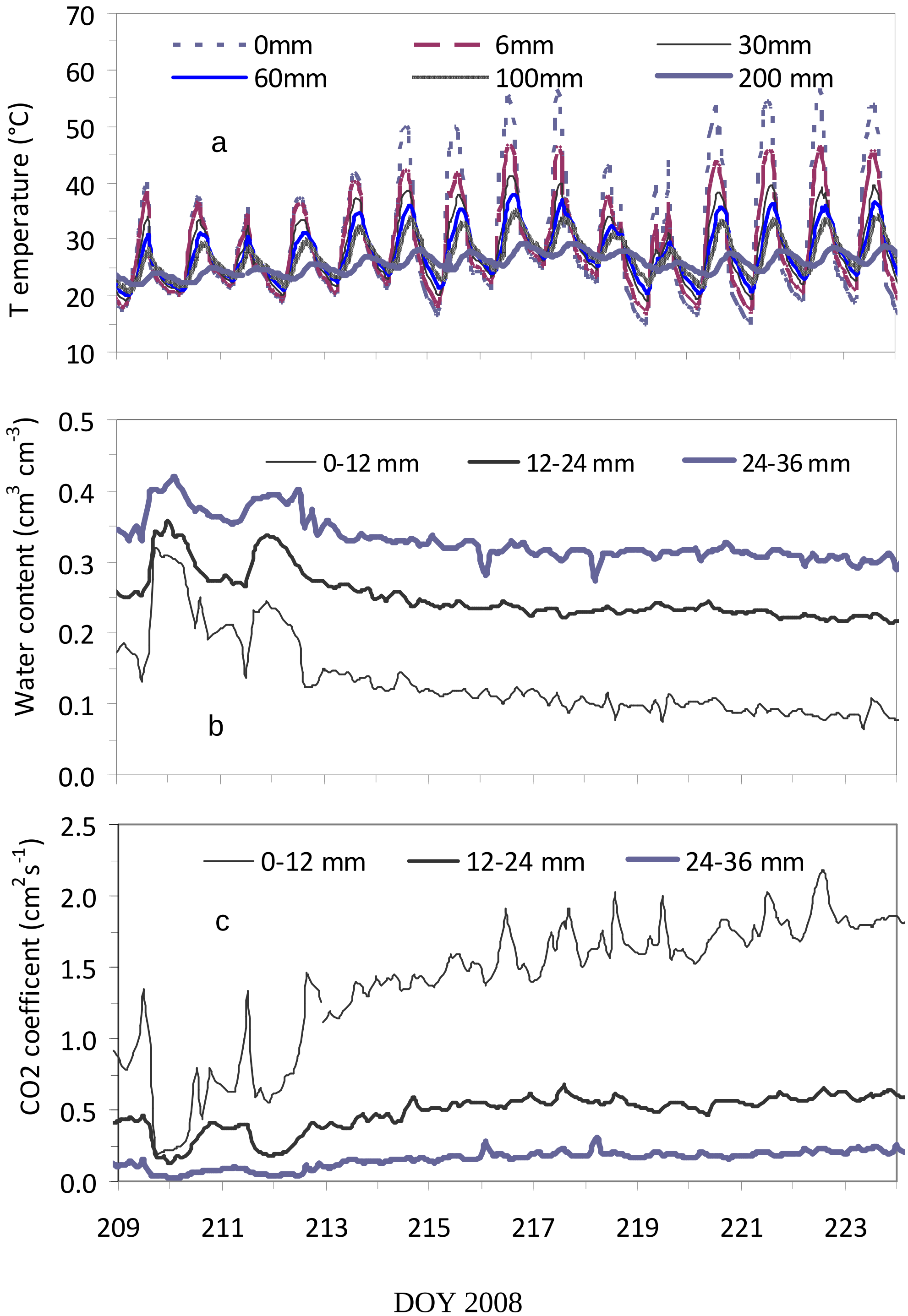

Fig. 2. Soil temperature, water content (θ) and CO2 coefficient at various depths.

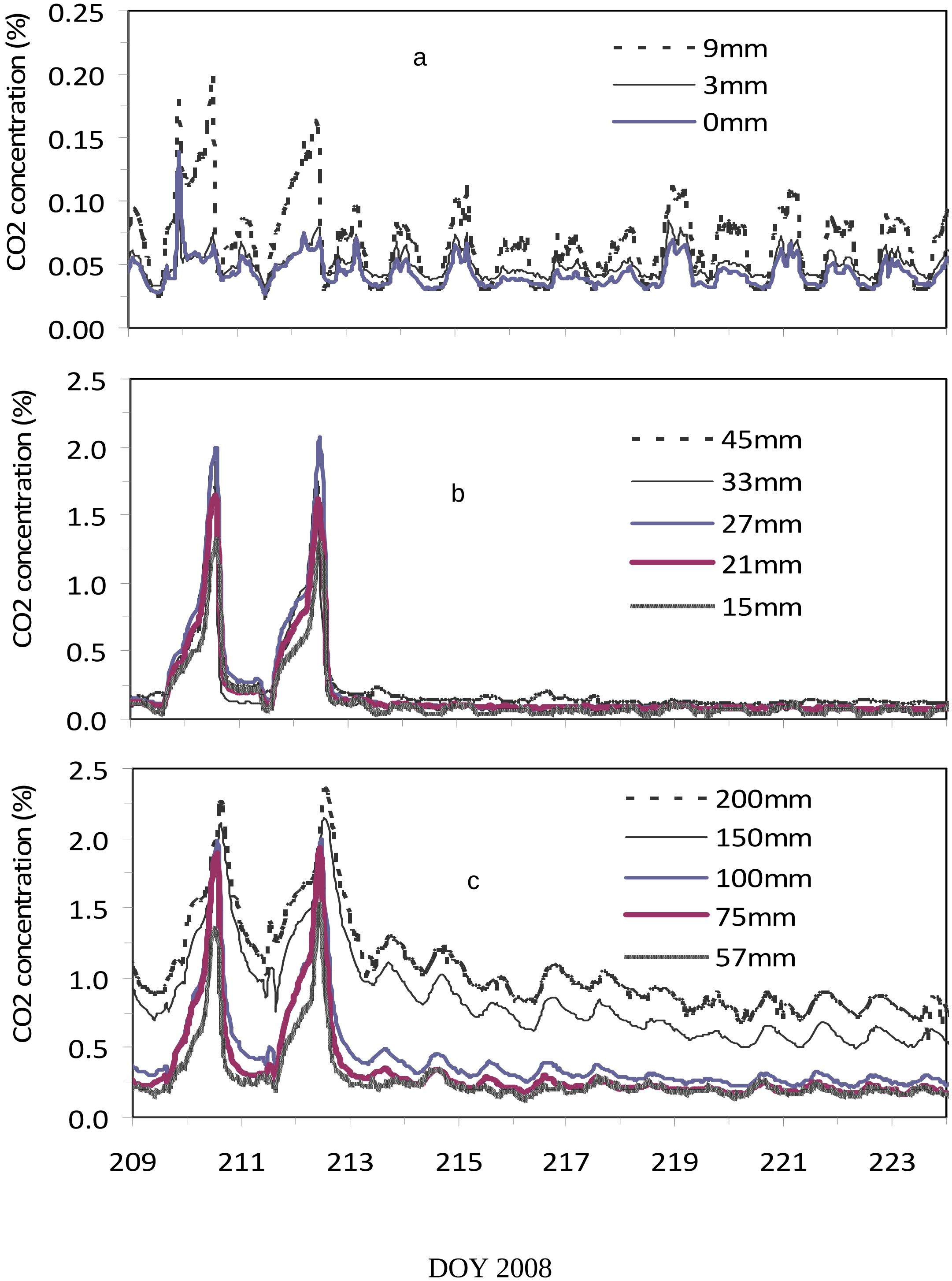

Fig. 3. CO2 concentrations measured at various depths by CO2 sensors.

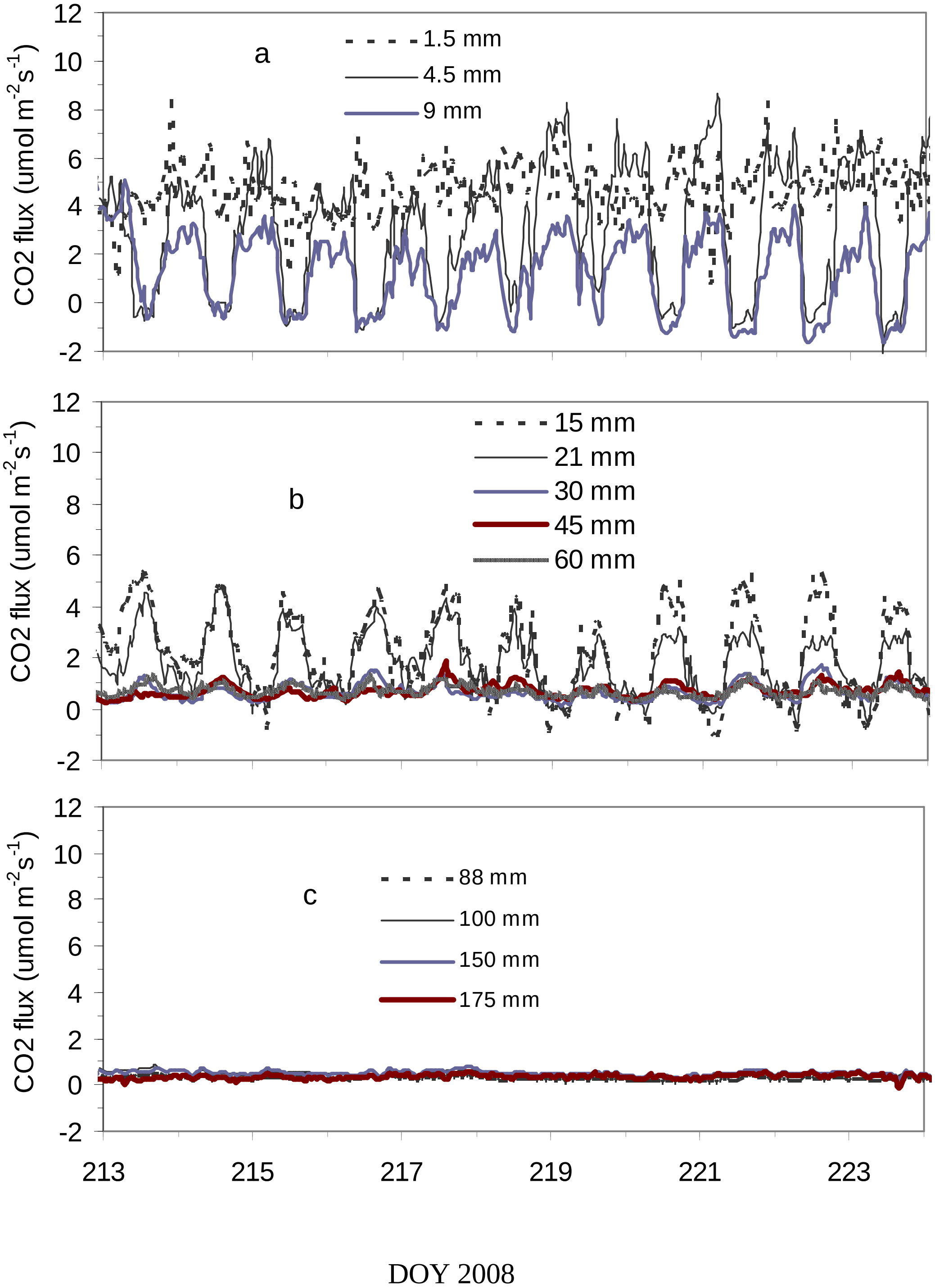

Fig. 4. Soil CO2 fluxes with time and depth.

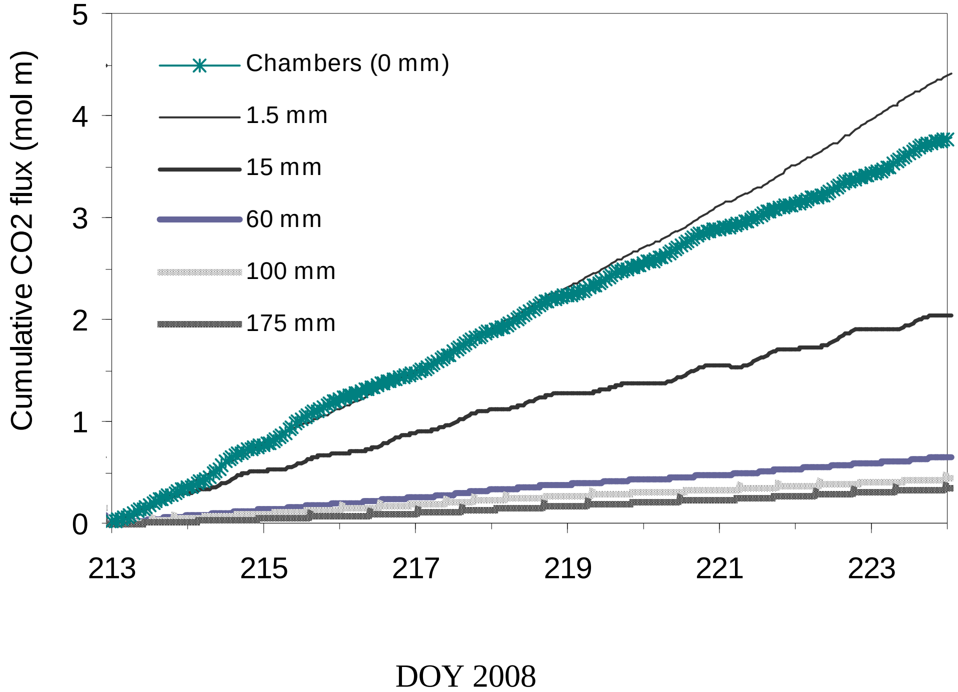

Fig. 5. Cumulative soil CO2 emitted with time and depth.

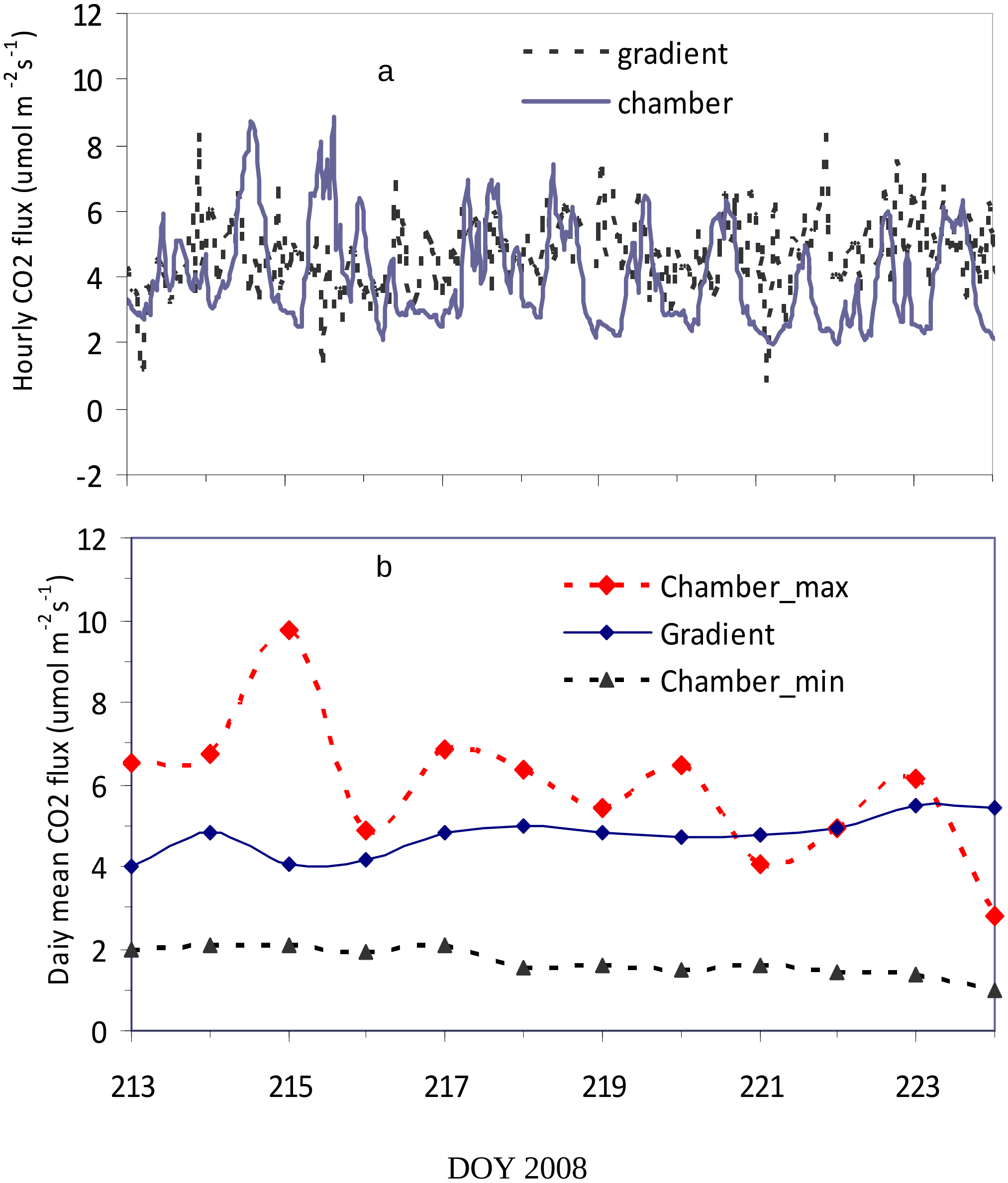

Fig. 6. a: Diurnal CO2 fluxes (μmol $m^{-2}s^{-1}$) from the gradient and chamber methods

b: Daily mean CO2 fluxes from gradient method and maximum and minimum CO2 fluxes from eight closed-chambers.

(Gradient method flux was at 1.5 mm soil depth).

Chapter 7 General Conclusions

Soil heat, water vapor and carbon dioxide (CO2) are interactive and impact the soil environment and physical, chemical, and biological processes occurring in the soil. Latent heat flux associated with soil water evaporation connects the surface water balance with the surface energy balance. Accurate and dynamic measurements of soil water evaporation and soil CO2 fluxes can enhance the understanding of water, energy, and carbon partitioning at the soil-atmosphere interface and the mechanisms of mass and energy movement in the soil. The overall objectives of this dissertation were to accurately determine transient soil water evaporation in bare soil and in different management zones of a corn field using heat pulse method and determine soil CO2 fluxes using a concentration gradient method in bare soil and to evaluate in situ measurement techniques. For those purposes, chapters 2, 3, 4 and 5 focused on the topic of soil water evaporation measurements, and chapter 6 focused the topic of soil CO2 flux measurement. For soil water evaporation specifically, chapters 2 and 3 evaluated the heat pulse method for determining surface and subsurface soil water evaporation with time and depth by using 3-needle heat pulse sensors in a bare soil. Using improved 11-needle heat pulse sensors, chapters 4 and 5 further evaluated the heat pulse method for determining soil water evaporation in different management zones of a corn field and in partitioning evapotranspiration in a corn field. In chapter 6, concentration gradient method was used to determine soil CO2 fluxes and production rates with time and depth and the method was evaluated. General conclusions are presented by topics and by chapters.

Soil water evaporation measurement: heat pulse method test and evaluation

The hypotheses of chapters 2, 3, 4, and 5 were that the heat pulse method could accurately and dynamically measure soil water evaporation with time and depth in bare and cropped soil. To test those hypotheses, 4 studies described in 4 chapters were conducted.

In chapter 2, the heat pulse method was used to measure bare field subsurface soil water evaporation with time and depth with 3-needle heat pulse sensors. Comparisons between daily estimates of heat pulse evaporation with Bowen ratio and micro-lysimeter estimates agreed well. This work demonstrated that heat pulse sensors could accurately determine bare field subsurface soil water evaporation with time and depth.

In chapter 3, the heat pulse method was further tested and evaluated in a bare soil with regard to determining cumulative surface and subsurface water evaporation. Cumulative water evaporation was calculated over 20 consecutive days in each of two years and compared with Bowen ratio measurements. The results showed that heat pulse and Bowen ratio measurements of cumulative water evaporation from bare soil were consistent in magnitude and time. Combined with Bowen ratio measurements, heat pulse measurements of cumulative evaporation with time revealed the dynamics of surface and subsurface soil water evaporation that developed in a bare field. These findings indicated that heat pulse sensors could accurately determine cumulative evaporation over consecutive days and wetting-drying periods.

From studies reported in chapters 2 and 3, the heat pulse method was tested and evaluated in bare soil. Because of its capability to measure evaporation with depth and time for field conditions, and because of its capability to accurately determine surface and subsurface cumulative evaporation, the heat pulse method promises to be a practical and valuable tool for a wide range of vadoze zone hydrology investigations..

In chapter 4, the heat pulse method was evaluated for determining soil water evaporation in three different management zones of a corn field: within-row (ROW), between-rows with roots (BR), and between-rows without roots (BRNR). Improved heat pulse sensors, 11-needle sensors, were used in this study. The results showed that the heat pulse sensor measurements provided realistic estimates of the soil water evaporation dynamics at the various locations. The cumulative soil water evaporation at the BARE location was larger than it was at the BRNR location which was slightly larger than evaporation at the ROW and BR locations. Soil water evaporation estimates from heat pulse and micro-lysimeter methods were consistent, with the total difference in evaporation of 0.5 mm out of 5.4 mm, and 0.8 mm out of 5.9 mm for 9 days at the ROW and BR corn field locations, respectively. Therefore, this work demonstrates that the heat-pulse method is a promising approach for measuring soil water evaporation at different management zones of cropped fields.

In chapter 5, the heat pulse method was applied to help partition evapotranspiration (ET) in a corn field. ET is a major component of the hydrological cycle and consists of soil water evaporation (E) and plant transpiration (T). In a corn field, soil water E was measured with improved 11-needle heat pulse sensors, T was measured with stem flow gauges, and ET was measured with an eddy covariance system. Potential evapotranspiration ET_0 was also calculated with the Penman-Monteith equation. The results showed that all three estimates of ET had similar trends and that E, T, E+T and eddy covariance ET accounted for 13%, 77%, 90% and 61% of ET_0, respectively, during the measurement period. This work demonstrated that the heat pulse method could be applied for evapotranspiration partitioning in a cropped field. Heat pulse sensors hold promise for providing accurate partitioning of ET into E and T and to improve water balance determination at the field and regional scales and help quantify components of the hydrological cycle.

Soil carbon dioxide (CO2) flux measurement

The hypothesis of chapter 6 was that soil CO2 fluxes could be accurately determined with time and depth in a bare field by concentration gradient method. To test this hypothesis, transient soil CO2 fluxes and soil CO2 production were estimated with depth using a concentration gradient method. The concentration gradient method was evaluated by comparing gradient method CO2 flux values with surface closed-chamber measurements of soil CO2 fluxes. The results showed that the *in situ* observed soil CO2 concentrations provided realistic CO2 distributions, and that soil CO2 fluxes kept stable below a depth of 90 mm with most of the CO2 produced in shallow soil. The gradient method calculated CO2 fluxes were compared with the surface closed-chamber CO2 efflux and they agreed well. This work applied high-resolution sensors in soil profile, and was the first effort to quantify *in situ* CO2 fluxes and production at a fine (mm) scale. It demonstrated that the concentration gradient method was able to accurately measure soil CO2 fluxes and production with time and depth in a bare soil, and it promises to be a practical and valuable addition for a wide range of CO2 flux and production investigation.

Overall, this dissertation focused on heat transfer, evaporation and CO2 transfer in soil. Specifically, for studying heat transfer and water evaporation in soil, the heat pulse method for measuring soil water evaporation in various applications was evaluated. The heat pulse method was able to accurately measure soil water evaporation with time and depth in a bare field, in different management zones of a corn field, and it enabled accurate evapotranspiration partitioning in a corn field. For CO2 transfer in soil, a concentration gradient method for determining CO2 flux and production in a bare soil was evaluated. The concentration gradient method was able to accurately determine CO2 fluxes and production rates with time and depth in a bare soil. Overall, the evaluations indicated that the heat pulse method for determining water evaporation and the concentration gradient method for determining CO2 flux are practical and valuable tools for a wide range of vadoze zone investigations. Simultaneous soil water evaporation and soil CO2 flux measurements are helpful for evaluating coupled models for heat, evaporation and CO2 transfer in soil and for guiding the management of soil properties and processes.

Future research

Accurate and dynamic measurements of soil water evaporation and soil CO2 fluxes can help to enhance the understanding of water, energy, and carbon partitioning at the soil-atmosphere interface and the mechanisms of mass and energy movement in soil. While this dissertation has evaluated some techniques for determining in situ soil water evaporation and CO_2 fluxes in various soil management conditions and made adequate progress in determining these soil gas fluxes, there are some potential research topics remaining to be explored in the future.

In this dissertation, soil water evaporation measurements using the heat pulse method were limited to the subsurface while surface evaporation was not determined. Accurate determination of soil water evaporation in the whole soil profile can provide a fuller insight of mass and energy balance in the soil. Further research could include two parallel directions: instrument design improvements and numerical analysis. By applying multi-needle heat pulse sensors with denser needles near the soil surface, or combing sensors with new detectors for surface thermal properties, improved measurements at the soil surface might be obtained. Alternatively, numerical analysis combining with surface and subsurface measurements could be used to infer surface and subsurface soil water evaporation. In addition, the heat pulse method used in this study to measure soil water evaporation in bare and cropped fields may be extended to determine solute transport and water flow under unsaturated, unsteady conditions.

In this dissertation, subsurface soil CO_2 fluxes and CO_2 productions rates with depth were determined with a concentration gradient method applied to drying soil in a bare field condition. Further studies on a range of field moisture and management conditions are needed to improve the determination of vertical CO_2 concentration gradients and in situ CO_2 diffusion coefficients at the soil surface and during rainfall events and in a more complex cropped field. Further research topics should address the determination of surface and subsurface soil CO_2 flux in more complex soil management conditions.

Numerical models used in conjunction with careful measurements provide a means to increase understanding of the complex soil system. The transfer of heat, water, and CO_2 in soil is coupled and interactive. Using and/or developing models for use in conjunction with soil heat, water and CO_2 measurements should lead to improve understanding of the mechanism of heat and mass transfer in soils.

Acknowledgement

I am grateful for all the help that I have received during my Ph.D study. I am so lucky to be a member of the Soil Physics group at Iowa State University. Group members gave me so much help on my research study and my personal life. Thanks to Dr. Toby Ewing, Dedrick Davis, Jacob Prater, Aaron Daigh, Yuki Kojima and Devinder Sidhu.

I thank my major professor Dr. Robert Horton. He has helped me to improve as a researcher and as a person. I am grateful for his consistent encouragement, patience, and teaching during my study. He is far more than a major professor to me. He is a role model for my future life. I also thank Drs. Tom Sauer, Brian Hornbuckle, Amy Kaleita-Forbes and Mahdi Al-Kaisi for serving as members of my Program of Study Committee. I especially thank Dr. Tom Sauer for his consistent support, guidance and encouragement to me, and I thank Dr. Brian Hornbuckle for all the opportunities he provided during my field experiments. I thank Dr. Jeremy Singer for his contributions to the sap flow measurements for plant transpiration. I thank Drs. Josh Heitman and Tusheng Ren for giving me so much advice and encouragement on my research study. I thank Tim Hart, Kevin Jensen, Jason Patton and Jenny Richter who gave me a lot of help on completing my field experiments.

At last, I want to thank my family. I thank my husband, Xianyan, who loves me and has been my constant support and encouragement always. I thank my two daughters, Ally and Emma, who have given me a lot of joy, encouragement and hope.